UNDERSTANDING THE EFFECT OF PHYSICO-CHEMICAL PROPERTIES OF PARTICLES ON CELLULAR INTERACTIONS

A Dissertation
Presented to
The Academic Faculty

by

Anusha Garapaty

In Partial Fulfillment
of the Requirements for the Degree
Doctor of Philosophy in the
School of Chemical & Biomolecular Engineering

Georgia Institute of Technology
[MAY 2017]

UNDERSTANDING THE EFFECT OF PHYSICO-CHEMICAL

PROPERTIES OF PARTICLES ON CELLULAR INTERACTIONS

Approved by:

Dr. Julie Champion, Advisor
School of Chemical & Biomolecular
Engineering
Georgia Institute of Technology

Dr. Athanassios Sambanis
School of Chemical & Biomolecular
Engineering
Georgia Institute of Technology

Dr. Julia E. Babensee
School of Biomedical Engineering
Georgia Institute of Technology

Dr. Sven H. Behrens
School of Chemical & Biomolecular
Engineering
Georgia Institute of Technology

Dr. Todd Sulchek
School of Mechanical Engineering
Georgia Institute of Technology

Date Approved: [February 23, 2017]

To my family who have helped me get to where I am today

ACKNOWLEDGEMENTS

First and foremost, I am greatly indebted to my family especially my grandparents who have played a huge role in shaping me as a person. My parents have always been there for me and have always made me their priority. Their unwavering support and encouragement constantly makes me explore and pursue my dreams. My brother, Bharat is always there to lend an ear and cheer me up during rough times. All of my uncles, aunts and cousins have been a great support system during my incredible PhD journey. Finally, my husband, for his incredible support as I finished my thesis.

I would like to convey my deepest gratitude to my advisor Dr. Julie Champion for her invaluable support, encouragement and guidance throughout my graduate study. Her enthusiasm has helped me be motivated during this long journey and her valuable insights have allowed me to grow scientifically. I am thankful to Dr. Todd Sulchek for helpful discussions on AFM during this project. I am also grateful to my committee members Dr. Julia Babensee. Dr. Sven Behrens and Dr. Athanassios Sambanis for their invaluable feedback during the course of this work.

My lab members have also played a huge role in this journey. Lina, Won and Trudy, the founding members of the lab for all the "know-how" when I joined. I am also thankful to Xingjie, with whom the layer-by-layer technique was conceptualized. Tim, Kevin and Trudy have been a great source of energy in the lab and have always been there for scientific and state of the world discussions. Matthew, my undergrad has been very resourceful during this work. Sung In, Yeongseon, Tianxin, Alex, Adam, Anshul and Kelly have all made this journey more memorable.

This journey would not have been fulfilling without the amazing friendship and emotional support of my wonderful friends and peers. The Chemie Desi Junta who always got together for countless celebrations, making it all the more fun and memorable. It's been an incredible journey and I am so thankful for all of the amazing people that have helped me along the way.

TABLE OF CONTENTS

LIST OF TABLES

LIST OF FIGURES

LIST OF SYMBOLS AND ABBREVIATIONS

PS	Polystyrene
PEG	Polyethyene glycol
IgG	Immunoglobulin G
TA	Tannic acid
PVPON	Poly (vinylpyrrolidone)
PLGA	Polylactic-co-glycolic acid
LbL	Layer- by- layer
PMA	Poly (methacrylic acid)
BSA	Bovine serum albumin
PAH	Poly (allylamine hydrochloride)
PSS	Poly (styrene sulfonate)
polyIC	Polyinosinic-polycytidylic acid
OVA	Ovalbumin

NP   Nanoparticle

CTL   Cytotoxic T lymphocyte

RBC   Red blood cell

ES   E-Selectin

TRAIL   TNF- related apoptosis inducing ligand

NK   Natural killer

ICAM-1 Intercellular adhesion molecule 1

MPLA   Monophosphoryl lipid A

aAPC   Artificial antigen presenting cell

MHC   Major histocompatibility complex

TCR   T cell receptor

CAR   Chimeric antigen receptor

LFA-1   Lymphocyte function associated antigen-1

RGD   Arginine-glycine-aspartic acid sequence

SWNT	Single walled carbon nanotubes
MZ	Marginal zone
Ag-SP	Antigen coupled to splenocytes
PD-L1	Programmed death ligand-1
MARCO	Macrophage receptor with collagenous structure
PEI	Poly-ethyleneamine
TNF-α	Tumor necrosis- alpha
IFN-γ	Interferon-gamma
PMA	Poly(methacrylic acid)
PAH	Poly-(allylamine hydrochloride
PSS	Poly-(styrenesulfonate)
TLR	Toll like receptor
polyIC	Polyinosinic–polycytidylic acid
MPC	2-methacryloyloxyethacrylate-PC

PC   Phosphorylcholine

IPA   Isopropyl alcohol

THF   Tetrahydrofuran

TEM   Transmission electron microscope

DLS   Dynamic light scattering

eGFP   Enhanced green fluorescent protein

LPS   Lipopolysaccharide

FITC   Fluorescein isothiocyanate

PBS   Phosphate buffered saline

MSR   Mesoporous silica rod

SUMMARY

Polymeric micro and nanoparticles are useful carriers for drugs and vaccines. During these applications, particles come into contact with macrophages of the reticuloendothelial system leading to their internalization. On one hand, uptake of particles by macrophages affects their ability to deliver therapeutics to the target cells. On the other hand, intracellular delivery of therapeutics is dependent on macrophage uptake in diseases or vaccines involving these cells. Previous research efforts have focused on identifying crucial particle physico-chemical properties like size, shape, surface chemistry and stiffness that are capable of enhancing drug delivery. However, as particle fabrication techniques advance to meet the growing need to develop complex particles for enhancing therapeutic delivery, identification of the inter-dependence between multiple physical properties on cellular interactions is critical. A major challenge with current particle fabrication techniques is the inability to tune each of their physical properties separately and thereby limiting investigation of influence of inter-dependent properties on cellular interactions. Additionally, it is crucial to identify how individual properties alter cellular functions like cytokine production.

To address these challenges, in this dissertation, we proposed a novel method that leverages the principles of self-assembly on soft templates to enable the tuning of multiple physical properties of particles while holding the surface chemistry constant. This technique provides insight on how an individual particle property influences cellular interactions when they work in concert with other properties. We investigated the combined effect of physical properties size, shape and stiffness on macrophage interactions

in Fc receptor-mediated phagocytosis. Our results highlight, for example, how reducing stiffness works in a complex way when combined with size and shape. For spherical shaped particles, decreased stiffness works in tandem with increased size to reduce internalization. In contrast, decreased stiffness increases internalization of rod shapes relative to spheres. These particles highlight the interplay between size, shape and stiffness during phagocytosis by macrophages and can be leveraged to identify combinations of parameters that improve particle-based delivery to cells.

In addition, this method enabled assembly of a phosphorylcholine co-polymer on microparticles in a single step, making it widely applicable and less time consuming compared to currently published covalent methods. We demonstrated that such a coating mechanism rendered the particles resistant to protein adsorption and phagocytosis by macrophages, two measures that are critical for use in biological systems. This highlighted the ability of this technique to be extendable to other polymers commonly used in the biomaterials community.

While prior research and our studies helped in understanding the effect of particle physicochemical properties on the outcome of particle-macrophage interactions, it is unclear how macrophage functions like cytokine production are affected while presenting active ligands through altered physical properties. Moreover, it is unknown if geometric presentation through an altered shape can elicit differential macrophage cytokine responses and if similar responses can be noticed across varying ligands. Therefore, we investigated the influence of geometric presentation of varying ligands (BSA, IgG, OVA, CD200) facilitated by the manipulation of shape of the particle on macrophage inflammatory cytokine response. We investigated the influence of geometric presentation of varying

ligands (BSA, IgG, OVA, CD200) facilitated by the manipulation of shape of the particle on macrophage inflammatory cytokine response- TNF-α. In addition, we examined the role of geometric presentation of different ligand densities between varying shapes. Further, this was correlated to TNF-α secretion and total particle association. This demonstrates how the geometric manipulation of diverse ligands through presentation on varying shapes alters inflammatory response in macrophage.

Overall, these studies enable identification of design rules for engineering cell interactions and responses. The identification of dominant properties such as size and the intricate interplay between stiffness and shape provide valuable information for the optimal design of advanced carriers to avoid or enhance macrophage internalization. Further, geometric presentation has been identified as an important design parameter that tunes cellular function like cytokine production. These findings are significant to both the biomaterials and the larger immunoengineering communities that actively employ various strategies involving particle properties and ligands to elicit immunological responses. These methods, techniques and results can be used to further fundamental research involving tunable particle-cell interactions and to inform particle design for specific therapeutic applications based on the disease.

CHAPTER 1.   INTRODUCTION

1.1   Approaches to synthetic carrier design

Free drugs such as chemotherapeutics often suffer from solubility, toxicity and stability issues when introduced into the body[1–3]. There is a pressing need to identify vehicles for enhancing their therapeutic activity. This has led to a rapid progress in the design of synthetic carriers such as polymeric micro-, nanoparticles, liposomes and micelles[4]. However, the major hurdle in the success of these synthetic carriers lies in their ability to overcome biological hindrances when introduced into the body. In these applications, particles come into contact with biological fluids that contain a complex mixture of proteins that can adsorb on the particle surface[5]. This process, called opsonization, fouls their surface and can prevent desired interactions. Opsonization helps phagocytic cells of the reticuloendothelial system, like macrophages, to rapidly clear particles from circulation through phagocytosis. This process of phagocytosis faced by synthetic carriers often limits particles' potential in biomedical applications. It has been established that biophysical particulate properties like size, surface chemistry, shape and mechanical properties influence phagocytosis[6–10].

The motivation to use physical properties to elucidate the clearance mechanisms employed by macrophages stems from the critical examination of native systems ranging from pathogens to cells[11]. Bacteria exhibit diverse properties like size, shape and surface chemistry, which contribute to their biological function. In addition, this also suggests that macrophages within our body must be able to recognize and clear such diverse bacteria. Cells like red blood cells possess unique biconcave shape and flexibility that enables them

to squeeze through tiny capillaries and any changes to these properties facilitates their clearance by macrophages upon aging[12]. Such examples have encouraged the design of synthetic particulates and the following sections illustrate the physico-chemical properties that have been explored in overcoming phagocytosis.

1.2   Size

Particles with sizes in the range of tens of nanometer to a few tens of microns have been studied actively for applications in drug delivery. Depending on the type of particle being made, numerous fabrication methods are being used including emulsion polymerization, microfabrication, self-assembly and jet breaking[13–16]. The processing parameters such as vortexing, sonication, stirring, nozzle diameter and flow rates, in addition to material and surfactant concentration play a prominent role in controlling the particle diameter[17]. The size of the particle in addition to other biophysical properties dictates *in vivo* functions such as circulation time, extravasation, internalization, targeting, clearance and uptake mechanism[18,19]. When introduced into the body intravenously, particles are cleared through varied mechanisms. Nanoparticles larger than 200 nm are cleared by the spleen through filtration where as those smaller than 100 nm have the ability to leave the blood vessels through fenestrations in the endothelial lining[20,21] The leaky vasculature in the case of tumors, can enable these particles to take advantage of the enhanced permeation and retention effect provided the heterogeneity in tumor vasculature is known[22,23]. Microparticles in the size range of 1-5 μm are cleared by phagocytic Kupffer cells in the liver or trapped in the capillary beds. In the case of pulmonary administration microparticles in the range 1-3 μm are desirable as they can travel deep into the lungs[24]. However, this size range is susceptible to phagocytosis by alveolar macrophages thereby

2

limiting their applicability. Overall, for many routes of administration, particles greater than 500 nm are cleared by macrophages which is highly undesirable for biomedical applications[25].

This has prompted numerous studies to examine the effect of size on phagocytosis. Phagocytosis of polystyrene particles by mouse peritoneal macrophages was reported to exhibit maximal phagocytosis for an intermediate particle size of 1.7 μm[6]. In another study, despite the heterogeneity of neutrophils their phagocytic ability was found to decrease with increasing size of polystyrene microparticles in the range 0.5-8 μm[26]. Though these studies identified the optimum phagocytic range, no clear mechanistic insight into the process was given. Polystyrene particles in the size range 2-3 μm exhibited maximal phagocytosis[7]. This was attributed to the membrane ruffles that enable this specific size recognition of the particle by the macrophage. In addition, this range coincides with the general size range of bacteria, further highlighting the role of biophysical attributes in pathogen recognition[27].

1.3 Shape

Various methods have been identified to produce diverse particle shapes, including mechanical stretching, soft lithography, microfluidics or self-assembly[28–33]. The local geometry of the particle at the point of attachment to the macrophages was established to dictate the outcome of phagocytosis[8]. It was shown that when a macrophage approached an opsonized polystyrene (PS) elliptical disc at its pointed end, internalization took place in a few minutes. Conversely, a macrophage attached to the flat region of the particle was not successful in internalizing even after 12 hours. In an extension of this study, high aspect ratio PS worms were prepared with the aim of minimizing local curvature and avoiding

uptake by macrophages[34]. Owing to the minimized curvature, these worms exhibited 6 times lower internalization than spheres of the same volume. Studies have elucidated that the shape of a particle can influence attachment to and internalization by a macrophage independently [35]. PS prolate ellipsoids have been shown to achieve maximum attachment compared to spheres and oblate ellipsoids. However, oblate ellipsoids exhibited higher internalization when compared to these two shapes. In another study, antibody-displaying micro-rods were shown to exhibit higher attachment and uptake compared to spheres in breast cancer cells[36].

In line with the prior *in vitro* studies, long and flexible diblock copolymers composed of poly(ethylene oxide)-b-poly(ε-caprolactone) filomicelles evaded the reticuloendothelial system and persisted longer in circulation compared to spheres *in vivo*[37]. The same group found that prolonged circulating filomicelles loaded with drug paclitaxel can penetrate into the tumor stroma and produce greater and more sustained tumor shrinkage and tumor cell apoptosis[38]. Discoidal silicon particles were also shown to exhibit unique tumbling and margination dynamics that enhanced their interaction with vessel walls than spherical particles[39]. These studies highlight that the shape of a particle is another essential property that plays an important role in particle adhesion, distribution and cell internalization.

1.4   Surface Chemistry

The major limitation of micro and nanoparticles is their inability to reach the diseased sites at therapeutically relevant doses owing to nonspecific uptake by the cells of the reticuloendothelial system; macrophages[5,40]. This nonspecific process is initiated by the

4

opsonization of proteins on the surface of the particles, involving plasma proteins such as serum albumin, apolipoproteins, complement components and immunoglobulins. This adsorption is dependent upon the particle surface charge, surface chemistry and size. Not only does opsonization enhance uptake by macrophages it is also detrimental to active targeting motifs present on the surface that often get masked by the adsorbed protein corona. Thus tuning the surface chemistry is critical to avoid opsonization and macrophage uptake and enhance the ability to retain targeting to diseased cells.

The surface charge of the particle is known to influence the outcome of phagocytic process[41]. Particles that are neutral in charge at physiologically pH avoid recognition by macrophages while those with high positive or negative charge are recognized by these cells. Another aspect that contributes to recognition by macrophages is particle hydrophobicity. Hydrophobic particles are preferentially coated by opsonins such as immunoglobulin, complement, albumin that aide in clearance of these particles by macrophages[42,43]. Therefore, hydrophilic coatings on particles is a common approach to delay such a recognition. PEGylation is the most common method to delay opsonization and increase the circulation time of particles[44]. However, of late there is growing evidence of generation of anti-polyethylene glycol (PEG) antibodies in the body in response to these materials[45,46]. Alternative zwitterionic polymers such as poly(phosphorylcholine), poly(sulfobetaine), and poly(carboxybetaine) have been observed to delay protein adsorption and enhance the circulation times when coated on particles[47]. In addition to synthetic polymers, biomimetic stealth coatings utilize mechanisms from cells to avoid phagocytic uptake. Cell mimics have been created by using cellular membranes to cloak nanoparticles[48–50]. These particles have the physical properties of the underlying synthetic

5

nanomaterial but the native membrane surface enables them to avoid opsonization, delay uptake by mononuclear phagocyte system, have long circulation times, bind to target cells and deliver a therapeutic load. Another approach is to use specific ligands to target particular cell receptors. Self-ligands such as, CD47 signal macrophages not to internalize cells that present this molecule on their surface. Peptides from CD47 were computationally designed and immobilized on the surface of nanoparticles[51]. These peptides substantially prolonged particle circulation by delaying phagocytic clearance. On the other hand, ligands such as immunoglobulin G (IgG) when displayed on particles can be used to enhance recognition and uptake by macrophages through interactions with the Fc receptor[7,9,52]. These studies highlight the role of surface chemistry and functionality in tuning interactions with macrophages.

1.5 Stiffness

Particle stiffness is an emerging physical property of particles. Its role in influencing cellular interactions is still unclear and depends on the materials, cells and range of stiffness. For the case of immune cells and macrophages, several studies have shown that hard particles are internalized more than soft particles. Soft poly (l-glutamic acid)-CpG capsules (800 nm) associated less with plasmacytoid dendritic cells than hard capsules[53]. Similar results were observed in the case of tannic acid/poly(vinylpyrrolidone) (TA/PVPON) soft cubical and spherical capsules[54], PEG hydrogel spheres[55], polyacrylamide spheres[9], and polylactic-co-glycolic acid (PLGA) -PEG lipid disks[56]. However, in another study, N,N-diethyl acrylamide and 2-hydroxyethyl methacrylate hydrogel particles (~170 nm) of intermediate elasticity were internalized more than those at either extreme[57]. For the case of cancer cells, softest hyaluronic acid capsules (2.4 µm)

exhibited highest association, both internalization and attachment by HeLa cells, compared to stiff capsules of similar size[58]. Similar results were observed in the case of dextran sulfate sodium salt and poly-L-arginine hydrochloride or poly(sodium 4-styrenesulfonate) and poly(allylamine hydrochloride) based capsules (sizes 4.1 and 4.7 μm), where soft capsules were internalized and transported to lysosomes faster than hard capsules in HeLa cells[59]. On the other hand, for PEG hydrogel bare or ICAM-1 functionalized spheres (200 nm) hard particles were internalized more than soft particles of similar size by 4T1 breast cancer cells[55]. From these cases it is clear that stiffness plays a complex role in cellular interactions and that it may be highly dependent on the cell type and the other properties of the particles being studied, such as size, chemistry or shape.

1.6   Layer-by-layer engineered capsules

Layer-by-layer (LbL) technique has the ability to tune particle properties based on the choice of polyelectrolyes, their properties and the interaction between the polyelectrolytes involved [60]. This method can form multilayer capsules after the deposition of polyelectrolytes on the surface of colloidal template particles, followed by removal of the sacrificial template. These capsules retain the size and shape of their template due to interactions between the polyelectrolyte layers such as electrostatic interactions[61], hydrogen bonding[62], hydrophobic interactions[63] and covalent coupling[64].   Another attractive feature of the method is its ability to incorporate a wide range of molecules such as organic dyes, quantum dots, biologically active molecules, electroactive polymers[65,66]. This flexibility in choice of template, interactions and materials to be assembled has been beneficial for drug delivery applications. The modular nature enables incorporation of biologics like proteins, peptides and nucleic acids into the intermediate layers. This is

particularly advantageous considering the high loadings achieved by this process through charge compensation of the material. In addition, the outermost layer of the assembly can be chemically modified to impart functionalities that can be useful in targeting or provide stealth properties for systemic delivery in the blood stream. This versatility in properties and function is difficult to achieve in traditional polymeric particles. Thus, this modular technique is promising in developing multifunctional capsules for a wide range of diseases based on the choice of templates and type of interactions.

The templates for capsule formation through LbL, can be broadly classified into hard or soft templates. Inorganic particles made from $CaCO_3$ [67], silica[64], gold[68] are commonly used hard materials in LbL applications. Soft templates are made from organic particles such as PS or PLGA. In addition to particles, LbL has also been performed on red blood cells and *E.Coli*.[69,70] The diversity of templates and the choice of coating materials has given rise to wide variety of LbL multilayered particles of different shapes, sizes and chemical composition. However, one is often restricted to choose between the size and shape of template that is readily available.

In addition to template choice, the type of interaction driving the formation of these capsules affects the final properties and applications of the capsules. Capsules made from hydrogen bonding interactions enables creation of different chemical composition of multilayers different from the traditionally used electrostatic interactions[60]. Single component capsule shells can be made by simple disruption of hydrogen bonding and removal of one of the polyelectrolytes. The ability to cross link such capsules can impart stability with pH dependence[64]. In addition, shells responsive to different environmental pH can be produced based on the choice of the polyelectrolyte combination[71]. The

intermolecular hydrogen bonding can also be used to alter the mechanical properties of the shell. For the case of (poly(methacrylic acid) /PVPON-co-NH$_2$)$_7$, the shell stiffness was altered based on the pH the multilayer was exposed to[71]. Similarly in the case of TA/ PVPON capsules, hydrogen bonding between the layers of capsules was also shown to substantially reduce elasticity in comparison to traditional LbL capsules based on electrostatic interaction[72].

Overall, LbL is a versatile technique that enables control of the physico-chemical properties of particles and can be used to understand particle interactions with cells. The influence of shape of capsules has been investigated though the trends are not clear. In the case of poly(methacrylic acid) (PMA) capsules with HeLa cells, spherical capsules were internalized more than rod shaped capsules[73]. In another study, bowl-like bovine serum albumin coated (BSA) poly-(allylamine hydrochloride)/poly-(styrenesulfonate) (PAH/PSS) capsules were found to mainly attach to cells from the convex-side and were subsequently internalized. It was hypothesized that less energy expenditure is required for membrane deformation in this geometry and that facilitates enhanced uptake of these capsules over spherical shapes[74]. Bio-inspired red blood cell discoid PMA capsule particles exhibited lower internalization compared to their spherical counterparts in endothelial, breast cancer and macrophage cells[75]. The elasticity of LbL capsules has also been observed to affect interactions with cells, though in a cell type specific manner. Soft poly (l-glutamic acid)-CpG spherical capsules (800 nm) associated less with plasmacytoid dendritic cells than hard capsules[53]. In the case of, (TA/PVPON) soft cubical and spherical capsules exhibited lower internalization when compared to their stiffer counterparts with macrophage cells [54]. The contrary trend is observed in the case of cancer cells, where soft

particles are internalized more than hard particles. This was the case for hyaluronic acid spherical capsules (2.4 µm) [58], dextran sulfate sodium salt and poly-L-arginine hydrochloride (4.1 µm), and poly(sodium 4-styrenesulfonate) and poly(allylamine hydrochloride) (4.7 µm) based spherical capsules[59].

In addition to understanding the role of particle-cell interactions, LbL engineered capsules are developing novel immunotherapies. Ovalbumin (OVA) containing PMA_{SH} capsules were internalized by antigen presenting cells resulting in presentation of OVA epitopes and subsequent activation of OVA-specific CD4 and CD8 T cells *in vitro*[76]. These capsules were further shown to exhibit at least 6-fold greater proliferation of OVA-specific CD8 T cells and 70-fold greater proliferation of OVA-specific CD4 T cells *in vivo* compared to the equivalent amount of soluble OVA, which could be beneficial for vaccination. LbL capsules have also been constructed entirely from immunologically active adjuvant and antigen polymers in order to simultaneously deliver both[77]. Sacrificial gold nanoparticles were functionalized by the deposition of the anionic adjuvant polyinosinic–polycytidylic acid (polyIC) and a cationic version of the SIINFEKL model peptide antigen. *In vitro*, this vaccine was able to induce dendritic cell maturation and antigen-specific $CD8^+$ T cell proliferation in a co-culture experiment, matching the activity of the free adjuvant/antigen pair. However, intradermal injection of this vaccine into mice was able to promote 5-fold stronger antigen-specific $CD8^+$ T cell proliferation than that of freely administered polyIC and antigen. These promising studies highlight the applicability of LbL method in immunotherapy. Additionally, targeting ligands can be incorporated to enhance interactions with specific cells of interest. LbL technique confers a high degree of

modularity, versatility and compositional heterogeneity to particles and has the potential to provide a unique platform to contribute to immuno-engineering.

1.7   Design strategies to tune cell responses

Immuno-engineering is an emerging field that seeks to understand and manipulate the immune system. Fundamental knowledge of the immune system is necessary to create molecules, materials, and strategies that can alter immune responses in a disease setting. In such a setting, immune responses in the body are initiated between cells, cell and infectious agent, or cell and endogenous molecules. During infection, pathogens activate the innate components of the immune system that help in controlling the infection. When the infection is not contained, an adaptive immune response is initiated. During such immune responses, contact based interfaces are often formed between immune cells including antigen presenting cells (APCs), B cells, T cells and phagocytes[78]. This interface sustains contact dependent receptor engagement, polarization of molecules in partner cells, and confined release of secreted products to partner cells[79]. Contact independent mechanisms also contribute to the stimulation or suppression of cells through secretion of signaling molecules by the source cells. This indicates that cell based interactions provide opportunities to direct immune responses.

Native and synthetic particulates can be engineered to achieve such responses through the formation of new immune-material interfaces. Native materials, such as extracellular vesicles, are an emerging class of materials ripe for engineering. These particles contain immune-active molecules and also display functional surface molecules that can be used for targeting and interacting with cells[80]. Synthetic particulates like

11

biomimetic materials are inspired from nature to recapitulate a natural immune function. These particulates are capable of interacting with cells and eliciting specific cellular responses by manipulating parameters such as geometry, presentation of ligands, and incorporation of adjuvants. In addition to replication of natural function, inherent material properties can also achieve a desired function. A wide variety of materials including solid polymer particles, liposomes, polymer micelles, gold, carbon materials, silicon oxide are also being used for biological applications. A major drawback of inorganic materials based particulates is their biodegradability[81]. Though natural particulates and biomimicry are valuable tools, the ability to create designer molecules with novel combinations of functions can access signaling and interactions that are not possible otherwise. These synthetic molecules may be more cost effective with advantages of precise control, enabling highly specific and tunable interactions with targets. The following sections deal with the design strategies of synthetic particles and the role of their inherent properties to tune cellular responses.

1.7.1 Biomimetic materials

Biomimetic strategies are ways to recreate interactions of cells with other cells, pathogens or molecules with the ability to tune the degree of complexity. This involves understanding key features of cellular communication such as antigenic components, cell entry mechanisms, surface ligands, and tolerization. This section highlights biomimetic particle strategies based on these features. Some designs seek to recapitulate the structure and chemistry of cell-cell, cell-particle, or cell-molecule interactions, with the hypothesis that function will follow structure. Other approaches are inspired by the natural function but design to achieve function directly, not necessarily with the same structure used in the

native system. In the examples below a wide range of particle physicochemical properties are used to elicit desired immune responses.

1.7.1.1   Cell Mimics

Cell mimics are created by using cellular membranes to cloak nanoparticles or preparing cell ghosts through a combination of hypotonic treatment and extrusion processes[50,82]. Extraction of cellular membranes has been incorporated in various applications. Cellular membranes contain diverse antigenic profiles and specific surface molecules that enable targeting. These membranes can be utilized to alter immune responses by their incorporation on nanoparticles (NPs). Cancer cell membrane coated NPs retain their membrane bound tumor antigens[82]. These particles, in combination with an adjuvant, were shown to induce anti-cancer immune responses such as stimulation of cytotoxic T lymphocyte (CTLs). Moreover, these coated particles were shown to use the homotypic binding mechanism, by which adhesive domains on tumor cells form multicellular aggregates, and target cancer cells *in vitro*.

Membrane isolation and cloaking was further extended to red blood cells (RBCs). In autoimmune diseases such as type II, type III, and type IV immune hypersensitivity, autoantibodies against RBC membrane components are produced in the body[49]. Nanoparticles that present natural RBC membrane and its associated surface antigens that are involved in antibody-mediated RBC clearance were prepared. RBC cloaked nanoparticles were shown to intercept the autoreactive antibodies of type II immune hypersensitivity reaction. These particles acted as 'antibody decoys' that bind to anti-RBC antibodies, protecting circulating RBCs. In another application, nanosponges made of RBC

membrane coated nanoparticles provided a platform to absorb pore- forming toxins that are common in bacterial infections and lyse host RBCs[83].

In contrast, "un-natural killer cell" mimics were made by functionalizing leukocytes with liposomes presenting E- selectin (ES) and TNF related apoptosis inducing ligand (TRAIL)[84]. ES and TRAIL are often used to target cancerous cells, and natural killer (NK) cells that take part in immunosurveillance present TRAIL on their surfaces. ES and TRAIL coated liposomes that mimic NK cells bound leukocytes via selectins on the cell surface under shear flow conditions. These liposomes induced apoptosis of circulating cancer cells in mice. The high compressive force experienced by the cancer cell upon collision with the liposome functionalized leukocytes induced flattening and binding of ligands on the cell surfaces.

Similarly, membrane receptors were immobilized on an artificial, cell-like protocell to prevent infection. Protocells bearing the entry receptor of henipavirus in lipid bilayers were supported on silica particles[85]. The protocells specifically and renewably inactivated henipavirus envelope glycoprotein pseudovirus particles. A protein, Ephrin-B2, on the surface of the particle allowed fusion of the viral envelope with the protocell. The protocells were hypothesized to disarm the virus by deactivating a protein that causes the virus to enter the cell. Such biomimetic combination approaches, containing both antigenic information and natural surface properties of cells, could lead to new therapeutics for disease intervention.

In another application, biomimetic leuko-polymersomes were assembled from block co-polymers and functionalized with sialyl Lewis X (selectin) and an antibody against

intercellular adhesion molecule 1 (ICAM-1, integrin)[86]. These polymersomes bound exclusively to inflamed HUVECs. By optimizing the ratios of selectin and integrin receptor mimics on the surface of the polymersomes, selective binding to inflamed sites and mimicry of leukocyte adhesion was achieved. These can be used to selectively target sites of inflammation and has applications in imaging and drug delivery.

Cell mimetic nanoparticles produced through membrane coating recreate the cellular interface to enable complex cellular processes initiated at the membrane. These particles have the physical properties of the underlying synthetic nanomaterial and are able to avoid opsonization, delay uptake by mononuclear phagocyte system, have long circulation times, bind to target cells and deliver a therapeutic load[48–50]. In addition to the above-mentioned applications this technique is also being extended to develop vaccines for bacterial infections[87]. The prospects of this membrane coating application are exciting but the scaling of this technique and immunogenicity needs to be addressed. Synthetic versions can address the issue of scalability but *in vivo* testing of these still needs to be pursued.

1.7.1.2   Pathogen Mimicking

Pathogens such as bacteria and viruses evade and manipulate the immune system to induce favorable interactions with target cells. Particulate forms of antigen and co-delivery of danger signals and antigen have been identified as critical parameters for pathogen mimics for vaccine development. Nanoparticles composed of multilamellar lipid vesicles with antigen entrapped and expressed on the surface were shown to elicit a strong humoral response[88]. This strong response was attributed to the formation of germinal B

cell centers near the NP depot that facilitated B cell responses. In addition, activation of follicular T cells supported the induction of strong humoral response.

In another study, polyelectrolyte multilayer capsules composed of dextran sulfate and poly-L-arginine with surface-bound CpG adjuvant were engineered to mimic pathogens[89]. These CpG coated and OVA encapsulated capsules induced antibody, Th1 and CTL responses. In a similar approach, malaria antigenic tri-epitope peptide incorporated on a polypeptide layer-by-layer microparticle was shown to induce neutralizing antibodies and malaria-specific T cell responses *in vivo*[90]. These examples suggest understanding the synergistic effect of various pathogen structures and composition can enhance the effectiveness of vaccines. Lipid enveloped PLGA micro and nanoparticles modified with adjuvants monophosphoryl lipid A (MPLA) and α-galactosylceramide in the layers and OVA antigen on the surface were created to mimic pathogens[91]. These particles were shown to elicit strong immune responses such as antibody titers and $CD8^+$ T cell stimulation at doses lower than conventional doses of alum or protein-adjuvant solutions.

In another study, the effect of shape on antigen presentation on PS particles was investigated. Ovalbumin conjugated rod shaped polystyrene particles were shown to induce a Th2 type immune response against ovalbumin while their spherical counterparts induced a Th1 type response *in vivo*[92]. In another study, mannose functionalized poly(DL-lactide)-b-poly-(acrylic acid) long cylindrical nanoparticle induced inflammatory response in macrophages by the production of IL-6, stronger than spherical or short cylindrical nanoparticle[93]. These examples suggest the ability of immune cells to respond differentially to biological signals when biophysical attributes of presentation are altered. These studies

16

emphasize the need to explore the design strategy of ligand presentation on particulates for eliciting an immune response.

1.7.1.3   Artificial Antigen Presentation

Artificial antigen presenting cells (aAPCs) can be used for both adoptive and active immunotherapy. These aAPCs should be able to create a physical interface with T cells to present antigen, co-stimulatory factors, and stimulate cytokine release[94]. aAPCs can activate and expand T cells *ex vivo* which are then adoptively transferred into a patient[95,96]. They can also be injected *in vivo* to achieve T cell activation. RAFTsomes are liposomes derived from enriched major histocompatibility complex (MHC) class II lipid rafts of membranes from DCs that were stimulated with antigens[97]. They elicit CD4$^+$ T cell priming, antibody production, and antigen specific responses *in vivo*. This shows that membrane microdomains enriched in MHC-peptide complexes alone, without co-stimulatory factors, can achieve an immune response.

PS bead aAPCs have been functionalized with MHC class I tetramers and co-stimulatory molecules[98]. When coupled with melanoma associated self-antigen and injected intravenously and subcutaneously, they elicited specific CTL responses and delayed tumor progression in a melanoma model of naïve and antigen-primed mice. However, biosafety and organ toxicity is a concern with these systems.

Nanoscale iron-dextran and quantum dot particles coupled with MHC-Ig dimers and anti-CD28, were effective in T cell stimulation[99]. These nanoparticles induced antigen specific T cell responses *in vitro* and anti-tumor activity *in vivo*. This was attributed to the use of MHC-Ig dimers with a flexible hinge region and the ability of MHC-dimers to enhance TCR and MHC interactions. Unlike micro aAPCs, these nano-aAPCs were shown

to localize in the lymph nodes and distribute away from the injection site. In an extension of this study, these iron- dextran paramagnetic nano-aAPC were shown to facilitate magnetic-field induced T cell activation[100]. The magnetic field caused aggregation of these paramagnetic aAPC, which was associated with increased T cell receptor (TCR) clusters and T cell activation *in vitro*. This technique was suitable to activate naïve T cells, antigen-specific T cells and such activated T cells were shown to inhibit tumor growth in a melanoma adoptive immunotherapy *in vivo* model. These studies are the first demonstration of nanoscale aAPC particles with applications in adoptive immunotherapy through magnetic-field induced nano-aAPC based antigen specific T cell expansion.

Janus particles have also been used as aAPCs to activate T cells. Micron-sized silica particles with a "bull's eye" pattern, that resembles the immunological synapse were fabricated[101]. Anti-CD3 was enriched in the central domain and surrounded by fibronectin molecules for adhesion to mimic the native pattern. A reversed pattern with fibronectin as a central domain surrounded by anti-CD3 was also fabricated. The reverse "bull's eye" pattern enhanced polyclonal T cell activation over the native "bull's eye", which performed slightly better than particles coated with fibronectin. This enhanced activation was attributed to a combination of spatial organization and increased surface coverage by anti-CD3.

While Janus particles with the "bull's eye" pattern captured the importance of ligand spatial organization to enhance interactions between aAPCs and T cells, geometry of aAPCs has also been identified as a crucial parameter for such interactions. Ellipsoidal aAPCs displaying MHC-Ig dimers and anti-CD28 were shown to activate CD8+ T cells *in vitro* better than spherical aAPCs[102]. This improved activation was demonstrated to be

dependent on the shape of aAPCs and not differences in the density of the ligands on the surface. These ellipsoidal aAPCs were effective in increasing the survival of mice compared to spherical aAPCs in a subcutaneous melanoma tumor model.

The previous aAPC systems primarily incorporate antigen recognition and co-stimulation but not cytokine release. PLGA micro-aAPCs with peptide-MHC, co-stimulatory ligands and encapsulated IL-2 were fabricated to replicate all the key features of APCs[103]. CD4$^+$ and CD8$^+$ T cells were stimulated to a greater extent when co-cultured with these aAPCs than aAPCs that lack encapsulated IL-2 but were supplemented with the cytokine exogenously. Paracrine delivery of IL-2 upon aAPC contact with T-cell resulted in increased accumulation of synaptic IL-2 and increased proliferation of CD8$^+$ T cells *in vitro* than exogenous administration of IL-2. Furthermore, these T cell responses were found to be dependent on the sustained release of the cytokine and proximity between aAPCs and T cells.

aAPCs can also be used to activate T cells with chimeric antigen receptors (CARs). Adoptive transfer of T cells with CARs that recognize specific tumor antigens has been shown to be effective in tumor immunotherapy[104]. However, this method requires aAPCs to be tuned to the specific antigen recognized by CARs. A universal aAPC was developed with K562 lymphoblast cells expressing a ligand directed towards a conserved extracellular domain on CARs[105]. This contributed towards activation of CAR modified T cells, independent of their antigen specificity, but preserved their antigen specificity. These strategies and design parameters provide insight for the development of targeted therapies that circumvent the need for natural APCs to initiate immune responses.

1.7.1.4   Specific Ligand Immobilization

APCs present antigen to T cells within an immunological synapse that forms between the two cells. Adhesion molecules on these cells aid in the formation of this synapse[106]. Synthetic peptides LABL and cIBR have been developed to bind receptors ICAM-1 and lymphocyte function associated antigen (LFA-1) on DCs and T cells, respectively[107]. Functionalization of LABL peptides on NP inhibited binding of T cells to DCs through blockade of ICAM-1. Similarly, cIBR-NP pre-treated T cells interacted with DCs to a lesser extent than untreated T cells. These peptide-functionalized nanoparticles can be used to interfere with the maturation of DCs or T cell expansion.

T cells expand when activated with antigen and co-stimulatory signals. Activation of T cells is mediated through the TCR-CD3 complex. On naïve T cells, TCRs are present in nanoclusters on the cell surface that oligomerize into microclusters upon activation[108]. Anti-CD3 functionalized quantum dots exploited this difference in TCR clustering to selectively activate antigen-experienced T cells. The sensitivity of TCR clusters in antigen-experienced cells is greater than naïve T cells, which initiates this response. These nanoparticles enhanced antigen-specific T cell responses *in vivo* and exhibited increased recall response upon challenge. This strategy could also be extended to other clustered receptors such as CD20 on B cells.

CD200R is expressed on immune cells and is an inhibitory immune receptor. It associates with its ligand CD200, a known immune-modulatory protein[109]. CD200 functionalized 28 μm polystyrene microbeads bound CD200R on macrophages and reduced activation and inflammatory cytokine release. These particles also reduced inflammation *in vivo*. This strategy could be applied to other types of biomaterials to reduce the foreign material immune response.

1.7.1.5   Tolerance Induction

Apoptotic cells and their debris are removed from the body by immune cells without activation of the immune system[110]. When these antigens are processed by APCs in the absence of an inflammatory signal, tolerance is induced. This processing is a key mechanism through which peripheral tolerance is maintained. Apoptotic protein/peptide antigens covalently coupled to splenocytes (Ag-SPs) were shown to induce antigen-specific T-cell tolerance[111]. Upon intravenous administration, Ag-SPs initiated IL-10 production by marginal zone (MZ) macrophages. IL-10 production was found to regulate the expression of programmed death ligand-1 (PD-L1) on MZ macrophages, which was critical for tolerance induction. Regulatory (Treg) cell induction was also confirmed. In a recent Phase I clinical trial for multiple sclerosis, myelin peptide antigens were coupled to autologous peripheral blood mononuclear cells[112]. A reduction in myelin-specific autoreactive T cell response was observed.

A modular biomolecular approach was developed to induce immunological tolerance by exploiting apoptotic cell carriers. A targeted antigen that binds to the protein glycophorin-A on the surface of mouse erythrocytes was engineered[113]. This antigen induced anergy when processed by APCs following erythrocyte-apoptosis. In a mouse model of autoimmune diabetes, deletion of autoreactive T cells was achieved when β-cell antigen was bound to erythrocytes through a designed antibody construct. This technique could also be applied to other antigens for tolerization.

Particle based tolerogenic approaches are also being pursued to take advantage of their large-scale fabrication. Encephalitogenic antigen peptide covalently coupled to

polystyrene or biodegradable PLGA microparticles, was shown to induce T cell tolerance in a mouse model of experimental autoimmune encephalomyelitis[114]. MZ macrophages internalized these particles through scavenger receptor, macrophage receptor with collagenous structure (MARCO), and played a key role in regulating the response. This tolerance induction depended both on T cell anergy and activity of Tregs. In a related approach, iron oxide nanoparticles were coated with different peptide-MHC complexes to blunt the polyspecific autoimmune responses in a type 1 diabetes model[115]. Nanoparticles coated with disease-relevant peptide-MHC complexes were also shown to expand cognate "autoregulatory" T cells. This antigen experienced CD8+ autoreactive T cells were found to suppress the activation and recruitment of other non-cognate specificities. This technique can be extended to other diseases by incorporating relevant antigen.

Extending the particle strategy, synthetic nanoparticles encapsulating protein or peptide antigens and tolerogenic immunomodulator rapamycin were shown to induce tolerance towards the antigen[116]. These nanoparticles were effective in models such as allergic hypersensitivity disorder, multiple sclerosis, and hemophilia A. Rapamycin has been established to induce tolerance even in the presence of inflammation. Similarly, these nanoparticles retained their tolerogenic potential even when co-administered in the presence of antigen and TLR agonists. This technique can address the issue of anaphylaxis, where antigen administration during inflammation often leads to disease exacerbation.

A biodegradable PLGA nanoparticle platform was developed by an emulsion process using poly (ethylene-co-maleic acid) as a surfactant[117]. These particles were investigated for their ability to couple to antigen, and safety and protection in a mouse multiple sclerosis model. The incorporation of the surfactant into the PLGA particle

synthesis was shown to mitigate the disease, relapses and minimize epitope spreading during intravenous administration. These particles had superior performance than commercially available nanoparticles but the mechanism has not yet been established. These antigen-coupled particles were demonstrated to be safe and not induce an anaphylactic reaction. This biodegradable nanoparticle platform can be extended to other diseases by changing the antigenic epitopes.

Biomimetic materials take advantage of the physicochemical properties of nano and micro materials. The nanomaterials, owing to their size, can enable targeting of specific cell types such as those in the lymph nodes[118]. These materials can also be tuned to mimic cells or pathogens while retaining a key advantage of synthetic materials, mass production. They represent an exciting area where engineering principles can be applied to biologically inspired design to achieve immunologically active materials.

1.7.2 Material properties control immune cell responses

While immune engineering of synthetic materials through biomimicry is an active area of research, there is growing evidence of materials having intrinsic properties that influence immune responses. Inflammatory responses in immune cells are initiated by particulate matter like PLGA[119], gold[120] , aluminium[121] and mesoporous silica rods (MSR)[122] through the activation of inflammasome. The choice of the material and their physicochemical attributes seem to contribute to such activation. The surface curvature or texture of polystyrene-block-poly(ethylene oxide) microparticles was also shown as a contributing factor in activation of inflammasome in immune cells[123]. A combination of shape and hydroxyl surface chemistry was shown to cause inflammatory responses in the case of aluminium based particles[121]. Properties like shape are also critical in the activation

of inflammasome; rod shape was more effective than cubical or spherical virus functionalized gold nanoparticles[120].These studies suggest that not only do material properties alone or in combination with other biological molecules influence immune cell responses.

Shape of the particle can also lead to inflammatory responses in immune cells [124]. Rod shaped particles were shown to stimulate macrophages more than spherical shaped PMA polyelectrolyte capsules. While the mechanism in this case is not yet clear it can be through altered processing of these shaped particles by cells upon uptake. Like shape, hydrophobicity of particles also contributes to activation of innate and adaptive immune responses. Tuning the hydrophobicity of antigen encapsulated poly(glutamic acid) correlated with immune cell activation and cellular immunity *in vivo*[125]. In another study, hydrophobicity of gold nanoparticles was shown to activate immune cells *in vitro* and influence innate immune response *in vivo*[126].

Another way through which the innate immune system can be activated is through the complement system, and surface chemistry of particles plays a major role in this activation. Hydroxylated pluronic-stabilized poly)propylene sulfide) nanoparticles were shown to activate the complement system and induced a danger signal that drove dendritic cell maturation[127]. In addition, when conjugated with antigen on the surface these particles were shown to enhance cellular immunity. In an extension of this study, surface charge of the particles was shown to modulate the complement activation[128].

Another area where particle properties are being explored is for cytosolic delivery of antigens to facilitate cross-presentation. Acetalated dextran nanoparticles encapsulated with OVA were shown to enhance MHC-I presentation by an order of magnitude than

PLGA particles[129]. This was attributed to the tunable degradability of these particles in comparison to PLGA particles. Moreover, the degradability of these particles tuned the type of pathway for MHC-1 presentation. This study highlights how material properties can be explored to direct immunological processing and presentation.

Material properties can also contribute to the induction of autophagy that can be used to trigger an adaptive immune response. The induction of autophagy is an attractive mechanism particularly for diseases like cancer. Alumina nanoparticles conjugated with antigen and not metallic iron oxide nanoparticles were shown to utilize autophagy as a mechanism in dendritic cells to cross-present antigen to T cells *in vitro*[130]. These particles also promoted anti-tumor responses *in vivo* when conjugated to tumor antigen or tumor cell derived autophagosome. In another study, the surface functionalization of SWCT was being explored to induce autophagy[131]. Carboxylic acid functionalized SWCT were shown to induce autophagy in human lung adenocarcinoma cells. This surface functionalization was also shown to cause acute lung injury *in vivo*.

While the above examples illustrate the immunostimulatory properties of particles, their role in modulation is also being explored. The role of surface charge of polystyrene beads in modulation was highlighted in inflammatory disease models including colitis, peritonitis, and myocardial infarction[132]. It was established that negatively charged spherical particles without any specific antigen are engulfed by inflammatory monocytes, which then migrate to spleen resulting in their apoptosis and dampening of inflammation.

The above studies highlight the need to understand the reaction between a synthetic particle and the host system by characterization of relevant inflammatory mediators. This is critical especially when the particle is similar to pathogens in properties like size and

surface chemistry. While this replication in material properties is favorable for applications involving stimulation, it might have a counter effect in cases involving modulation.

As the field of immune-engineering grows, so will opportunities to manipulate immune interfaces with synthetic materials. Advances in understanding of immune cell function and signaling in health and disease will create new sources of bioinspiration and new ideas for therapeutic interventions. The exploration of intrinsic properties of synthetic materials will lead to new avenues in shaping immune responses. These will be coupled with improving chemical synthesis and molecular control, nano and microparticle fabrication, and practical scale up and production.

1.8   Motivations and Objectives

Most of the studies discussed in the previous sections have observed the effect of either one or two physical properties on cellular interactions. However, as particle synthesis techniques become more advanced, there can be interplay between more than two different physico-chemical properties on cellular interactions. A recent study has identified synergy between physical (shape), biological cue (antibody display) and route (cellular hitchhiking) for delivery to the lung endothelium[133]. It is thus crucial to be able to interrogate the role of properties size, shape, stiffness and chemistry independently in cellular interactions.

To understand specific and combined role of particle properties in tuning cellular interactions, each physico-chemical property (size, shape, stiffness, chemistry) needs to be tuned without affecting the others. This is a major drawback with current particulate fabrication techniques, including LbL. Moreover, as particle fabrication techniques advance to meet the growing need to develop complex particles for enhancing therapeutic

delivery, identification of the inter-dependence between multiple physical properties on cellular interactions is critical. Additionally, with the current LbL engineered particles one is restricted to choose from the size or shape combinations that are readily available. These limitations need to be addressed to endow polyelectrolyte capsule particles with controllable properties that can aide in tuning cellular interactions.

For the systematic fabrication of capsules using LbL, soft templates are attractive since independent manipulation of size and shape is possible[32]. Thus using soft templates could greatly increase the applicability of LbL to diverse shapes. However, capsules made using these templates suffer from severe aggregation issues during the centrifugation process and have incomplete template removal issues. Therefore, developing a LbL technique that addresses the issues with soft-template based capsule fabrication would have the ability to achieve independent control over particle properties- size and shape. The choice of the polyelectrolyte in combination with crosslinking chemistry during the LbL process can enable independent tuning of capsule stiffness. Thus, a modified LbL process on soft templates, is a promising solution to fabricate capsules with control over size, shape and stiffness that enable systematic investigation of the influence of physicochemical properties on cellular interactions. Further, such tunable particles will enable understanding the role of properties in influencing interactions when combined together. Additionally, it is crucial to understand the role of properties in affecting macrophage functions like cytokine production.

The objectives of this thesis are: (1) development of an LbL technique applicable to soft templates that enables independent control over the physical properties of size, shape and stiffness while keeping surface chemistry constant, (2) understand the interplay

27

between these physical properties in tuning macrophage interactions (3) application of the LbL technique to control surface chemistry for reduction of macrophage interactions (4) understand the role of geometric presentation of varying ligands through manipulation of particle shape on macrophage function.

1.9   Thesis Overview

To achieve these objectives a modified LbL technique was developed in Chapter 2 that is applicable to soft templates and overcomes aggregation issues common to soft template based LbL. In Chapter 3 this technique is adapted to enable independent control over each of the physical properties size, shape and stiffness while retaining the same surface chemistry. These engineered capsules are also employed in this chapter to investigate the role of the physical properties and interplay between them in macrophage interactions. In chapter 4, a modified LbL technique is presented that applies a zwitterionic polymer to impart stealth surface chemistry to particles for reduction of biological interactions. Chapter 5 combines active surface chemistries with particle shape and assesses their effect on macrophage interactions and inflammatory response. Finally, the work is summarized and an outlook is provided in Chapter 6.

CHAPTER 2.   FABRICATION OF CAPSULES THROUGH

MODIFIED LAYER BY LAYER TECHNIQUE

Particles are actively being used in biological applications such as drug delivery, vaccination to improve specificity or efficacy of drugs[134]. However, advances in the field have suggested that it is first critical to understand the role of physicochemical properties such as size[7,41,52], shape[34,35,135], surface chemistry[6,136,137] and stiffness[55,58,59] of the particles to achieve this. Hence tuning these properties to control biological behavior of particles is an active area of research. Polyelectrolyte capsules are a promising class of particles that have the ability to be tuned in each of these properties[134]. However, the major drawback with the current systems is their inability to tune these properties while keeping others constant.

To meet this challenge, we have fabricated novel polyelectrolyte capsules whose parameters size, shape can be independently controlled. In this chapter, these materials have been fabricated by combining soft organic templates created by the particle stretching method and a modified layer by layer (LBL) deposition process. The successful fabrication of these capsules is attributed to the weak hydrogen bonding and loose structure imparted to the capsules by this modified LbL method. In addition, the applicability of this method to generate diverse nano-scaled capsules is also highlighted.

2.1   Experimental section

2.1.1   Particle Preparation

Polystyrene (PS) particles were obtained from Polysciences. The shaped particle were fabricated based on a previously reported method[32]. In brief, 1 mL of 2.6 wt% PS spheres was combined with 9 mL polyvinyl alcohol (hydrolyzed degree 99+%, Mw 85-

124 kDa, 1 mg mL^{-1}, Sigma Aldrich) and dried in air to form a film with thickness of ~75 μm. The air-dried film was stretched in a hot oil bath maintained at 120°C. The stretch ratio was defined as the ratio of the length of stretched film to the length of the original film. The stretched film was allowed to cool to room temperature and dissolved in 70/30 v/v% water-isopropyl alcohol (BDH) at 65°C. The particles were centrifuged for 15 min at 1k, 10k, and 30k rcf for 3 μm, 500 nm and 200 nm particles, respectively using Allegra X-15R Centrifuge (Beckman Coulter). The particles were washed in this water-isopropyl alcohol 4 times and the particles were finally dispersed into 80% ethanol (Sigma- Aldrich).

2.1.2 Synthesis of PAA-FITC

Fluorescein isothiocyanate (FITC, Sigma Aldrich) was dissolved in dimethyl sulfoxide (DMSO, BDH) to 0.1 M. Polyacrylic acid (PAA, Mw ~100 kDa, Alfa Aesar) was dissolved in 80% DMSO to 0.1 M. 12 mg N-(3-dimethylaminopropyl)-N-ethylcarbodiimide (EDC, Thermo Scientific) was added to 3 mL PAA solution, 8 mg) N-hydroxysuccinimide (NHS, Sigma-Aldrich) was added after 10 min to this mixture. The reaction was allowed to proceed for 5 minutes after which 20 μL FITC solution was added. The reaction was carried out overnight after which the solution was dialyzed against 80% ethanol for 24 hours. The entire reaction and dialysis process was protected from light.

2.1.3 LbL Assembly on PS Particles and Capsule Fabrication

Layer-by-layer (LbL) on spherical and shaped particles was carried out in ethanol. Polyelectrolytes polyvinylpyrrolidone (PVP, Mw ~ 55 kDa, Alfa Aesar), branched polyethylenimine (PEI, Mw ~ 120 kDa, Alfa Aesar) and PAA were chosen to facilitate LbL on particles. The stock solutions of bPEI (5 mg/mL), PVP (5 mg/mL) and PAA (5 mg/mL) were prepared in 80% ethanol.

100 µL of a 2.6 wt% suspension of PS particles were dispersed in 4 mL 80% ethanol. To this suspension 1 mL of the first adsorbing solution (bPEI) was added, and adsorption was allowed to proceed for 10 min with sonication. Then particles were collected by centrifugation for 10 min (1k, 5k, and 10k rcf for 3 µm, 500 nm and 200 nm particles respectively). The supernatant was removed and the particles were washed two times by resuspending in 80% ethanol. Particles were further functionalized with other polyelectrolytes PAA, PAA-FITC, or PVPON using the procedure mentioned above with the same washing protocol. The final multilayer obtained on the particle is as follows: PS/PEI/(PAA/PVPON)$_{4.5}$.

For capsule fabrication, the layered particles were dissolved in 4 mL of tetrahydrofuran (THF, Alfa Aesar) for 2 min. The particles were centrifuged for 25 min (1k, 5k, and 8k rcf for 3 µm, 500 nm and 200 nm particles respectively). The supernatant was removed and the pellet was rinsed with THF 2 times, using 200 µL THF each time. Finally, the capsules were dispersed in water (500 µL).

2.1.4   FTIR Characterization of LbL assembly

PAA and PVPON samples were prepared from the stock solutions, and were dialyzed against water (pH ~ 3.0) overnight for FTIR. The solutions were freeze dried prior to testing. The PVPON/PAA films were prepared on glass substrate from the same conditions mentioned in the previous section by the typical LBL process. The formed multilayers were scratched off by a razor and dried under vacuum, PS particles, layered PS particles, and capsules were freeze dried (Millrock Bench Top Freeze Dryer) after fabrication. In order to avoid any interference from water, all the samples (particles or films) were kept in vacuum for at least 3 days before grinding with KBr for FTIR measurements.

2.1.5 Particle characterization

Particle size distribution was measured by dynamic light scattering using a Zetasizer Nano ZS90 (Malvern Instruments Ltd.). The samples were measured in water at 25°C and a scattering angle of 90°. Average particle size was calculated as the arithmetic mean of the distribution of at least three batches of particles. Zeta potential was determined by measuring the electrophoretic mobility of nanoparticles in water using the same instrument. FTIR spectra were obtained on a Bruker Vertex 70 FTIR spectrometer equipped with a DTGS detector. Transmission electron microscopy (TEM) was carried out on a JEM-2010 microscope operating at 100.0 kV. A Zeiss Axio Observer Inverted Microscope Z1 was used for fluorescence microscopy images. Scanning electron microscopy (SEM) images were taken on a JEOL JSM 5600LV scanning electron microscope operating at 15 kV.

2.2 Results and Discussion

2.2.1 Modified LbL for the fabrication of tunable capsules

Soft templates like polystyrene (PS), polylactic-co-glycolic acid (PLGA) offer the advantage of fabrication of particles of varying sizes and shapes with independent control unlike hard templates like calcium carbonate[32,138,139]. However, the major challenge in using soft templates to fabricate capsules is the aggregation of particles during LbL process when carried out in water, based on traditional electrostatic interactions between the polyelectrolytes. These particles are susceptible to aggregation during the collection step of this process due to the comparable densities of the soft templates and water. In addition, realizing capsule fabrication on the nano-scale based on electrostatic interactions is challenging due to increased surface energy for nano-sized particles.

In order to circumvent these issues, we explored the use of organic solvents. Mixtures of organic solvents with water has a lower dielectric constant than water effectively screening electrostatic interactions and thus enabling favorable multilayer interactions[140]. In addition, switching the solvent to organic solvent-mixture like 80% ethanol reduces the centrifugal force required to collect particles and thereby potentially avoiding aggregation. More importantly, the decreased surface energy of particles in ethanol, as compared to water, ensures re-dispersion of the particle pellet under slight sonication or shaking.

Polyacrylic acid (PAA) and polyvinylpyrrolidone (PVPON) were chosen as building blocks for capsule fabrication because of their good solubility in ethanol. Previously, hydrogen bonding based LbL has been executed in water or methanol between the proton donor of the COOH in PAA and the proton acceptor of C=O in PVPON[140–142]. However, the formation of hydrogen bonding between PAA and PVPON in ethanol considering its low polarity than water or methanol is unknown.

Hydrogen-bonding based LbL was executed in ethanol on carboxylated PS particles (diameter 3 μm and aspect ratio 1, $PS_{3\mu m-r1}$). The buildup of the layers was monitored by zeta-potential, which changed as a function of the charge of the end group in the depositing polyelectrolyte (Figure 2.1a). PEI was coated first on the PS particle to impart a high charge density critical for subsequent layer deposition. [53] The size dependence of the particle with each depositing layer was monitored. No size dependence on the number of depositing layers was observed confirming good dispersion and no aggregation during the LbL process (Figure 2.1b).
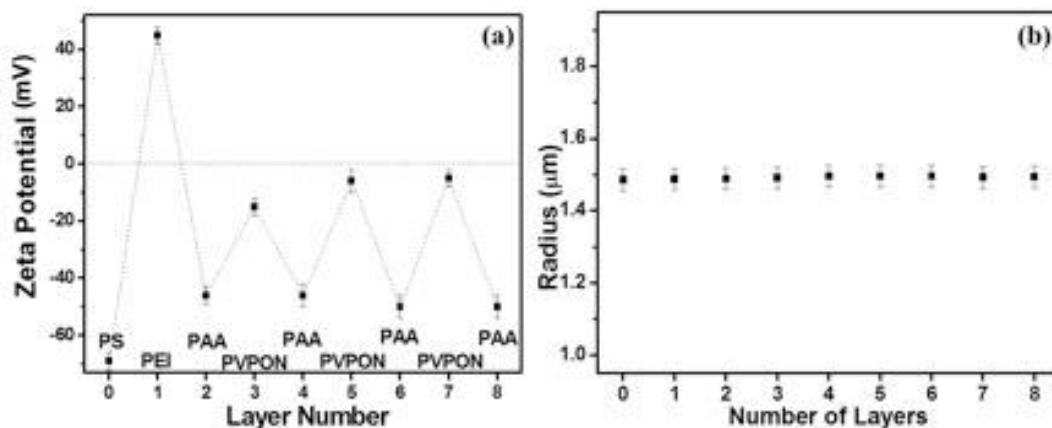
Figure 2.1. Zeta-potential and size characterization of layered particles. (a) The dependence of zeta-potential of PS$_{3\mu m\text{-}r0}$/PEI/(PAA/PVPON)$_{4.5}$ on the number of layers. (b) Particle size dependence on the number of polyelectrolyte layers as measured by dynamic light scattering. The values reported are the average of at least 3 batches and the error bars indicate standard deviation.

The final multilayered particles (PS$_{3\mu m\text{-}r1}$/PEI/(PAA/PVPON)$_{4.5}$) were incubated in THF to remove the PS core and form hollow capsules. The size of the capsules was measured, as shown in is similar to the layered particles but slightly larger, due to the swelling of the capsule wall[62]. The formation of hydrogen bonds between PAA and PVPON in ethanol was confirmed by Fourier transform infrared (FTIR) spectroscopy[142,143]. As shown in Figure 2.2b the peak centered at 1666 cm^{-1} in the top spectrum is assigned to the vibration of the carbonyl groups in PVPON, while the peak centered at 1714 cm^{-1} in the middle spectrum is attributed to the vibration of the carbonyl function of PAA carboxylic acid groups in the associated state. Compared to the spectra of pure polyelectrolytes, the carbonyl vibration of PAA in the film shifted to a higher wavelength number, 1728 cm^{-1}, revealing that the carbonyl group is in a less-associated state than in pure PAA. Meanwhile the carbonyl vibration of PVPON in the film shifted lower, with the center at 1652 cm^{-1}. These data demonstrate that hydrogen bonding between PAA and PVPON is the driving force for the film growth[140,142].

34
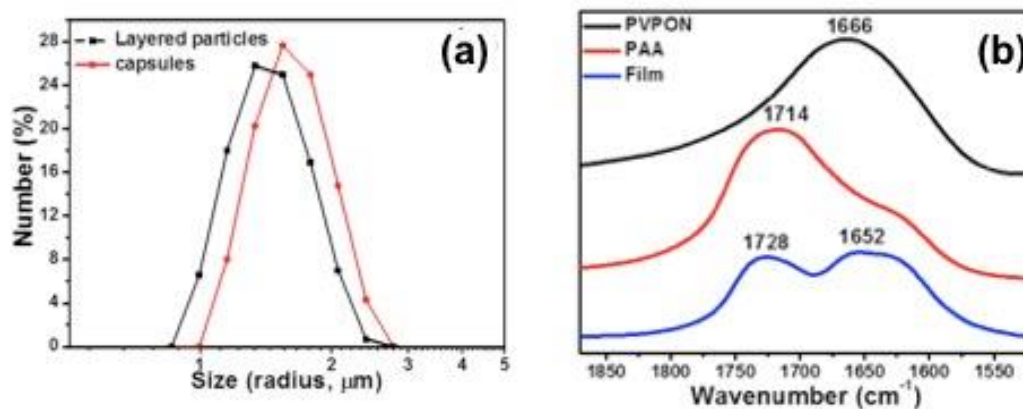
Figure 2.2. Size distribution and FTIR characterization of capsules. (a) Size distributions of layered particles (PS$_{3\mu m\text{-}r1}$/PEI/(PAA/PVPON)$_{4.5}$, black line), and capsules after removal of the PS template (PEI/(PAA/PVPON)$_{4.5}$, red line), (b) FTIR spectra of pure PVPON (top, black), PAA (middle, red) and LBL PAA/PVPON films (bottom, blue) prepared in ethanol.

Fluorescent capsules were also prepared using the same technique by functionalizing PAA with FITC. Fluorescent microscopy images indicate the ability of the capsules to retain the template shape, confirm their dispersability and the absence of any aggregation (Figure 2.3a). Conversely, serious aggregation was observed when the same particles were fabricated in water (Figure 2.3b). We hypothesize that good dispersion was mainly due to the lower surface energy and lower density of ethanol. The lower density reduced the centrifugal force from 6000g in water to 1000g in ethanol enabling control of aggregation during the LbL process.
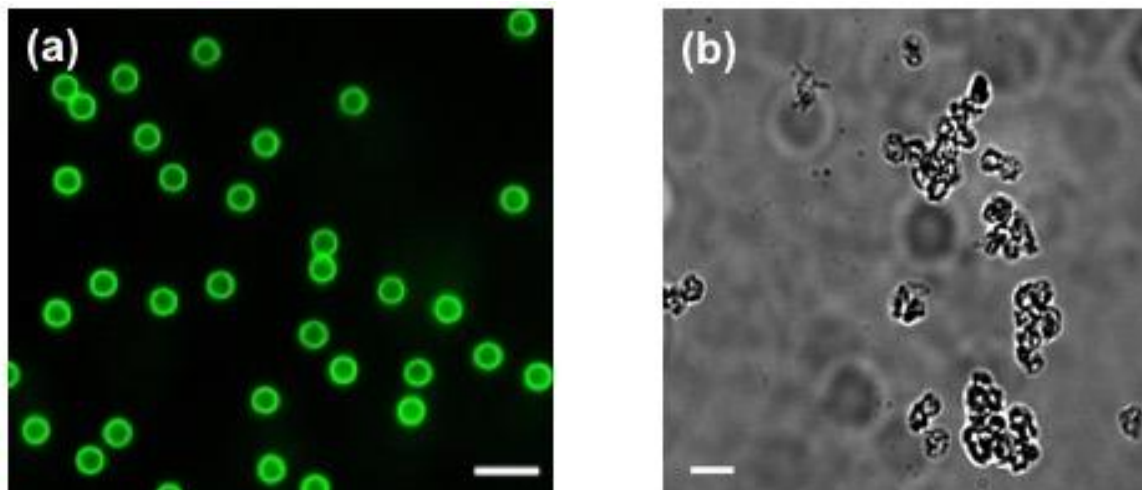
Figure 2.3. Capsule images after LbL process. (a) Fluorescent image of the capsules PEI/(PAA-F/PVPON)$_{4.5}$ fabricated with ethanol as solvent. Scale bar is 5 μm. (b) Optical image of the capsules, PEI/(PAA-F/PVPON)$_{4.5}$ fabricated with water as solvent. Scale bar is 5 μm.

2.2.2   Altering solvent composition enables formation of capsules

For the intact formation of capsules, it is critical to ensure complete removal of the core. Previously, removal of the polystyrene core from LbL systems based on electrostatic interactions suffered from long treatment times and low yield of good quality capsules[61,72]. However, in our system only a two-minute incubation led to complete removal of the polystyrene core.

We believe that our choice of the solvent enabled quick removal of the template. The solvent composition is considered as an important parameter in tuning the polyelectrolyte interactions[140,143,144]. The combination of organic solvent and water lowers the dielectric constant compared to water thereby enabling effective screening of electrostatic interactions. It has been shown that presence of organic solvents causes a great deal of structural changes in the polyelectrolyte multilayer shells leading to permeability

changes. In our case, the ethanol-water solution caused structural changes in the polyelectrolyte and the weak hydrogen bonding between the multilayers contributed to a loosely bound multilayer. This loose structure enabled removal of the organic templates which comprises swelling of the template, then dissolution and diffusion out of the capsule.

Removal of the PS template was verified by FTIR in Figure 2.4a. The top spectrum was obtained from the original PS particles, where the peaks centered at 758 cm^{-1} and 698 cm^{-1} are assigned to the out-of-plane hydrogen deformation of a mono-substituted phenyl group and the out-of-plane ring deformation for a mono-substituted phenyl group, denoted as characteristic peaks of PS[145]. After assembly of PEI/(PAA/PVPON)$_{4.5}$ layers on PS particles (middle spectrum), the peaks between 1550 cm^{-1} to 1850 cm^{-1} widen, demonstrating the successful deposition of the layers without losing the characteristic PS signals. After incubation in THF to produce capsules (bottom spectrum), the characteristic PS peaks disappear while the peaks at 1728 and 1652 cm^{-1} from the carbonyl vibration of PAA and PVPON remain. TEM images of the capsules confirmed the absence of core as seen in Figure 2.4b. This indicates complete removal of PS template.
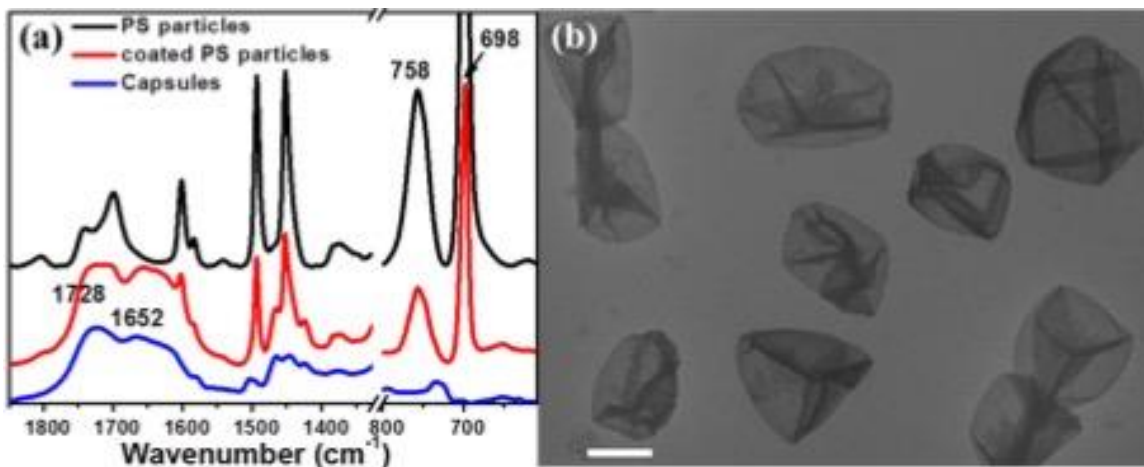
Figure 2.4. PS Core dissolution confirmation by FTIR and TEM (a) FTIR spectra of the original PS$_{3\mu m\text{-}r1}$ particles (top, black), coated particles (PS$_{3\mu m\text{-}}$

r1/PEI/(PAA/PVPON)4.5, middle, red), and capsules obtained by incubating PS3μm-r1/PEI/(PAA/PVPON)4.5 in THF for 2 min (bottom, blue). (b) TEM image of the capsules. Scale bar is 2 μm.

The role of weak hydrogen bonding in supporting the loose structure of the capsules was tested by the incubation of capsules in THF for long period of 40 minutes. This led to the breakage of capsules (Figure 2.5a-b) unlike the capsules formed by electrostatic interactions which can endure at least several hours of THF treatment without breaking[146]. The loose structure theory was also tested by making crosslinked capsules. As a control, PAA in the layered particles was crosslinked by EDC/NHS in the presence of hexamethylenediamine. After crosslinking the template could not be removed because of the limited space in the compacted network structure of the crosslinked layers (Figure 2.5c-d). Increasing the incubation time (2 days) or the incubation temperature (37°C) in THF did not help core removal. These results illustrate that the loose structure of the layers was critical for core removal.
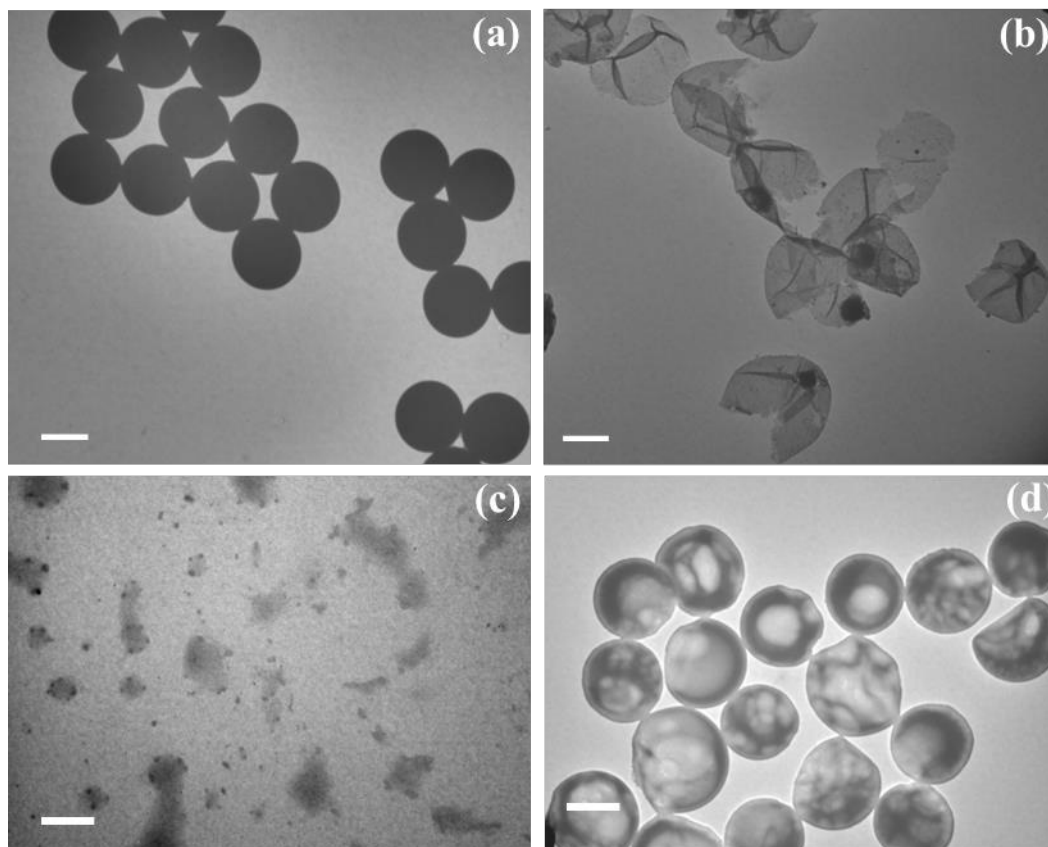
Figure 2.5. Transmission electron microscopy (TEM) images of layered particles PS$_{3\mu m-r1}$/PEI/(PAA/PVPON)$_{4.5}$ (a) before and after (b) 40 min, (c) overnight THF treatment to remove the core, and (d) incubated in THF for 2 days after crosslinking by EDC/NHS in the presence of hexamethylene diamine Scale bar 2μm.

2.2.3   Independent control over size and shape of capsules

The ability of the modified LbL technique to exercise independent control over size and shape was tested was by stretching PS particles into different shapes. The same PS particles were used as the starting material thereby conserving volume. The layered template was then treated with THF to form capsules. The capsules were monitored by fluorescence microscopy and are shown to retain the template shape and be well dispersed (Figure 2.6a). By TEM, the capsules were observed to be intact without broken or damaged walls (Figure 2.6b). We also tested the applicability of the method to fabricate capsules of

the same shape and size but higher stretch ratio, 3, $PS_{3\mu m-r3}$ particles. Stretching causes significant changes to the shape of the particles, affecting the charge distribution on the surface which is critical to LBL layer deposition. Another concern is the ability to maintain the shapes of capsules after the template dissolved. The layered capsules $PEI/(PAA/PVPON)_{4.5}$ layers were monitored after core removal using fluorescence microscopy (Figure 2.6c) and TEM (Figure 2.6d). This confirms that the template shapes were preserved and well dispersed, indicating the capsule walls were stiff enough to support the shape without deformation.
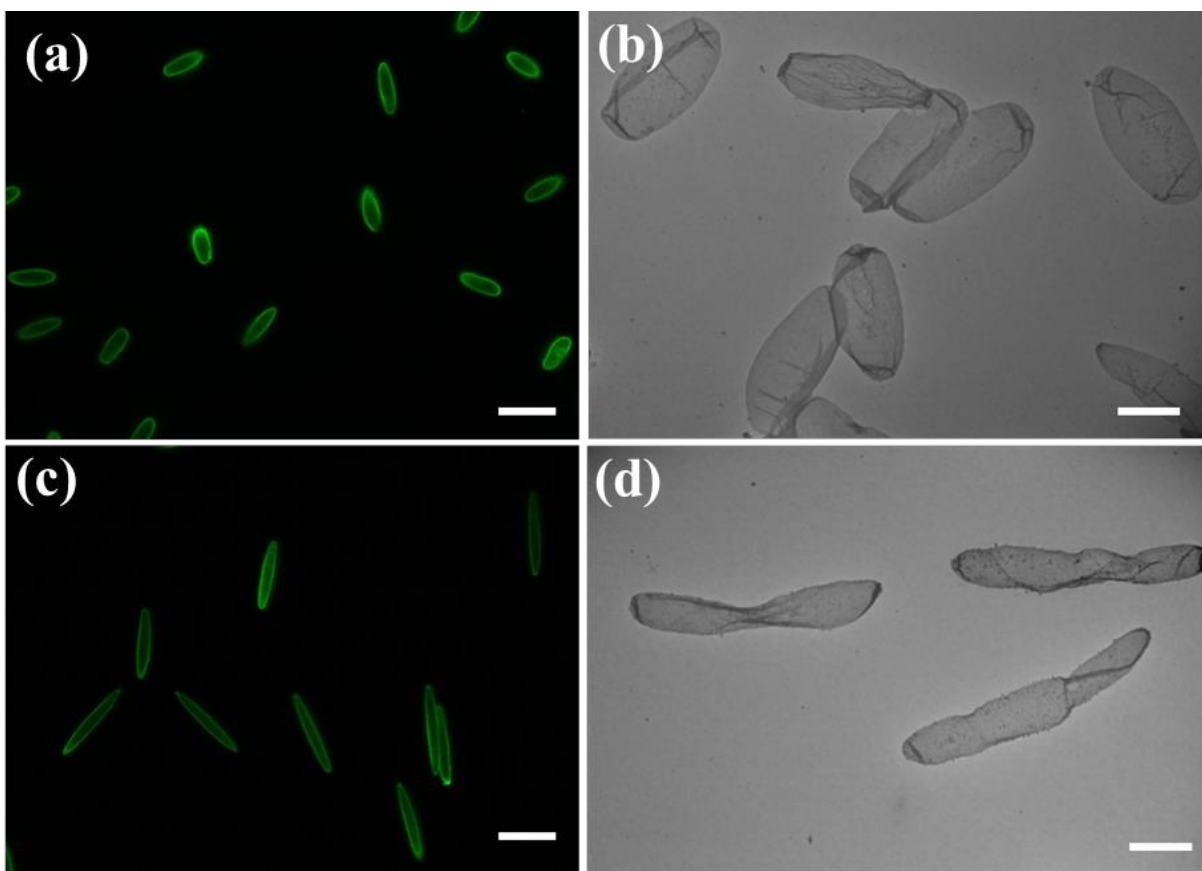
Figure 2.6. Fluorescent images of $PEI/(PAA-F/PVPON)_{4.5}$ shaped capsules. (a) $PS_{3\mu m-r2}$ and (c) $PS_{3\mu m-r3}$ template particles. TEM images of $PEI/(PAA-F/PVPON)_{4.5}$ capsules, fabricated from (b) $PS_{3\mu m-r2}$ and (d) $PS_{3\mu m-r3}$ template particles. Scale bars are 5 μm for (a) and (c), and 2 μm for (b) and (d).

2.2.4 Fabrication of nanocapsules

The fabrication of nanocapsules is challenging due to their higher surface energy making it difficult for re-dispersion and are prone to high aggregation during centrifugation. The applicability of this technique was tested to templates of size 500 nm with stretch ratio 3 ($PS_{500nm-r3}$) and 200 nm with stretch ratio 2 ($PS_{200nm-r2}$). The size distributions were assessed by DLS. As shown in Figure 2.7a-b, a single population of layered particles was observed, with size distributions centered at radii of 240 nm and 120 nm for $PS_{500nm-r3}$ and $PS_{200nm-r2}$, respectively. This is coincident with the size of original particles, though DLS cannot accurately measure the size of anisotropic particles. The size distribution of the capsules after core removal as shown in Figure 2.7a-b, the peak of the size distribution shifted larger, as with spherical templates, but remained a single population. These data illustrate good dispersion of the shaped nanocapsules. As observed by TEM in Figure 2.7c-d, the shapes of the capsules were maintained and the capsules were intact.
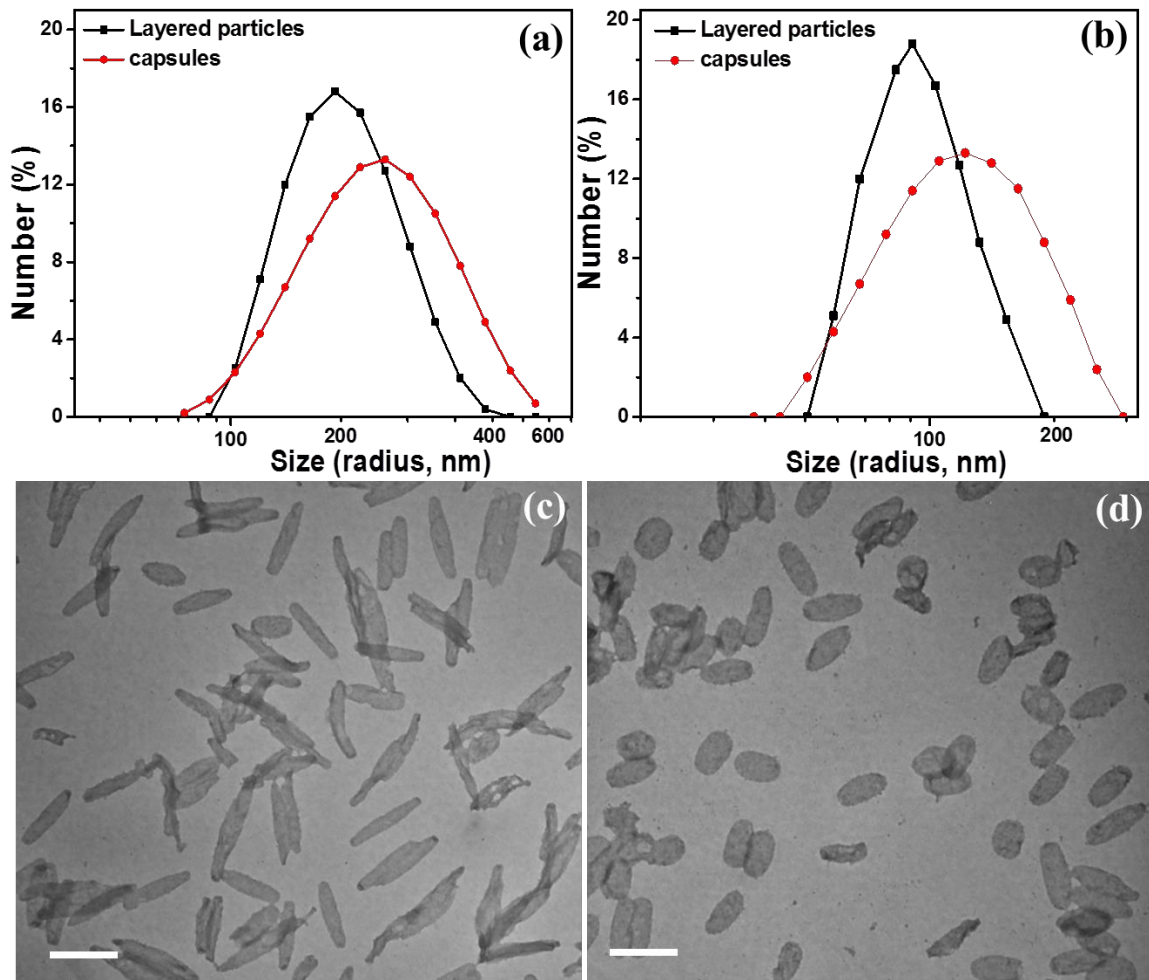
Figure 2.7. Size distributions of particles and TEM images of capsules. (a) PS$_{500nm-r3}$ layered particles (black line) and capsules (red line), (b) PS$_{200nm-r2}$ particles layered particles (black line) and capsules (red line). TEM images of PEI/(PAA-F/PVPON)$_{4.5}$ capsules, (c) PS$_{500nm-r3}$ and (d) PS$_{200nm-r2}$ particles. Scale bars are 1 μm and 500 nm for (c) and (d) respectively.

2.3   Summary

In summary, we developed a method for fabrication of polyelectrolyte capsules with constant surface chemistry and independently controlled size and shape by combining particle stretching with soft template LBL. Capsule aspect ratio can be tuned by template stretching independent of the size (volume), and the size (volume) of capsules can be tuned by selection of the initial sphere size without altering the shape and aspect ratio of the

capsule. Switching the solvent, enabled multilayer formation on particles through hydrogen bonding and facilitating a loose structure of the shell when treated with tetrahydrofuran for capsule fabrication. This method is highly versatile for the production of capsules with a wide range of sizes and shapes. This method will enable the optimization of physical properties of particles for drug-delivery applications or to further elucidate the interaction of particles with cells.

CHAPTER 3. FABRICATION OF TUNABLE PARTICLES AND ELUCIDATION OF COMBINATORIAL EFFECTS OF PHYSICAL PROPERTIES ON MACROPHAGE UPTAKE

Polymeric micro and nanoparticles are useful carriers for drugs and vaccines[147,148]. However, their fate in the system is dependent upon their interaction with macrophages. Particle properties such as size[6,7,149], surface chemistry[6,40,150–152], shape[37,75,153], and elasticity[53–56,58,59,154] have been identified as crucial in tuning interaction of particles with these cells. Most of these studies above have elucidated the effect of either one or two physical properties on cellular interactions. However, as particle synthesis techniques become more advanced, there can be interplay between more than two different physico-chemical properties on cellular interactions. A recent study has identified synergy between physical (shape), biological cue (antibody display) and route (cellular hitchhiking) for delivery to the lung endothelium[133]. It is thus crucial to be able to fabricate tunable particles with independent control over properties to understand the interplay between properties on cellular interactions.

In this chapter, we have adapted the template based layer-by-layer assembly process from the previous chapter to fabricate tunable particles whose size, shape, elasticity, and ligand immobilization can be controlled independently while retaining the same surface chemistry. We systematically investigated the combined contributions of these properties on cellular interactions during Fc- mediated phagocytosis, revealing complex interplay between the properties. Particles varying in multiple physical properties exhibit very different trends during interactions with macrophages. We demonstrate the

interplay between size, shape and stiffness in tuning the specificity of Fc ligand functionalized particle interactions with macrophages during phagocytosis.

3.1 Experimental methods

3.1.1 Particles and fabrication of rod shaped particles

The geometry of the particle has been recognized as an important design parameter for phagocytic interactions. In this work, spherical or rod shaped geometries were used to illustrate the combinatorial effects on such interactions. Spherical carboxyl functionalized polystyrene (PS) particles (3μm, 6μm) were used without any modifications from the manufacturer (Polysciences). Rod shaped particles were fabricated using our previously reported method. Briefly, 1 ml of 2.6 wt% spheres was suspended in polyvinyl alcohol (PVA, hydrolyzed degree 99+%, Mw = 85-124 kDa, Sigma Aldrich) solution (0.1 g/ml) and the solution was dried to yield a film of thickness of ~70 μm. The film was stretched in a hot oil bath at 120˚C to an aspect ratio of 2.5. The film was cooled to room temperature and the particles were extracted from the film by heating the film in 30% isopropyl alcohol-water (BDH) solution maintained at 65˚C. The particles were then centrifuged at 2500 g using Allegra X-15R Centrifuge (Beckman Coulter) for 15 minutes. This process of washing was repeated 6 times and the particles were dispersed in 80% ethanol (Sigma-Aldrich).

3.1.2 Functionalization of polyacrylic acid with fluorescein isothiocyanate and thiol molecules

Fluorescein isothiocyanate (FITC) was first modified to enable its conjugation to polyacrylic acid (PAA). FITC was dissolved in dimethyl sulfoxide (DMSO, BDH) to 0.2

M. N-(3-dimethylaminopropyl)-N-ethylcarbodiimide (EDC, Sigma-Aldrich) and N-hydroxysuccinimide (NHS, Sigma-Aldrich) were added to the mixture at a molar ratio of 1.4:1.2:1 (EDC:NHS:FITC). The reaction was carried out for 10 minutes and 1,6 diamine hexane (Alfa Aesar) was added to the mixture at a molar ratio of 0.9:1 (1,6 diamine hexane:FITC). The reaction was protected from light and carried out overnight. The solution was centrifuged to remove any precipitates.

The functionalization of PAA was carried out as follows. PAA (36 mg/ml, Alfa Aesar) was dissolved in 50% DMSO. EDC (43 mg) was added to the mixture followed by NHS (26 mg) and allowed to react for 10 minutes. pyridine dithioethylamine hydrochloride (44 mg/ml, Chem-Impex International Inc.) and modified FITC as described above (0.2 M) were added simultaneously to the above mixture and the reaction was allowed to proceed overnight. The resulting mixture was then dialyzed against 50% ethanol with 0.025 v/v% β- mercaptoethanol (Sigma-Aldrich) overnight. The functionalized polymer was finally reduced with dithiothreitol (1 M, G-Biosciences) for at least three hours. PAA functionalized with FITC and thiol will be referred to as PAAm in this chapter. For the non–fluorescent version of PAAm with thiol, the same protocol was used without FITC.

3.1.3 Layer-by-layer assembly on particles and capsule fabrication

Layer-by-layer (LbL) on spherical and rod shaped particles was carried out in ethanol. Polyelectrolytes polyvinylpyrrolidone (PVP, Mw ~ 55 kDa, Alfa Aesar), branched polyethylenimine (PEI, Mw ~ 120 kDa, Alfa Aesar) and PAA were chosen to facilitate LbL on particles. The stock solutions of PEI (5 mg/mL), PVP (5 mg/mL) and PAA (5 mg/mL) were prepared in 80% ethanol.

150 µl of 2.6 wt% suspension of PS particles were dispersed in 4 ml of 80% ethanol. To this, 1 ml of each adsorbing polyelectrolyte layer from the stock solution was added. The suspension was sonicated for 10 minutes and centrifuged at 1000 g for 10 minutes. The polyelectrolyte adsorbed particles were then washed in 80% ethanol through sonication and collected through centrifugation. In this way $(PVP/PAA)_2PEI(PAAm/PVP)_2PAA$ coated particles were obtained. Particles were crosslinked using 1 mM chloramine trihydrate (CaT, Acros Organics) solution for 2 minutes. Polyelectrolyte coated particles were suspended in 750 µl tetrahydrofuran (THF, Alfa Aesar) for 2 minutes to remove the PS and form capsules. The capsules were then centrifuged at 1000 g for 2 min and this process was repeated once. The capsules or coated particles retaining their core (referred to as core-shell particles) were suspended in phosphate buffered saline (PBS, 10 mM NaH_2PO_4, 137 mM NaCl, 2.7 mM KCl, 2mM KH_2PO_4; pH 7.4) for cell studies.

3.1.4 IgG functionalization of particles

The particles (core-shell or capsule) were functionalized with IgG by coating first with bovine serum albumin (BSA, Fischer Scientific) using 10 times excess of the surface monolayer saturation as calculated from the manufacturer's protocol. The particles were incubated with BSA (1 mg/ml) in PBS for two hours, washed three times in PBS and collected by centrifugation at 1000 g for 2 minutes. BSA coated particles were incubated for one hour with rabbit anti-BSA IgG antibody (ThermoFisher Scientific) at a mass ratio of 1:1 (BSA: IgG). The IgG functionalized particles were washed three times with PBS. To confirm the presence of IgG, particles were incubated for 30 minutes with FITC goat-anti-rabbit IgG (BD Life Sciences) and washed with PBS three times. The washed particles

were assessed by flow cytometry (Accuri C6, Beckton Dickenson Biosciences).

3.1.5   Particle imaging

Fluorescent images of particles were taken using a Zeiss Axio Observer Z1 inverted microscope. The ability of spherical capsules to conform to a circle was measured using the circularity function in ImageJ software. Transmission electron microscopy was carried out using JEOL 100CX-II microscope operating at 100.0 kV. Particles were dropped on a Cu grid 400 mesh (Electron Microscopy Sciences) and allowed to settle for 10 minutes. Any excess solution was wiped off and the grid was left to dry overnight before imaging.

3.1.6   Stability of capsules in media

The stability of capsules was tested by incubating 10^6 particles in DMEM media supplemented with 10% FBS for 48 hrs. The particles were gated by their forward and side scatter and retained similar fluorescence. The particles were then counted at 0, 24, and 48 hrs by flow cytometry. Experiments were performed in triplicate and data represented as the mean +/- standard deviation.

3.1.7   Cytotoxicity assay

The cytotoxicity of the capsules was evaluated using lactate dehydrogenase (LDH) assay. J774 cells, 10,000 in number were plated in triplicate in a 96 well plate. Particles at the ratio of 10:1 particles:cell or 10 μl of sterile water were added to the wells and incubated for 24 hrs. Controls for maximum LDH activity were also run according to the manufacturer's instructions (Pierce LDH Cytotoxicity Assay, Thermo Scientific). 50 μl of each sample condition was transferred to a 96 well plate. 50 μl of reaction mixture was added to each well and mixed. The reaction was protected from light for 30 minutes and

50 µl of stop solution was added to each well. The absorbance values were measured at 490nm and 680 nm using Biotek Synergy H4 Multimode plate reader (Biotek Instruments Inc) and reported as % cytotoxicity according to the manufacturer's instructions.

3.1.8 Size and zeta-potential of particles

The size of the capsules was determined by dispersing 10^5 capsules stored in PBS for 24 hours into a counting chamber glass slide and their size distribution was determined using a Cellometer Auto M10 Counter (Nexcelom Biosciences). Zeta-potential was determined by measuring the electrophoretic mobility of particles in 10 mM NaCl using a Zetasizer Nano ZS90 (Malvern Instruments Ltd.). Non- fluorescent PAAm was used to determine the zeta-potential of particles.

3.1.9 Thiol quantification

The thiol content was determined from Ellman's test (Uptima). Briefly, 50 µl of (DTNB solution- 2 mM Dithio-bis-(2-nitrobenzoic acid), 50 mM sodium acetate), 100 µl of Tris solution (1 M), and 840 µl water were mixed. To this working solution either 10 µl of PAAm sample or standard was added. The solution was mixed well and incubated at room temperature for 5 minutes. The absorbance values were recorded at 412 nm. Based on the calibration curve, the thiol content was computed. The thiol content was estimated for three different batches of PAAm.

3.1.10 Cell Culture

J774 macrophages (American Type Culture Collection (ATCC)) were grown in Dulbecco's Modified Eagle's Medium (DMEM) (ATCC) at 37˚C in a humidified

atmosphere containing 5% CO_2. The media was supplemented with 10% fetal bovine serum (Seradigm) and 1% penicillin/streptomycin (Amresco). The cells were used between passages 4 and 15.

3.1.11 Particle association with cell

The particle association with cells was assessed by flow cytometry and confocal microscopy. For flow cytometry, 10^5 J774 cells per well were plated in a 24 well plate overnight. Particles were added to the cells in supplemented media at 10 particles/cell. The cells were incubated with particles for two hours. The cells were then washed with cold PBS three times and scraped from wells. Duplicate samples were centrifuged at 3000 g for 3 minutes, treated with 200 μl trypan blue, and immediately interrogated on the flow cytometer. Control samples were run at 4°C and corresponding duplicate samples were treated with trypan blue to determine the effectiveness of quenching attached particles. Cell populations were gated and threshold fluorescence was established based on the auto-fluorescence of J774. Cell events beyond this threshold were reported as particle positive cells. The phagocytic assay was repeated three times using three different batches of prepared particles. Particle quenching by trypan blue was confirmed by incubating 10^5 fluorescent particles in 200 μl of trypan blue and interrogating immediately on a flow cytometer.

For confocal microscopy, 10^4 cells were plated in a Lab-Tek II chamber slide (Thermo Fisher Scientific) and allowed to adhere at least 6 hours. Particles were added to cells at 10 particles/cell and incubated with cells for one hour. The cells were washed with cold PBS twice and fixed with 3.7% formaldehyde for 15 minutes at room temperature.

The cells were then washed with PBS once quickly and two times for 5 minutes. 1% Triton–X 100 in PBS was used to permeabilize cells for 15 minutes at room temperature. The cells were washed three times with PBS after permeabilization. Phalloidin-rhodamine (Sigma Aldrich) was used to stain the actin at a volume dilution of 1:500 for 15 minutes at room temperature. The cells were washed three times before imaging using a Zeiss LSM 700-405 Confocal Microscope (Carl Zeiss Microscopy, LLC).

3.2   Results and discussion

3.2.1   *Fabrication and characterization of tunable particles*

With the aim of understanding the combinatorial effect of physical properties on the process of phagocytosis by macrophages, tunable particles in the form of core-shells or capsules were prepared through a self-assembly process called layer-by-layer. Polyacrylic acid (PAA) and poly(vinylpyrrolidone) (PVPON) and polyethylenimine (PEI) were chosen as the precursors for this process due to their solubility in ethanol. The choice of the solvent has been shown to be critical to prevent aggregation of particles during layer-by-layer (LbL) on soft templates[155.] Despite the low polarity of ethanol, hydrogen bonding between PVPON and PAA is strong enough to sustain LbL on polystyrene (PS) particles. PEI is used as a middle layer to impart high charge density for subsequent layer deposition. Zeta potential was used to monitor the progress of LbL on the particles. The zeta potential values changed as a function of the charge of the end group in the depositing polyelectrolyte (Figure 3.1). Depending on the choice of polyelectrolyte, the interactions of the hydrogen-bonded layers are susceptible to disintegration at physiological pH [156,157]. At a pH above the pKa of PAA, 4.2[158], its ionization disrupts hydrogen bonding, rendering capsules

unstable. In such cases, crosslinking of hydrogen bonded layers through amide or thiol

chemistry is commonly used to endow stability to capsules for biological applications[64].

Hence, we functionalized PAA with thiols in the presence of EDC and NHS yielding PAA

with 10 mol% of thiol containing units. This polyelectrolyte was further modified with

FITC (PAAm) to fluorescently label the particles enabling monitoring upon interaction

with macrophages. Functionalization of PAA did not affect the build-up of layers, as seen

from the zeta potential in Figure 3.1.
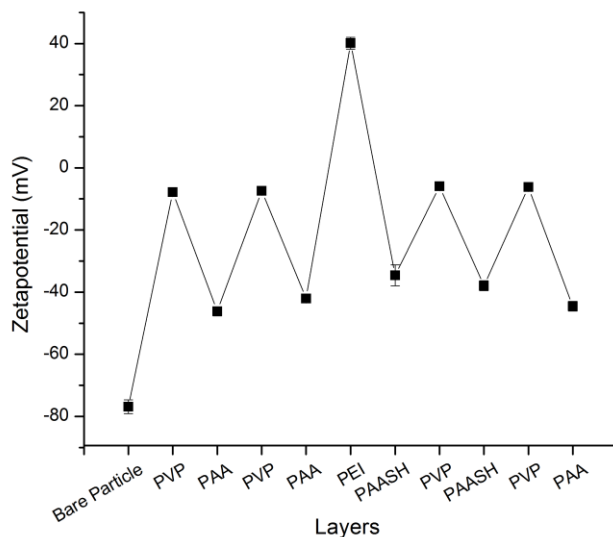
Figure 3.1. Zetapotential of particles during LbL process. Data represented as mean +/- standard deviation (n = 3).

These layers were crosslinked with chloramine trihydrate (CaT) which has been

shown to oxidize thiols controllably[157]. The layered templates

(PVP/PAA)$_2$PEI(PAAm/PVP)$_2$PAA were incubated in THF to remove the PS core. The

core removal was further confirmed by TEM as seen in Figure 3.2. The removal of the core

was shown to result in reduction of the elasticity of tannic acid/ polyvinylpyrrolidone

capsules when compared to their core-shell[54,72]. Hydrogen bonding between the layers of capsules was also shown to substantially reduce elasticity in comparison to traditional LbL capsules based on electrostatic interaction[72].
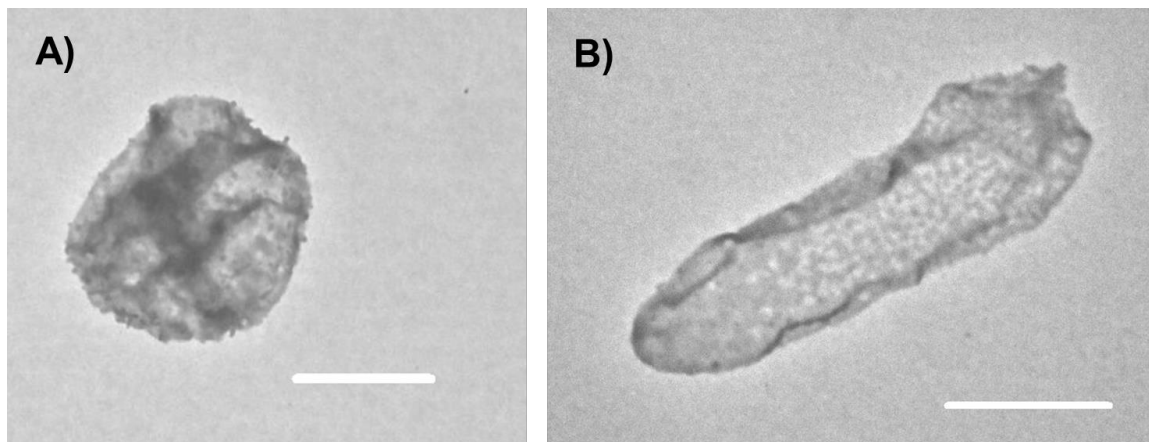
Figure 3.2. TEM images of capsules A) 3µm sphere, B) rod (scale bars 2 µm).

Figure 3.3 shows fluorescence images of the particles. The capsules retain the morphology of the template and 6 µm capsules appear more deformable than 3 µm capsules. Rod shaped core-shell particles and corresponding capsules were also made using the same LbL technique on rod-shaped templates (12 +/- 0.2 µm in length and 2.5 +/- 0.23 µm in width) stretched from 3 µm polystyrene spheres, thereby conserving particle volume. The rod capsules retain the shape of the template as seen in Figure 3.3c-d.
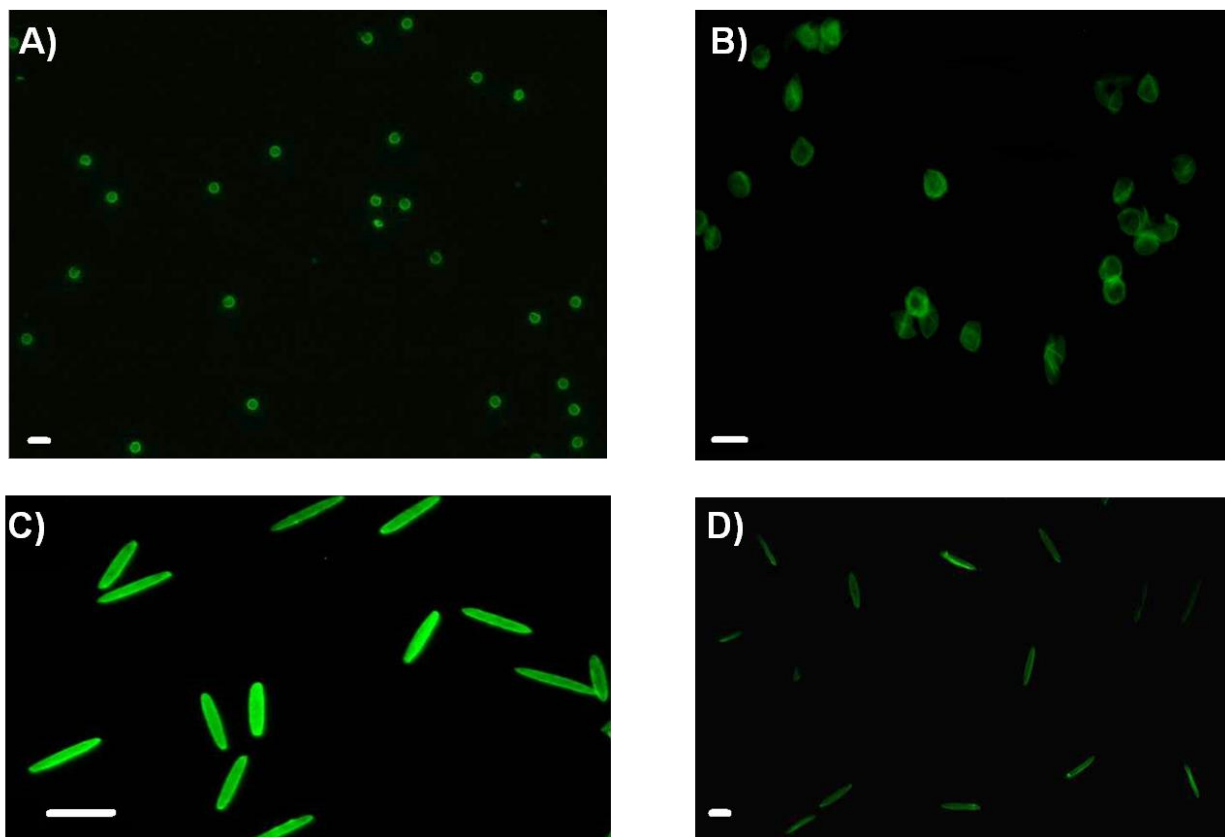
Figure 3.3. Fluorescence images of particles. A) 3 µm spherical capsules (scale bar 5 µm), B) 6 µm spherical capsules (scale bar 10 µm), C) rod shaped core-shell particles (scale bar 10 µm), D) rod shaped capsules (scale bar 5 µm).

The particles were also characterized for their size, stability and cytotoxicity to macrophages. The size distribution of the hollow spherical capsules (3 µm and 6 µm) in PBS was found to be similar to that of corresponding core-shell particles as evident in Figure 3.4A-B. This confirms the conservation of size and the dispersability of the capsules. Through this layer-by-layer technique we fabricated core-shell particles (3 µm sphere, 6µm sphere, rod) and corresponding capsules (3 µm sphere, 6µm sphere, rod) of the same surface chemistry yet varying in size, shape and elasticity. The stability of capsules was tested in biologically relevant media, DMEM supplemented with 10% serum as shown in Figure 3.4C, and they were found to be stable for at least two days. The

particles were determined to be non-cytotoxic to macrophages after incubation for 24 hrs in Figure 3.4D.

Isolating the effects of physicochemical properties on cellular interactions is critical to understand the roles that these properties can have when combined. Choice of particle size often depends on the *in vivo* application[159]. The advancement of techniques such as particle replication in non-wetting template (PRINT), stretching and liquefaction, step flash imprint lithography and self-assembly have enabled the fabrication of various non-spherical particles[135]. Stiffness of capsules can be altered by varying the number of layers, cross-linking, choice of material or maintaining/removing the core[160]. It is crucial to maintain similar size and shape during these processes while tuning stiffness. Our platform based on the choice of template particle size, method of stretching, and hollow preparation enables control over these properties and can help understand any interplay that exists between size, shape and stiffness.
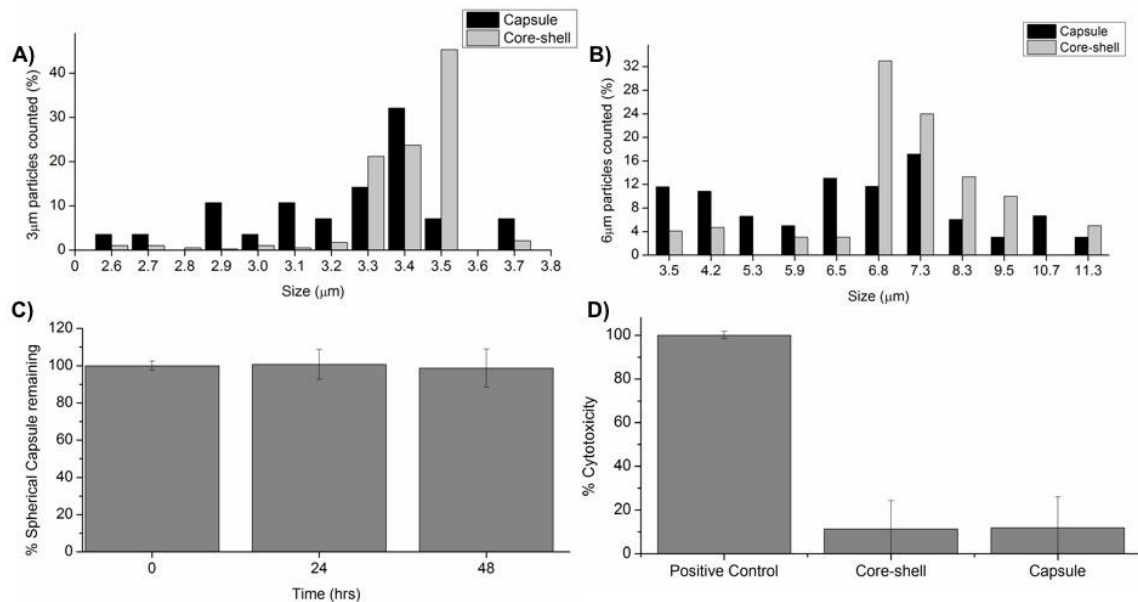
Figure 3.4. Characterization of particles. A) Size distribution of 3 µm core-shell and capsule particles measured in PBS, B) Size distribution of 6 µm core-shell and capsule particles measured in PBS, C) Stability of spherical 3 µm capsules in DMEM supplemented with 10% serum, D) Cytotoxicity of 3 µm core-shell and capsule particles to J774 cells following 24 hrs incubation. Positive control indicates a strongly cytotoxic agent provided by the manufacturer.

3.2.2   Interaction of tunable particles with macrophages

3.2.2.1   Opsonization of tunable particles

When particles are introduced systemically or locally into the body they encounter macrophages[5,161]. Macrophages are capable of phagocytosing particles through varied mechanisms, though Fc receptor mediated is the most widely studied[162]. Hence, to promote specific particle interactions with macrophages, core-shell and capsule particles were opsonized with Immunoglobulin-G (IgG). To achieve proper orientation of IgG Fc domain to Fc receptors, the particles were first coated with BSA followed by incubation with anti-

BSA IgG antibody. IgG functionalization of particles as shown in Figure 3.5 was confirmed by flow cytometry.

Recently, the density of Fc-ligand functionalization on spherical particles of different sizes has been shown to affect overall phagocytosis by macrophages[52]. The influence of such biological cues was shown to be negligible for spheres of sizes beyond 3 μm. Hence, for our 3μm and 6 μm spherical particles any effects of Fc-ligand density on phagocytosis would be negligible. For the case of rods, the influence of Fc density on shaped capsules and corresponding core-shells has been eliminated by equivalent antibody functionalization (Figure 3.5B).
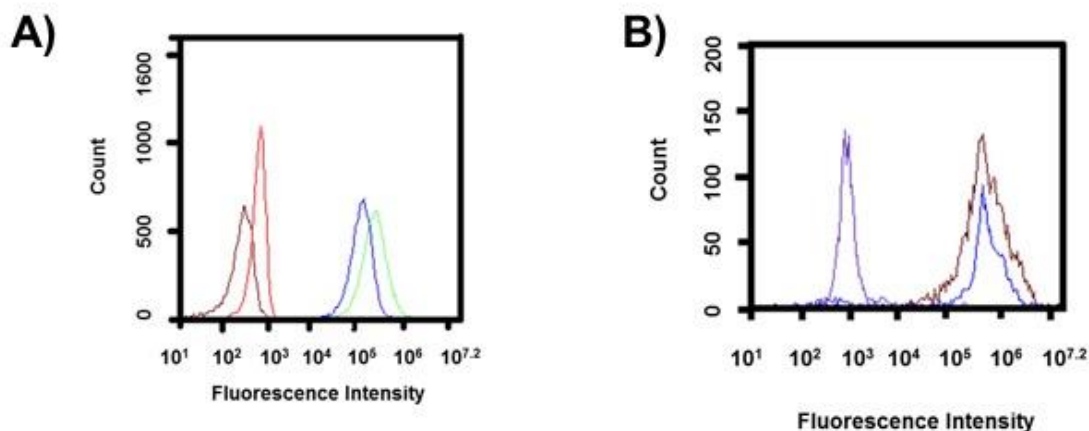
Figure 3.5. Opsonization of particles with anti-BSA IgG antibody and incubated with secondary antibody to confirm IgG presence. A) Spherical 3 μm core-shell and capsule particles after opsonization: core-shell (blue), capsule (green), and negative controls incubated with BSA and secondary antibody only, core- shell (red) and capsule (brown), Rod core-shell and capsule particles after opsonization: capsule (brown), core-shell (blue), negative control incubated with BSA and secondary antibody only: core-shell (purple). Traces were consistent across two independent replicates.

3.2.2.2   Effect of trypan blue on attached and internalized particles

The effect of various particle physico-chemical properties size, shape, surface chemistry and stiffness has been extensively studied to tune phagocytic interactions between macrophages and particles[6,7,9,153]. Attachment and internalization are the first two steps of the phagocytic process. To understand the independent effect of particle properties on internalization at 37˚C we used trypan blue quenching of FITC to differentiate between cells with membrane bound particles from cells that had completely internalized particles. Trypan blue quenched the fluorescence of particles as shown in Figure 3.6 by at least an order of magnitude. To confirm the applicability of this technique to differentiate between attached and internalized particles with cells, particles were incubated with macrophages at 4˚C, which prevents energy-dependent internalization processes including phagocytosis. As with free particles in solution, trypan blue also quenched the fluorescence of all the different types of particles attached to macrophages at 4˚C, establishing the ability to distinguish between attached and internalized particles at 37˚C (Figure 3.7).
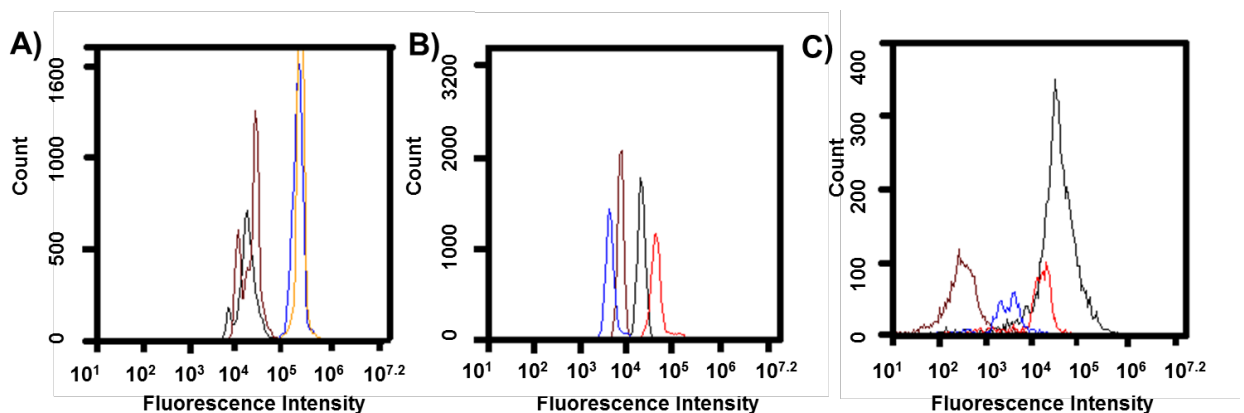
Figure 3.6. Trypan blue quenching of particles. A) 6 µm particle- core-shell (yellow), capsule (blue), core-shell quenched (brown), capsule quenched (black). B) 3 µm particle- core-shell (black), capsule (red), core- shell quenched (brown), capsule

quenched (blue). C) Rod shaped particle- core-shell (red), capsule (black), core-shell quenched (blue), capsule quenched (brown). Traces were consistent across two independent replicates.
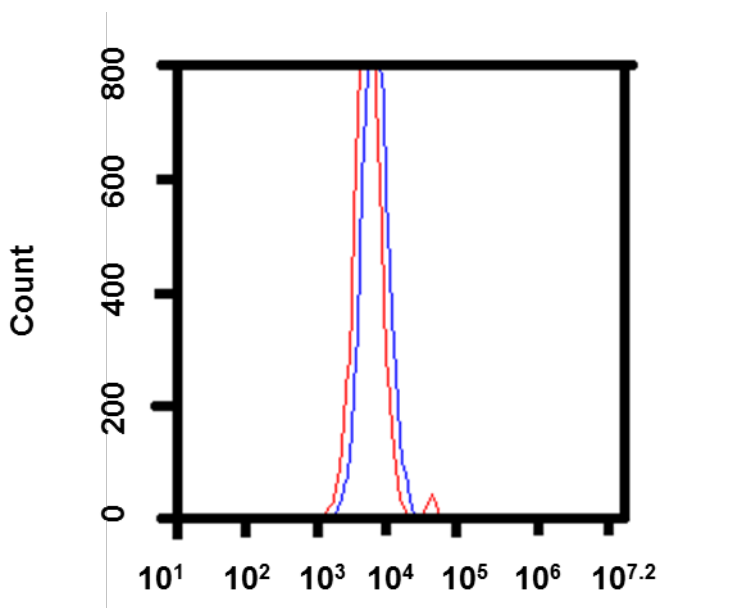
Figure 3.7. Trypan blue quenching of core-shell particles attached to J774 at 4 ˚C: no trypan blue treatment (red), trypan blue treated (blue). Traces were consistent across two independent replicates.

3.2.2.3   Effect of tunable particles on phagocytic process

The effect of IgG functionalized capsule or core-shell particles on total association (attached and internalized) and internalization by macrophages was evaluated after two-hour incubation with cells at 37˚C. The dependence of total association and internalization by macrophages due to varied particle physical properties is summarized in Figure 3.8. There was no statistical difference between the total association of core-shell particles or capsules of any kind.

Despite similar total association for particles of varying physical properties – size, shape, and stiffness, the internalization trend is different when any of these physical properties is altered. However, from one-way ANOVA analysis it is unclear if there exists any interplay between physical properties. For example, it is not clear if the effect of size for a spherical particle on phagocytic interaction is the same across varying stiffness. Likewise, the effect of altering shape from sphere to a rod on such interactions across varying stiffness is also unknown. Even when particles being compared appear to have only 1 physical parameter varied between them, the physical parameters size, shape and stiffness are inherently related to each other. Therefore, two-way ANOVA was performed to delineate the interplay between any two physical parameters on internalization by macrophages[163].
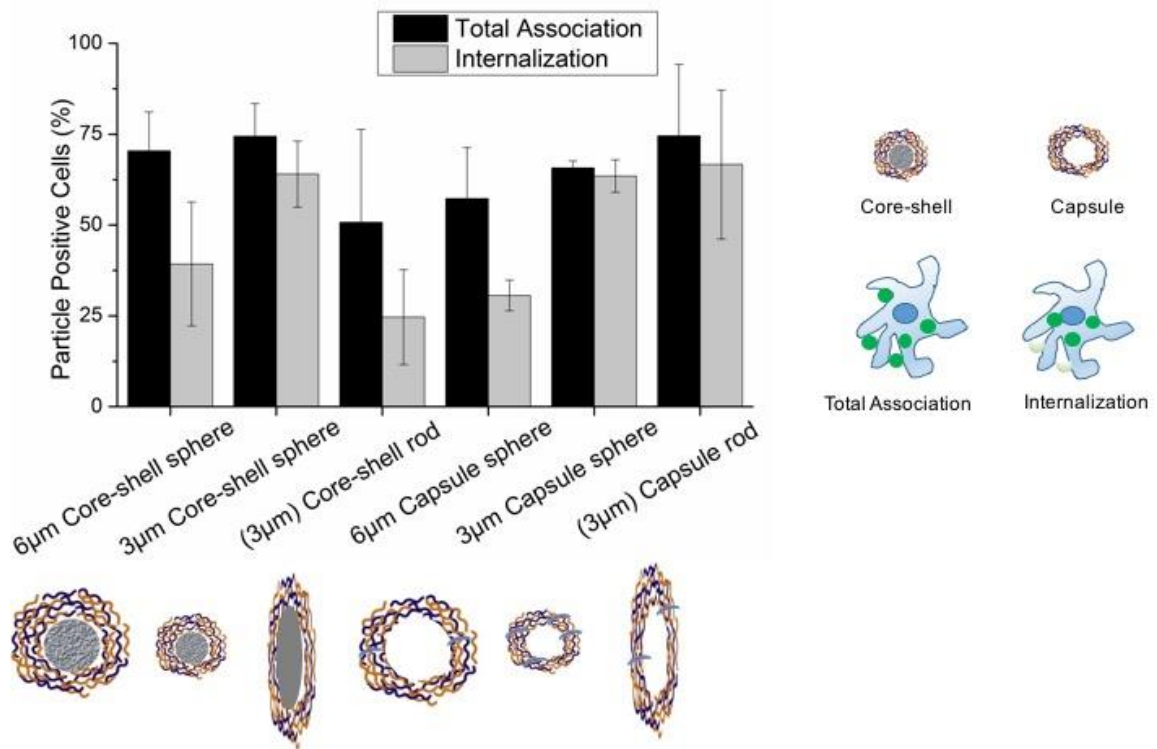
Figure 3.8. Percentage of J774 macrophages that associated with particles of varied physical properties, as measured by cell fluorescence: total association (black), internalized (gray). Data represented as mean +/- standard deviation (n = 3).

3.2.2.4   Interplay between size and stiffness of spherical particles

The interdependence between size and stiffness on internalization of spherical particles is shown in Figure 3.9A . The internalization enhancement seen with decreased size is greater for capsules than for stiffer core-shell particles. This could be due to differences in the sizes or differences in the stiffness of particles. Two-way ANOVA analysis, summarized in Figure 3.9B, determines that size (p=0.001) plays a dominant role over stiffness (p = 0.4568) for these spherical capsules in affecting internalization. There is no significant interaction between size and stiffness on influencing internalization by macrophages (p= 0.5058). In a recent study, measurement of single-event engulfment of 3 μm silica spheres by RAW macrophages exhibited ~2.8 times slower engulfment time than 1.85 μm spheres[164].This could be attributed to the energetics associated with deformation of the macrophage membrane during internalization of particles. Larger spherical PS particles (3 μm) have been reported to be taken up more slowly compared to 1.5 μm sized particles, suggesting that higher energy requirement for membrane deformation of large particles could abate uptake[165]. In addition, modeling of flexible nanoparticle interactions with membranes has identified the relative size between the particle and the interacting cell as a parameter in dictating the ability of the cell to execute complete wrapping of the particle[166]. The energy required for wrapping relatively larger particles is higher, which suggests this is the reason for the dominant effect of size in internalization.

It has been established that stiffness is inversely proportional to the radius of a thin hollow spherical shell (Appendix A), so larger capsules exhibit reduced stiffness[167]. Analysis of fluorescent images of capsules in solution (such as those in Figure 3.3) revealed that 6 μm capsules have 67% conformation to a circular shape, suggesting that 6 μm capsules are less stiff than 3 μm capsules, which have 85% conformation. This is also evidenced from confocal microscopy images in Figure 3.10, where 6 μm capsules are deformed by the cell membrane while 3 μm capsules maintain their spherical shape. While these measurements ascertain the differences between these capsules qualitatively, obtaining quantitative measurements of spherical capsules has been challenging due to fouling of AFM tip with particles upon contact. To prevent this, two strategies were employed. Polyelectrolyte treated surfaces were used to ensure that the capsule was immobilized on the surface. The surface was treated with various polyelectrolytes like PVP, poly-L lysine and PEI to facilitate adequate interactions of particles with the surface. Secondly, thiols can contribute to sticky interactions and hence the amount of thiols on the particles was lowered. However, neither of these strategies reduced fouling sufficiently to collect useful measurements.

The stiffness of capsules is also dependent on the choice of polyelectrolyte and the number of the layers that constitute the capsule so a different selection of either of these could alter the results and highlights the difficulty of selecting fabrication conditions and comparing to the literature. For example, capsule elasticity was greater by 3.5-5 times when poly(allylamine hydrochloride) was the choice of polyelectrolyte over poly(diallyldimethyl ammonium) chloride for capsule formation with poly(styrene sulfonate sodium salt)[168]. An increase in the number of layers has been correlated to increased stiffness of capsules in

the case of poly(styrene sulfonate)/ poly(allylamine hydrochloride) and hyaluronic acid capsules[58,59]. In addition, it has been suggested through modeling that the stiffness ratio between the particle and the membrane, is critical in dictating either partial wrapping or complete wrapping by the cell[169]. It is possible that our particular materials system could be beyond this critical ratio for the cell type we are using and thus not influencing the interaction between capsules and the membrane. However, as discussed below, the difference between core-shell particle and capsule stiffness does play a role in internalization of rod-shaped particles, which underscores the complexity of the interactions and difficulty in making broad conclusions.

When size and stiffness are altered for a spherical shape, our results show that a larger size and decrease in stiffness reduces internalization but also that altering the size plays a dominant role compared to stiffness in affecting internalization. This could depend on the crucial role of size in governing the number of attachment points of the particle to the cell and the energetics required for engulfment[7,165]. Altering the stiffness can affect the ability of actin cup formation, leading to reduced internalization[154]. Though the influence of stiffness in our case is negligible, the adhesion strength between the particle and the membrane for a particular stiffness could be explored with our particles to achieve full or no wrapping by macrophages. Models for relatively stiff particles have established that altering the adhesion strength alone can help achieve either no wrapping or full wrapping[169].
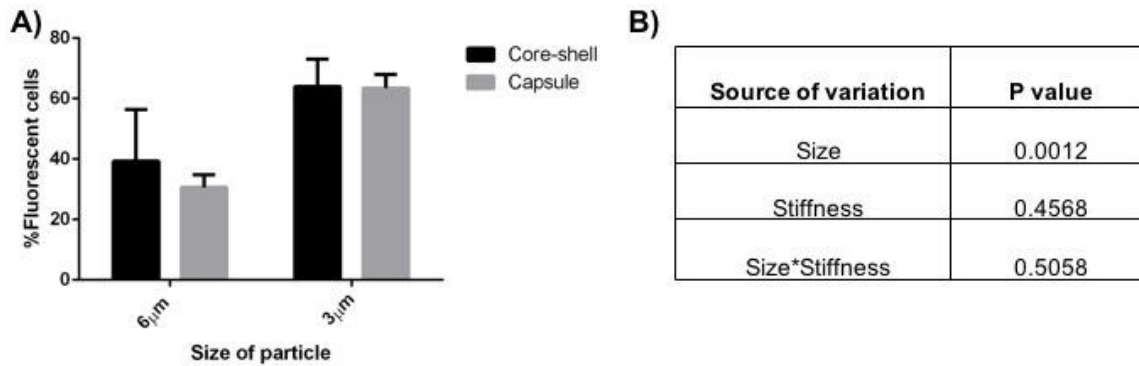
Figure 3.9. A) Role of size and stiffness on internalization: core-shell (black), capsule (gray). Data represented as mean +/- standard deviation (n = 3). B) P values calculated for each source of variation by two-way ANOVA.
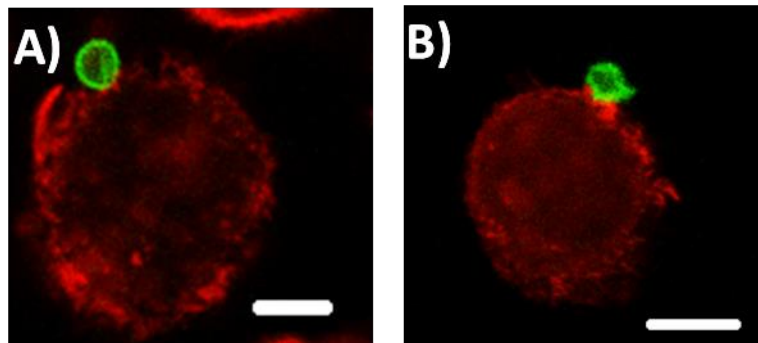
Figure 3.10. Confocal microscopy images from the center of the stack of J774 cells incubated with particles for one hour: A) 3 µm capsule (scale bar 5 µm), B) 6 µm capsule (scale bar 10 µm).

3.2.2.5   Interplay between shape and stiffness of spherical particles

To understand the effect of shape and stiffness, spheres and rods of identical volume were used. As seen in Figure 3.11, both the shape and stiffness together affect internalization (interaction shape*stiffness p = 0.023). When we look at the individual effects of shape for core shell particles in Figure 3.11, switching from sphere to rod shape decreases internalization while it has no effect on capsule rods and spheres. Studies have elucidated that shape of a particle can influence attachment to and internalization by a

macrophage independently [35]. Prolate ellipsoids have been shown to achieve maximum attachment compared to sphere and oblate ellipsoids. However, oblate ellipsoids exhibited higher internalization when compared to these two shapes. In another study, antibody-displaying micro-rods were shown to exhibit higher attachment and uptake compared to spheres in breast cancer cells[36]. The data in Figure 3.8 suggests that the rod shaped core-shell particles are able to attach to the macrophage but are unable to efficiently convert attachment into internalization. Our prior work with core particles hypothesized this was due to minimized curvature at the point of contact[153]. Switching the shape from sphere to rod has no effect on internalization of capsules. As evident from the analysis, this difference from core-shell particles must be due to the combined effects of shape and stiffness. Our results contradict a previous study where PMA spherical capsules were shown to be internalized more than rod shaped capsules[73]. This could be due to the different size (~300 nm) and mechanism of internalization, or the type of capsules and cells used, which make comparison difficult.

When we isolate the role of stiffness in these interactions; for 3 μm spheres, altering stiffness seems to have no effect on internalization. However, decreasing stiffness of rods has a significant 2.6-fold increase in internalization. The reduced stiffness of the rods enables their bending and twisting by the cell upon internalization, as seen in Figure 3.12. The stiffness of anisotropic particles is dependent on their orientation during interrogation methods like atomic force microscopy[170,171]. In the case of hollow tubes made from glass fiber templates, the stiffness varied with the location of probing on the tube, highlighting the challenges involved in characterizing mechanical properties of anisotropic shapes. Recently, a non-contact mode of determining axisymmetrical pendant capsule elasticity

was developed based on the pendant drop method. This method determines the capsule's resistance to stretching and its bending stiffness from shape and wrinkle analysis during deflation of the capsule[172]. However, it may not be possible to analyze different geometries through this method. Models to establish the global bending of shaped capsules like tubes is actively being pursued[173]. Such investigations can help identify the dependence of elasticity on shape. Another aspect to be considered when comparing core-shells and capsules is the density differences between these particles, as this physical property affects the ability of feeders such as ciliated protozoa to efficiently capture particles[174]. Though the mechanisms of encountering particles are different between these cells is different, the number of particles that are associated can be influenced by this parameter. The similar total association trends between these type of particles in Figure 3.8, suggests that particle density is not influencing macrophage interactions.
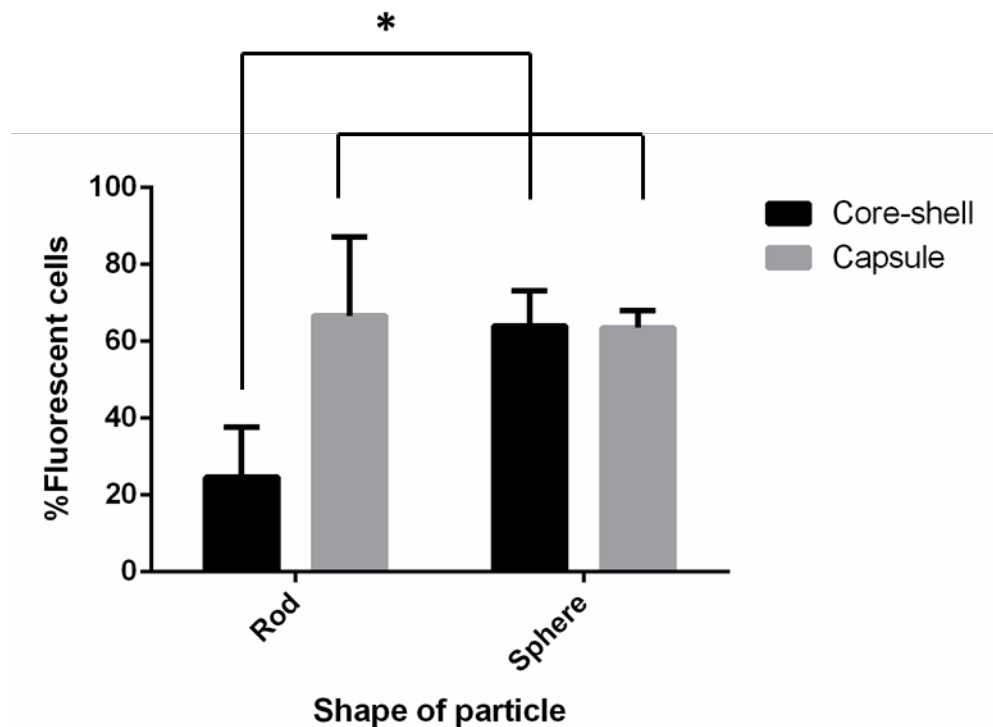
Figure 3.11. Role of shape and stiffness on internalization: core-shell (black), capsule (gray). Data represented as mean +/- standard deviation (n = 3). (p = 0.044 for shape, p = 0.026 for stiffness, p = 0.023 for shape*stiffness, by two-way ANOVA followed by Sidak's multiple comparison test).
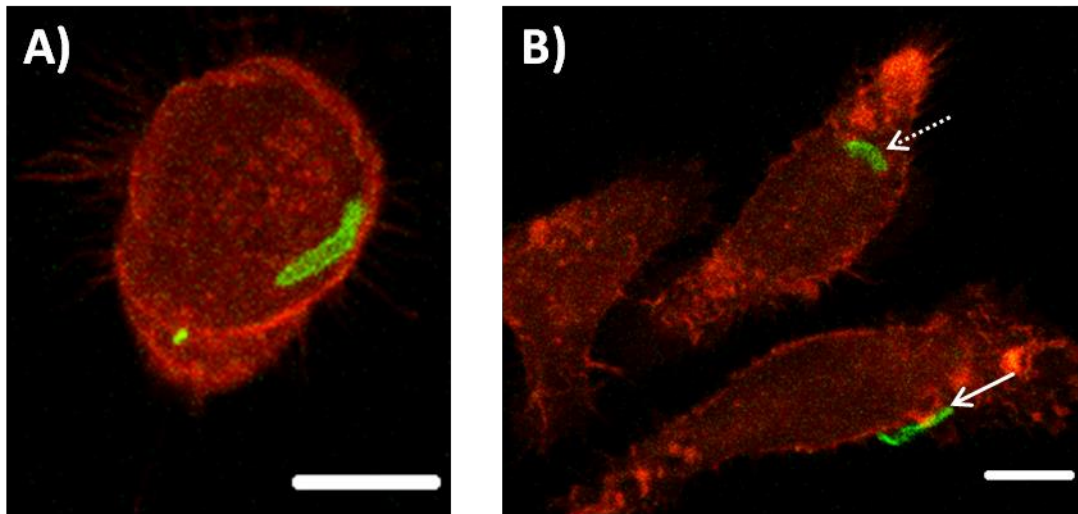
Figure 3.12. Confocal microscopy images from the center of the stack of rod capsules incubated for one hour with J774 cells: A) bent rod and B) rod folded in half (dotted arrow), twisted rod (solid arrow), scale bar 10 μm.

Varied stiffness has a complex interaction with shape, affecting internalization in the case of rods while having negligible effect on spheres. Particle shape has been widely investigated to alter cellular attachment and internalization of particle based therapeutics[35,37,153]. Oblate ellipsoids were found to be internalized more than prolate ellipsoids or spheres during phagocytosis[35]. A 2D model for phagocytosis of non-circularly symmetric particles predicts similar results for oblate ellipsoids when presented on the flat side to the macrophage membrane[175]. Despite the usual convention of high particle curvature promoting fastest engulfment, the model suggests that orientations like the flat side of oblate ellipsoids can also promote uptake. The mechanism of this is still to be

67

investigated. In another study, BSA coated poly (allylamine hydrochloride)/ poly(styrenesulfonate) bowl-like microcapsules were found to be internalized greater than spherical microcapsules in smooth muscle and macrophage cells. Bowl-like capsules were found to mainly attach to cells from the convex-side, and it was hypothesized that less energy expenditure is required for membrane deformation and that facilitates enhanced uptake of these capsules over spherical shapes[74]. Though the field does not yet have a unified theory, these studies contribute to the role of shape and orientation of the particle in enhancing uptake.

The effect of particle elasticity on cellular interactions, to a certain extent, shows consensus for immune cells that soft spherical or non- spherical particles are internalized to a lesser extent than their stiffer controls[53,54,56,154]. TA/PVPON cubical or spherical microcapsules exhibited less uptake in macrophages compared to their respective stiff counterparts. In addition, no difference in uptake between spherical or cubical stiff core-shells was reported, highlighting that a cubical shape for stiff core-shells has no effect on internalization. Reduced stiffness in this case worked in concert with shape (cubical or spherical) to reduce internalization by macrophages, emphasizing the complex interaction that stiffness can have on internalization for different shapes [54]. In the case presented here, internalization by macrophages is enhanced due to a combination of non-spherical, rod shape and reduced stiffness. For two particles of the same volume, an increase in surface area increases the probability of adhesion when comparing rods and spheres. This increase in adhesion contact area will also enhance the interaction between the particle and membrane, facilitating full wrapping through adequate compensation of membrane bending[176]. In addition to shape, reduced stiffness can increase the ability of the

macrophage to feel the particle by deformation, causing changes in the local curvature of the particle at the point of attachment[177,178]. This can facilitate wrapping by the cell membrane, resulting in enhanced internalization of shaped capsules over their corresponding core-shells. These tunable particles thus highlight the interplay between physical properties size, shape and stiffness to alter cellular interactions.

3.3 Summary

The results in this chapter illustrate the development of a system where the effect of multiple physical properties on cellular interactions can be evaluated. Using these particles, we have analyzed the effects of size, shape and stiffness on macrophage interaction and internalization. Stiff core-shell particles of the same volume but different shape, exhibit very different trends in internalization when compared to capsules. Core-shell rods reduced internalization compared to core-shell spheres, while capsule rods behaved quite similarly to spherical capsules.

Though these properties have an individual effect on cellular interactions, the way each of these influence interactions changes when they work in concert with other properties. In our results it is evident that stiffness behaves in a complex way when combined with size or shape. Increase in size reduces internalization of spherical particles, while changes in stiffness have no effect. However, varying stiffness had a significant effect on internalization for rod shaped particles. These results reveal the complex interplay between physical properties and highlight the challenges in making broad conclusions about the roles of size, shape, and stiffness on phagocytosis, as is evident from the seemingly conflicting reports in the literature. This system can be used to fabricate

advanced carriers or understand membrane mechanics and can be leveraged to identify combinations of properties that improve particle-based delivery systems or reveal new insight into phagocytosis.

CHAPTER 4.   IMMOBILIZATION OF STEALTH PHOSPHORYLCHOLINE COATING ON PARTCILES

Micro and nano-particles when used in biological applications such as drug delivery come into contact with biological fluids that contain a complex mixture of proteins that can adsorb on the particle surface. This adsorption process facilitates their clearance from the body by the cells of the reticuloendothelial system like the macrophages. The most common approach- PEGylation of materials suffers from drawbacks like initiation of an immune response when introduced into the body through the production of anti-PEG antibodies and complement activation[45,46].

Zwitterionic polymers containing phospholipids such as phosphorylcholine (PC) are alternative coatings that are being used for various biological applications [179]. PC is a component of the cell membrane and is known to be non-thrombogenic[180]. 2-methacryloyloxyethacrylate-PC (MPC) based polymers have been synthesized to mimic the cell membrane and have been shown to be highly resistant to adsorption of proteins[181] and adhesion of mammalian cells[182] and bacteria[183]. It has been proposed that the PC group strongly associates with several water molecules through electrostatic interactions, enabling formation of a hydration layer that inhibits protein adsorption[45,46]. MPC surfaces have been generated either as self-assembled monolayers on gold substrates or as alcohol-based coatings on medical devices such as cardiovascular stents, oxygenators, catheters, artificial blood pumps and blood filtration devices[152,184]. Though MPC polymers exhibit desirable properties when used as coatings for surfaces or particles in biological media, the techniques described require specific design of MPC co-polymer, as well as identification

of suitable solvents and process parameters to achieve sufficient coating. It would be beneficial to self-assemble MPC polymers as a layer on particles without such restrictions.

In this chapter, an alternative and general method has been developed. This method is based on solvent composition enabling the self-assembly of MPC polymer as seen in the previous chapters. We show the assembly and characterization of a positively charged MPC polymer coat on model polystyrene microparticles by the simple ethanol coating process. We investigated the resistance of the assembled MPC coating to protein adsorption and phagocytosis, and compared its effectiveness to PEG conjugated microparticles. Our results show that, MPC coated particles exhibited reduced protein adsorption and macrophage internalization; as low as PEG conjugated particles. In addition, these particles demonstrate a balanced charge on their surface which further confirms their non-fouling nature.

4.1   Experimental methods

4.1.1   Phosphorylcholine coating on particles

Poly(2-(methacryloyloxyethyl)-2-(trimethyl-ammoniumethyl)phosphate,inner salt / 3-(2-amminoethylsulfanyl)-2-hydroxypropyl methacrylate hydrochloride) (MPCAM)was a generous gift of NOF Co. Ltd. (Tokyo, Japan). 18 mg of MPCAM polymer (5 wt% in water) was added to 1 ml of an 80% ethanol-water solution (Sigma Aldrich). 1.64 mg of carboxyl functionalized 3μm particles (Polysciences) were added to the solution and sonicated for 15 min. The particles were centrifuged at 5000g for 3min Allegra X-15R Centrifuge (Beckman Coulter), washed twice in phosphate buffered saline (PBS, 10 mM NaH_2PO_4, 137 mM NaCl, 2.7 mM KCl, 2mM KH_2PO_4; pH 7.4), and stored at 4°C

4.1.2 Polyethylene glycol conjugation on particles

1.64 mg of carboxyl-functionalized particles was washed twice in 0.1 M 2-(N-Morpholino) ethanesulfonic acid hydrate (MES buffer,pH 5.5, Acros Organics). The activated particles were then suspended in 0.1 M MES buffer containing 8 mM Sulfo-NHS and 15 mM EDC and reacted for 15 min. Then, 0.625 mM PEG was added to the solution and the reaction was continued overnight at 4°C. The particle suspension was centrifuged at 7500g for 5 min and washed twice with PBS and stored at 4°C

4.1.3 Characterization of Particles

Zeta potential was determined by measuring the electrophoretic mobility of particles in 10 mM sodium chloride (BDH) using Zetasizer Nano ZS90 (Malvern Instruments Ltd.). The existence of 2-methacryloyloxyethyl phosphorylcholine (MPC) groups on the particle surface was confirmed by X-ray photo- electron spectroscopy (XPS; Thermo K-Alpha XPS). A small drop of MPCAM coated particles was placed on a glass slide and allowed to dry for 24 hours prior to XPS characterization.

4.1.4 Ovalbumin Adsorption on Particles

MPCAM coated, PEG conjugated, and carboxyl uncoated particles (14.9 μg each) were incubated with 0.01 mg/ml fluorescent Alexa 647 ovalbumin (OVA, Life Technologies) for one hour. The particles were spun down at 7500g for 5min and washed twice with PBS. The particles were interrogated by a flow cytometer (Accuri C6, Beckton Dickenson Biosciences) to monitor any increase in particle fluorescence due to OVA adsorption.

4.1.5   Ovalbumin Adsorption on Particles at High Concentration Condition

MPCAM coated, PEG conjugated, and carboxyl uncoated particles (0.149 μg each) were incubated with 10.01 mg/ml OVA protein solution for twenty-four hours at room temperature. The OVA protein solution was a combination of fluorescent and non-fluorescent OVA. The fluorescent OVA constituted 0.1% of the total OVA protein by mass. The particles were spun down at 17900g for 10 min and washed twice with PBS. The particles were interrogated by a flow cytometer to monitor any increase in particle fluorescence due to OVA adsorption.

4.1.6   Stability of MPCAM Coating on Particles

The stability of the MPCAM coating on particles was tested in PBS buffer. The particles were left in PBS for four weeks at 4°C and their effectiveness against OVA adsorption was tested as described above and compared to PEG conjugated particles.

4.1.7   Adsorbed OVA Secondary Structure

Circular dichroism (CD) spectra were acquired on a Jasco J-810 spectrometer (Easton) with the sample chamber maintained at 25°C. Measurements were made using a 0.2 mm path length quartz cell. The average spectra of five measurements were obtained from a wavelength range of 200-250 nm with 1 nm increments. PBS without protein was used as a blank. Spectra for ovalbumin (OVA) (0.01 mg/ml) were measured in solution and in the presence of MPCAM coated, PEG conjugated, and carboxyl uncoated particles (0.07μg each). The particle concentration was optimized to reduce scatter and absorbance.

OVA and particles were incubated for one hour prior to acquisition. Spectra were acquired in millidegrees and converted to mean residue ellipticity using the following equation.

$$[\theta] = \frac{[\theta]_{obs}\, MW}{10lCn}$$

The mean residue ellipticity in units of degrees cm^2/dmol ($[\theta]$) is a function of the observed signal in millidegrees, $[\theta]_{obs}$, the average molecular weight of the protein (MW), path length in cm (l), protein concentration in g/L (C), and the total number of amino acids (n). Estimation of secondary structure content was performed with the CDSSTR program provided in the CDPro software package.

4.1.8 Phagocytosis Assay

Cells were seeded in 24 well plates at a concentration of 10^5 cells per well and were allowed to adhere overnight. Particles (MPCAM coated, PEG conjugated, carboxyl uncoated) were added to cells in supplemented media at 10 particles/cell and incubated for two hours at 4°C. After cold incubation, samples were moved to 37°C, 5% CO2, humidified for one hour. Cells were then scraped from the wells, washed three times with cold PBS to remove unattached particles and analyzed by flow cytometry. For serum independent experiments, particles were incubated with OVA for one hour and subsequently added to cells in serum free media with the same incubation procedure described above. 10,000 cells were counted in each condition and was repeated with freshly coated particles.

4.1.9 Statistical Analysis

All quantitative experiments were performed in triplicate and are presented as arithmetic mean ± SD. Phagocytosis assay was performed in duplicate. One-way ANOVA was used to determine significance among groups. p values <0.05 among groups were considered statistically significant.

4.2   Results and discussion

4.2.1   *Fabrication of phosphorylcholine coated, polyethylene coated particles*

Carboxyl 3 µm polystyrene particles were used as model particles. Poly (2-(methacryloyloxyethyl)-2-(trimethyl-ammoniumethyl) phosphate, inner salt/3-(2-amminoethylsulfanyl)-2-hydroxypropyl methacrylate hydrochloride) (MPCAM, Appendix B) (a kind gift of NOF Co. Ltd.) was assembled on the particles by incubating them in a 2 wt% polymer solution containing 80% ethanol. Polymer with MPC content of 85 mol% was used in this work. It has been shown that polymer with 50 mol% MPC is sufficient to prevent protein adsorption on flat surfaces[182]. Carboxyl particles were also conjugated with PEG MW 5000 through EDC-NHS conjugation chemistry. PEG MW 5000 has been established as the critical molecular weight threshold for maximum reduction in protein adsorption and was thus used in this study for comparison to MPCAM[185]. Zeta potential measurements confirmed coating of MPCAM polymer and conjugation of PEG on carboxyl particles. The zeta potentials of particles, measured in 10 mM NaCl, were +22.1 +/-3.28, -8.1 +/-3.57, and -70 +/-6.20 for MPC coated particles, PEG conjugated particles, and carboxyl uncoated particles, respectively. The PEG conjugated particles are neutral, consistent with high surface coverage[148,186]. Conversely, MPCAM coated particles are positively charged. This is attributed to the protonization of

the amine groups present in the copolymer of the MPCAM polymer. This indicates that the MPC coating has shielded the charge of carboxyl groups on the polystyrene particle.

4.2.2   Determination of fouling by proteins on MPCAM particle surface

When exposed to serum proteins, polymeric micro and nanoparticles develop a protein corona on their surface[187]. This corona is dominated by albumin, as it is abundantly present in serum. Fluorescently tagged OVA was used as a model serum protein. Figure 4.1(A) shows fluorescence intensity of particles measured by flow cytometry after incubation with 0.01 mg/ml OVA for one hour. In comparison to carboxyl uncoated particles, OVA adsorption was reduced by 80% on the MPCAM coated particles (Figure 4.1(B)), similar to the reduction in OVA adsorption observed for PEG conjugated particles. The MPC polymer forms a strong hydration layer via electrostatic interactions that plays a major role in preventing protein adsorption[188]. It has been established in the literature that PEG chains associate with water molecules to help achieve protein resistance[185]. Carboxyl uncoated particles exhibited high OVA adsorption due to hydrophobic interactions between the exposed polystyrene surface and protein.
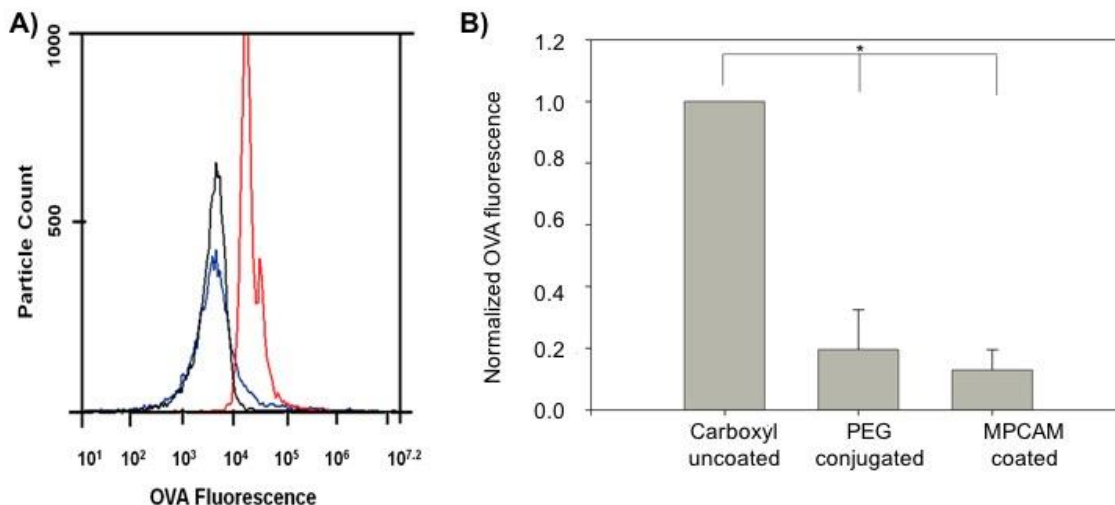
Figure 4.1. OVA adsorption measured by particle fluorescence after one hour of incubation with Alexa-647 OVA at room temperature. (A) MPCAM coated (blue), PEG conjugated (black), carboxyl uncoated (red) particles upon OVA adsorption directly after particle coating. (B) Normalized OVA fluorescence of particles was obtained with respect to adsorption on carboxyl particles. The median fluorescence value of particles from (A) was normalized with respect to median fluorescence value of carboxyl particles upon OVA adsorption.

4.2.3   Determination of stability of MPCAM coating on particle surface

We next assessed the stability of MPCAM coated particles. OVA adsorption was tested after storing particles for 4 weeks in PBS at 4°C. As seen in Figure 4.2(A), their effectiveness in preventing adsorption was preserved and comparable to PEG conjugated particles. We also tested MPCAM coated, PEG conjugated and carboxyl uncoated particles after 6 months storage in PBS at 4°C, in a high (10 mg/mL) concentration of OVA and a longer time period of incubation with the protein (Figure 4.2B). We observed similar results as in Figure 4.2(A). This demonstrates that although there is no covalent interaction, there is a strong association between the adsorbed MPCAM polymer and particle surface.
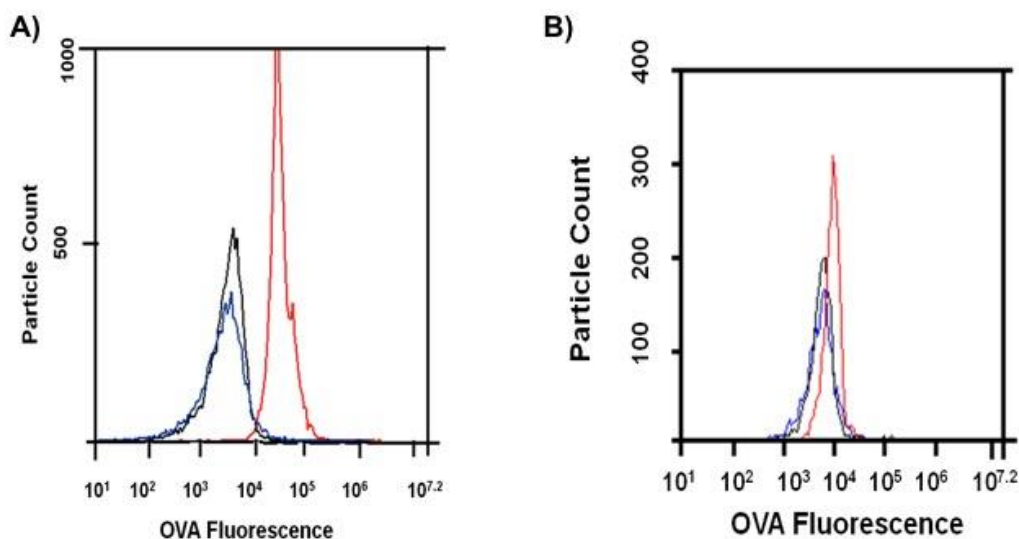
Figure 4.2. Stability of MPCAM coating measured by fluorescent OVA adsorption on particle surface. (A) MPCAM coated (blue), PEG conjugated particles (black) and carboxyl uncoated (red) particles after storing for 4 weeks in PBS at 4°C (B) MPCAM coated (blue), PEG conjugated (black), Carboxyl (red) particles upon OVA adsorption after storing in PBS for 6 months at 4°C. Fluorescent OVA adsorption measured by particle fluorescence after twenty-four hours of incubation with a high concentration mixture of fluorescent and non-fluorescent OVA at room temperature.

4.2.4 Determination of fouling by proteins on MPCAM particle surface

We probed the influence of coating on OVA secondary structure upon adsorption to MPCAM coated, PEG conjugated, and carboxyl uncoated particles. Adsorption of serum proteins on the surface of polymeric particles often alters protein structure[150]. Structural changes can influence the type of cell receptors engaged by adsorbed proteins during particle-cell interactions. In a recent study, it was established that the secondary structure of adsorbed protein is influenced by the surface chemistry of nanoparticles and alters interactions between particles and cell receptors[150]. Cationic amine and anionic carboxyl nanoparticles have been shown to exhibit net anionic protein-NP complexes on their surfaces when in contact with serum. However, there is a loss in secondary structure of

79

proteins on cationic, but not anionic nanoparticles. Further this loss in secondary structure caused alternate receptor engagement[189]. Such alternate engagement by receptors can result in inflammatory responses[190]. Circular dichroism (CD) spectroscopy was used to determine the structural content of OVA following incubation with particles for one hour. OVA incubated with MPCAM coated, PEG conjugated, and carboxyl uncoated particles showed similar α-helical content to soluble OVA, suggesting no significant change in OVA secondary structure. All surfaces, including MPCAM coated particles, support retention of adsorbed protein secondary structure as seen in Table 4-1. It has been reported that proteins adsorbed to PEGylated nanoparticles do not exhibit loss of secondary structure[191]. Surface carboxylation of particles also helps in retaining protein secondary structure upon adsorption [150].

Table 4-1. Secondary structure content of OVA in the absence and presence of particles obtained using the CDSSTR program with raw CD data.

Sample	α-helix (%)	β-strand (%)	Turns and unordered (%)
OVA	42.3	21.8	35.4
MPCAM coated	40.7	22.1	37
PEG conjugated	39.8	25	35
Carboxyl uncoated	40.5	22.2	36.9

4.2.5   Influence of MPCAM coating on particle uptake by macrophages

Evasion of immune cells is a primary challenge for particle based therapeutics[192]. We investigated the ability of MPCAM coated and PEG conjugated fluorescent particles to suppress uptake by J774A.1 mouse macrophage cells. Uptake by J774A.1 was performed in 10% serum (equivalent to 10mg/ml of protein[193]) representing biological conditions requiring high concentration of protein. To understand the influence of serum proteins on uptake, serum-free incubation of cells and particles (MPCAM coated, PEG conjugated, carboxyl uncoated) was carried out following incubation of particles with OVA. Just as MPCAM coated and PEG conjugated particles exhibited similar OVA adsorption (Figure 4.1A), they also had similar resistance to phagocytosis in serum-free conditions (Figure 4.3). There was no difference in uptake by macrophages when the media was supplemented with media for either MPCAM coated or PEG conjugated particles as seen Figure 4.3. However, carboxyl uncoated polystyrene particles are hydrophobic and are taken up by macrophages to a significantly greater extent. There was no difference in phagocytic uptake in the presence or absence of serum proteins, indicating no role of serum proteins on phagocytosis.
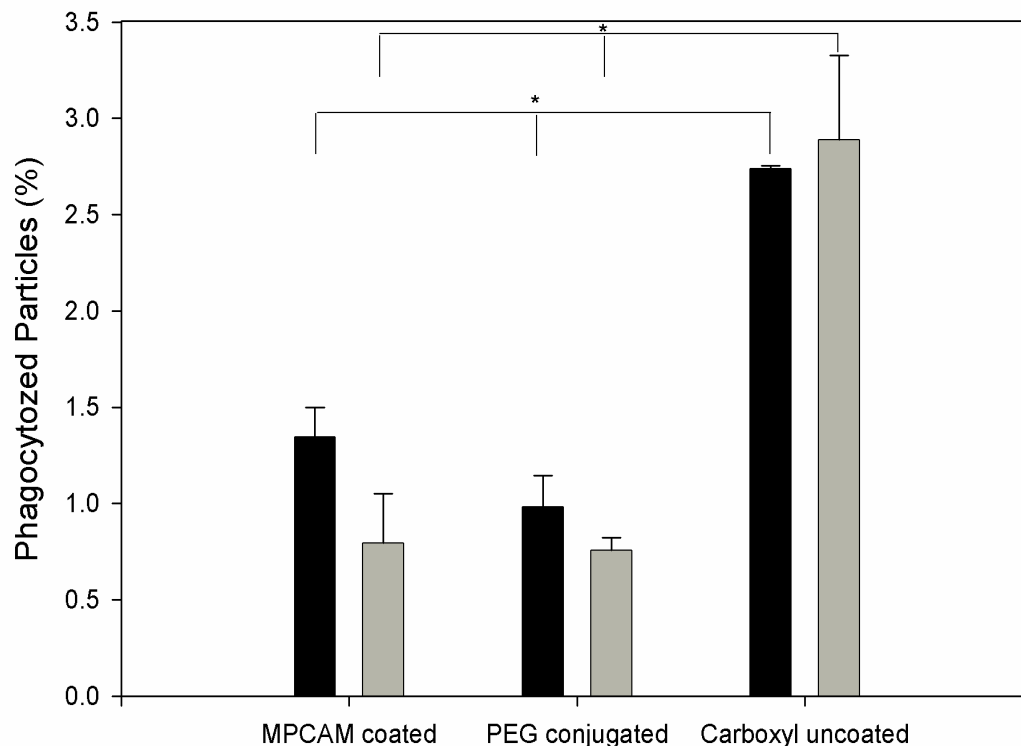
Figure 4.3. Percent internalized particles after incubation with macrophages at 37°C for one hour. Media was not supplemented with serum and particles were incubated with OVA for one hour prior to incubation with macrophages (black), or media was supplemented with 10% (v/v) fetal bovine serum (gray).

4.2.6 Surface characterization of MPCAM coated particles

Though MPCAM coated particles have a positive zeta potential, which the literature would predict to result in poor performance, the data indicate that MPCAM coated particles resist protein adsorption and phagocytosis as well as covalently bound PEG 5000. Surfaces with positive zeta potential are known to induce protein adsorption. It has been shown that negative or neutral nano and microparticles have lower levels of protein adsorption and internalization than positively charged particles[6,194–196]. However, in a biological environment, irrespective of the surface functionalization, particles display

a negative charge on their surface resulting from protein adsorption[136]. Zeta potential alone is not sufficient to establish how the interactions of particles and cells are influenced by surface functionalization and protein adsorption. X-ray photo-electron spectroscopy (XPS) characterization is commonly used to characterize zwitterionic coatings[197]. The non-fouling nature of zwitterionic surfaces is determined by the nitrogen to phosphorus or N/P ratio. This ratio indicates the charge balance for a surface. A ratio of N/P = 0.87 was shown to resist fibrinogen adsorption effectively on a PC thiol self-assembled monolayer[197]. Further, the study demonstrated that such ratios could serve as an indicator of the non-fouling nature of the surface. XPS elemental analysis of MPCAM coated particles shown in Table 4-2 revealed a ratio of N/P= 0.89. This ratio further supports the non-fouling nature of the MPCAM coated particles.

The XPS data supports that the PC groups are exposed to the surface. It has been proposed that PC groups on the surface can help in reducing the interfacial energy when in contact with water[198]. The hydrophobic moieties of the co-polymer might be buried within the assembly of the polymer and thus the MPC groups are oriented in aqueous environments to dominate the surface chemistry[198]. The electrostatic interactions between the charged groups on the co-polymer and proteins do not appear to play a significant role. However, the co-polymer could aid in the assembly of the MPC polymer. We hypothesize that the solvent quality enhances the hydrophobic attraction between the MPCAM polymer and the polystyrene surface. It has been established that for zwitterionic polyelectrolytes in poor solvents, as ethanol is for MPCAM polymer, the change in their conformation facilitates such hydrophobic attraction[199,200]. Therefore, this technique could be further

extended to other hydrophobic particles used in biological applications such as poly (lactic-co-glycolic acid) or polycaprolactone.

Table 4-2 Elemental characterization by XPS of MPCAM coated particles.

Element	Atomic (%)
C	65.55
O	23.01
P	3.28
N	2.93

4.3   Summary

The results in this chapter illustrate the potential of ethanol based layer-by-layer technique in immobilizing stealth coatings on particles. We demonstrate a simple technique of assembling a positively charged MPC polymer on model polystyrene particles through the 1-step ethanol coating process. Our results show that, despite positive zeta-potential protein adsorption and macrophage internalization were low for MPCAM coated particles; as low as for PEG conjugated particles. Balanced charge on the surface dictates the behavior of zwitterionic non-fouling surfaces and the N/P analysis ratio of MPCAM coated particles confirmed balanced surface charge. MPCAM coated particles retained adsorbed protein secondary structure, which is a critical design benefit that can influence the interactions of particles with cells and other proteins for diagnostic and therapeutic uses. This technique can be extended to biological applications that are incompatible with covalent coating methods, such as backfilling of particle surfaces to prevent protein

adsorption while retaining the targeting ability of attached ligands, or to endow stealth

properties easily to hydrophobic drug carriers.

CHAPTER 5.   THE ROLE OF GEOMETRIC PRESENTATION OF LIGANDS ON MACROPHAGE INFLAMMATORY CYTOKINE RESPONSE

Biomaterials such as nano- and micro particles have been developed to tailor immune responses. These materials are being used to enhance vaccine responses to pathogens, drug delivery to inflamed cells, and modulate inflammation in an antigen-specific or non-specific manner[201]. New strategies are actively being explored to control the immune system by enhancing or suppressing immune functions, and particle properties play a key role in programming biologic responses. Particle physicochemical properties such as size[7,52,202], shape[34,54,92], surface chemistry[150,203], ligand density[52,107], surface topography[204] have been identified as crucial in governing cellular responses in a wide range of cell types. In addition, these properties have the ability to determine the type of immune response[92,202]. Immune cells and functions, in particular, appear to be quite sensitive to particle properties[92,124,153].

Shape of the particle when functionalized with active ligands not only replicate native immune interfaces but also augment interactions and initiate signaling from cognate receptors on immune cells of interest [92,102,153]. While the field has made tremendous progress in understanding the effect of particle physicochemical properties on the outcome of particle-macrophage interactions, it is unclear how macrophage functions like cytokine production are affected while presenting active ligands through altered physical properties. Moreover, it is unknown if geometric ligand presentation through an altered particle shape

can elicit differential macrophage cytokine responses and if responses are ligand dependent.

In this chapter, we investigated the influence of geometric presentation of varying ligands (BSA, IgG, OVA, CD200) facilitated by the manipulation of shape of the particle on macrophage inflammatory cytokine response- TNF-α. In addition, we examined the role of geometric presentation of different ligand densities between varying shapes and correlated to TNF-α secretion and total particle association. Evidence indicates that, presentation of diverse ligands on rod shaped particles is inflammatory to macrophages compared to the same ligands presented on spherical shaped particles. This effect was observed for varying ligand densities and does not correlate to total particle association. This study demonstrates the ability of geometric manipulation of ligands to alter macrophage cytokine response irrespective of the nature of the ligand.

5.1 Experimental methods

5.1.1 Fabrication of rod shaped particles

Our previously reported method was used to fabricate rod shaped particles[32]. Briefly, 1 ml of 2.6 wt% fluorescent or plain polystyrene spheres (Polysciences) was suspended in PVA solution (0.1 g/ml, hydrolyzed degree 99+%, Mw = 85-124 kDa, Sigma-Aldrich) and the solution was dried to yield a film of thickness of ~65 μm. The film was stretched in a hot oil bath maintained at 120˚C to an aspect ratio of 2.5. The film was cooled to room temperature and the particles were extracted from the film by heating the film in 30% IPA-water solution maintained at 65˚C. The particles were collected by centrifugation at 2500 g using an Allegra X-15R Centrifuge (Beckman Coulter) for 15 minutes. This

process of washing was repeated at least 7 times to remove all PVA from the particle surface.

5.1.2 *Ligand functionalization of particles*

Plain or fluorescent particles (spherical or rod-shaped) were coated with BSA (Fischer Scientific) or OVA (Invivogen) using 10 times excess or with human IgG1 (R & D Systems) using 20 times excess of the surface monolayer saturation as calculated from the manufacturer's protocol.

5.1.2.1 BSA and IgG functionalized particles

The particles were incubated with BSA (1 mg/ml) in PBS for two hours, washed three times in PBS and collected by centrifugation. To functionalize with IgG, BSA coated particles were further incubated for one hour with rabbit anti-BSA IgG (Life Technologies); antibody at a mass ratio of 1:1 (BSA:IgG). For variable IgG density on particles a dilution of 1:5 or 1:100 of IgG to BSA was used. The IgG functionalized particles were washed three times with PBS. To confirm the presence of IgG, particles were incubated for 30 minutes with FITC goat-anti-rabbit IgG (BD Life Sciences) and washed with PBS three times.

5.1.2.2 OVA functionalized particles

The particles were incubated with OVA (1 mg/ml) in PBS for two hours, washed three times in PBS and collected by centrifugation. OVA coated particles were incubated for one hour with primary rabbit anti-chicken ovalbumin antibody at a mass ratio of 1:1

(OVA:IgG). To confirm the presence of OVA, particles were incubated for 30 minutes with FITC goat-anti-rabbit IgG (BD Life Sciences) and washed with PBS three times.

5.1.2.3 CD200 functionalized particles

The particles were first incubated with human IgG_1 Fc antibody (100 µg/ml) for two hours, washed three times in PBS and collected by centrifugation. These particles were further functionalized with CD200-Fc (100 µg/ml, R & D Systems) for one hour and washed with PBS. The presence of CD200 was confirmed by incubation with rat anti-mouse CD200:FITC (Bio-Rad) for 30 minutes, and washed with PBS three times.

All centrifugation steps were carried out at 2500g for 5 minutes. Plain particles were used to confirm the presence of ligands to avoid overlapping fluorescence between fluorescent particles and secondary antibody. The washed particles were assessed by flow cytometry (Accuri C6, Beckton Dickenson Biosciences) to confirm the respective ligand functionalization.

5.1.3 Cells

J774 macrophages (American Type Culture Collection (ATCC)) were grown in Dulbecco's Modified Eagle's Medium (DMEM) (ATCC) at 37°C in a humidified atmosphere containing 5% CO_2. The media was supplemented with 10% fetal bovine serum (Seradigm) and 1% penicillin/streptomycin (Amresco). The cells were used between passages 4 and 15.

5.1.4 Cytokine Assay

J774 cells were plated overnight at 10^5 cells per well in a 24 well plate. Plain or fluorescent ligand coated particles were added to the cells in supplemented media at concentration of 10 particles/cell. The cells were incubated with particles for eight hours. The supernatants were collected and stored at -80 ℃ to measure TNF-α production. TNF-α production was measured by standard ELISA kit (R&D Systems) as per manufacturer's instructions. The cytokine assay was repeated three times using three different batches of particles.

5.1.5 Particle association with cells

J774 cells were plated overnight at 10^5 per well in a 24 well plate. BSA, IgG or OVA functionalized fluorescent particles were added to the cells in supplemented media at 10 particles/cell. After incubation for 8 hours, the cells were washed with cold PBS three times and scraped from wells. Cell populations were gated based on the side and forward scatter of J774 cells without particles. The number of particles per cell was determined by measuring the mean fluorescence intensity (MFI) of the curve and dividing by the average MFI of one particle[205]. The phagocytic assay was repeated two times and 10000 cells were counted in each condition.

5.1.6 Cytokine assay for CD200 functionalized particles

All protocols involving animals were in compliance with the NIH Guide for the Care and Use of Laboratory Animals, as well as with relevant laws and institutional guidelines as prescribed by Georgia Institute of Technology's Institutional Animal Care and Use Committee. Femurs from 6 to 12 week old female C57BL/6J mice (Jackson Laboratory) were harvested following euthanasia. Mouse C57BL/6 cells obtained from

bone marrow were treated with red blood cell lysis buffer (155 mM NH_4Cl, 12 mM $NaHCO_3$, 0.1 mM EDTA; pH 7.4). The cells were cultured in Dulbecco's Modified Eagle Medium/F12 (DMEM/F12; Invitrogen) supplemented with 10% heat-inactivated FBS (Hyclone), 10 mM l-glutamine, 100U/ml M-CSF, 100 U/mL penicillin, and 100 μg/mL streptomycin. On day 7 of growth, the differentiated macrophages were dislodged using cell-dissociation buffer (Cellgro) after washing twice with Dulbecco's phosphate-buffered saline without calcium or magnesium (Cellgro)[206]. Macrophage response was examined by seeding 1×10^5 of bone marrow derived macrophages (BMDM) in culture media described above in a 96 well plate. Macrophages were pre-incubated with particles at a particle: cell ratio of 10:1 for two hours and then stimulated with murine IFN-γ (0.5 ng/ml) and *E.coli* LPS (0.05 ng/ml, Sigma) for 18 hours. Cell culture supernatants were collected and analyzed for secretion of pro-inflammatory cytokine TNF-α, by ELISA following the manufacturer's instructions (R&D Systems). The cytokine assay was repeated with freshly coated particles.

5.1.7 *Enhanced green fluorescent protein (eGFP) adsorption to shaped particles*

Spherical or rod shaped particles, 30000 in number were incubated with eGFP for 15 minutes at room temperature. The particles were spun down at 2500g for 5 minutes and resuspended in PBS. The particles were then immediately interrogated on the flow cytometer. For heat denaturation experiments, eGFP coated particles from the previous step were added to a PBS solution maintained at 55°C or 65°C for 10 minutes. The solutions containing the particles were run on the flow cytometer. All experiments were repeated in triplicate.

5.1.8   Statistical analysis

One-way or two-way ANOVA was performed followed by Tukey's post-hoc test for multiple comparisons. $p < 0.05$ was considered to be statistically significant in all analysis. Statistics were performed using the GraphPad Prism6 software.

5.2   Results

5.2.1   Ligand functionalization on spherical and rod shaped particles

Rod shaped particles were prepared by our previously developed method[32]. All ligands were immobilized by passive adsorption on the surface of spherical and rod-shaped particles. For ligands BSA and OVA direct adsorption on particles was carried out. For the case of IgG immobilization, the particles were first coated with BSA and then incubated with anti-BSA IgG antibody to orient the Fc portion of the antibody to relevant Fc receptors on macrophages. The coating of all ligands, BSA, IgG and OVA, was confirmed by incubation with relevant secondary antibodies and assessed with flow cytometry as seen in Figure 5.1. Irrespective of the ligand, similar levels of immobilization were observed for both spherical and rod shaped particles.
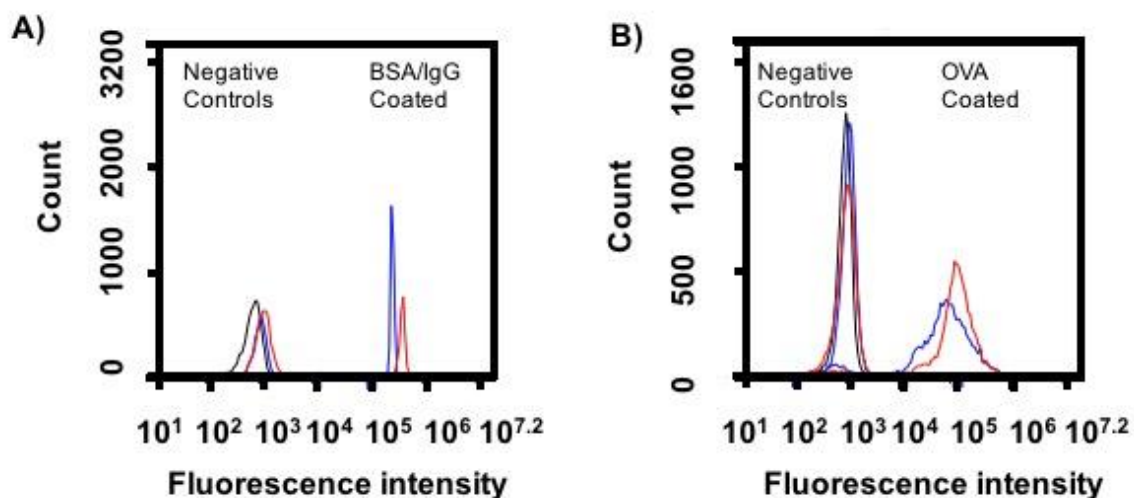
Figure 5.1 Ligand immobilization on spherical and rod shaped polystyrene particles.
Spherical (blue) and rod (red) shaped particles were adsorbed with ligand A) BSA
and rabbit anti-BSA IgG antibody B) OVA and rabbit anti-ovalbumin antibody and
probed with the same fluorescein isothiocyante labeled anti- rabbit IgG secondary
antibody to confirm BSA or IgG and OVA presence. Negative controls were
incubated with BSA (A) or plain particle (B) and fluorescein isothiocyante labeled
anti- rabbit IgG secondary antibody only. Plain PS particles (black) presented to
indicate particle fluorescence. Traces were consistent across two independent
replicates.

5.2.2   *Effect of geometric presentation of ligands on macrophage response*

The effect of presentation of ligands on varying shapes on inflammatory response

was assessed with TNF-α production by macrophages. For the case of BSA, IgG and OVA

coated spherical and rod shaped particles, TNF-α production was measured using the J774

macrophage cell line by ELISA. Regardless of the type of ligand, TNF-α production was

greater when ligands were immobilized on rods compared to spherical particles as seen in

Figure 5.2. In addition, TNF-α secretion varied based on the identity of the ligand when

immobilized on rods but there was no difference between the ligands immobilized on

spheres.
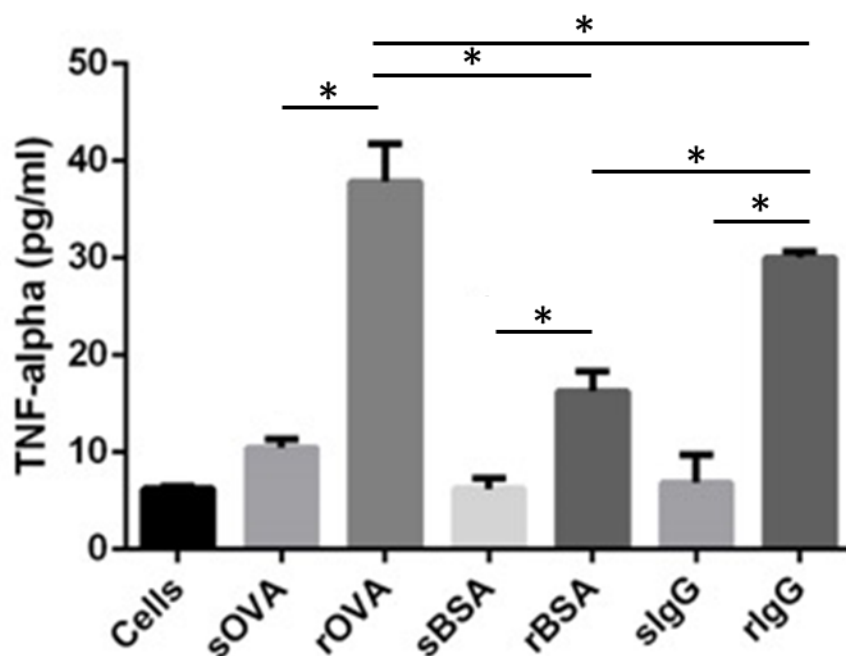
Figure 5.2 Geometric presentation of ligands on spherical (s) and rod shaped (r) particles alters TNF-α production in J774 macrophages. TNF-α values are averages +/- standard deviation of n=3 and * denotes $p<0.05$ as determined by one-way ANOVA followed by Tukey's multiple comparison test.

5.2.3   Relation between varying IgG ligand density and geometric presentation on

macrophage response

BSA coated particles were exposed to varying concentrations of anti-BSA IgG antibody to alter the IgG ligand density on each shape. The reduced IgG densities are denoted as a ratio between BSA:IgG. Similar densities were maintained between shapes for a corresponding ligand density as seen in Figure 5.3.
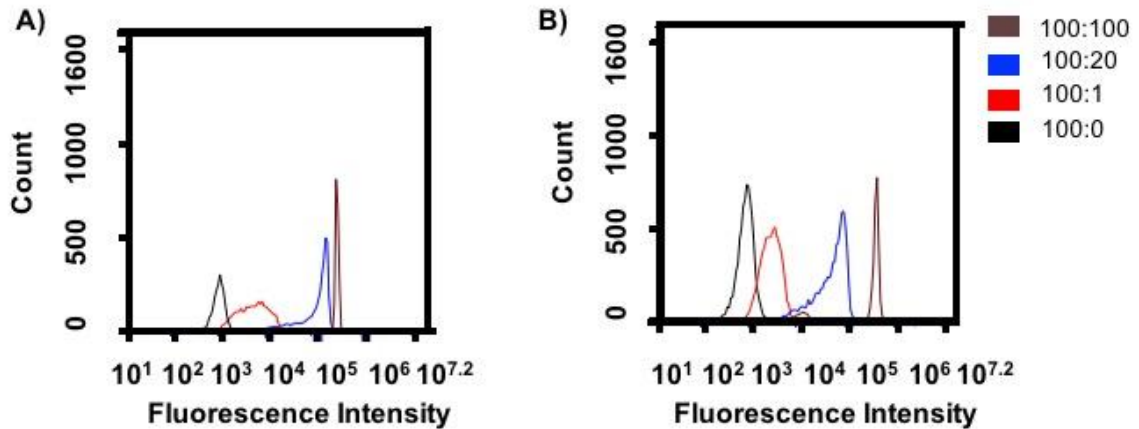
Figure 5.3 Variable IgG density on spherical and rod shaped particles. The histograms of fluorescent intensity of fluorescein isothiocyante labeled anti-rabbit IgG secondary antibody added to each a) spherical and b) rod shaped particle condition and measured by flow cytometer. The density is presented as a ratio between BSA:IgG in each condition. Traces were consistent across two independent replicates.

We measured the amount of TNF-α produced for each IgG ligand density on the shapes by ELISA. Reducing IgG density on spherical particles did not influence TNF-α production by macrophages, as seen in Figure 5.4A. However, reduced IgG density on rod shaped particles correspondingly reduced TNF-α production in J774 macrophages. Presentation of matched IgG densities on rod shaped produced greater TNF-α production than when presented on spherical particles in all cases except the lowest IgG density, 100:1.

Using variable IgG functionalized fluorescent spherical and rod shaped particles we assessed total particle association with J774 macrophages by flow cytometry. Total particle association is the combination of particles attached to and internalized by cells. Two-way ANOVA was used to determine the influence of both IgG ligand density and its presentation on varying shape on total particle association as seen in Figure 5.4B. Maximum IgG functionalization at a ratio of 100:100 increased the macrophage association of spherical particles compared to non-IgG-functionalized (BSA only coated) spherical

particles. Conversely, for rods, functionalization with IgG at the same maximum density (100:100) did not enhance total macrophage association in comparison to BSA coating. Altering IgG density on spherical particles had no influence on total particle association with macrophages. Conversely, reducing IgG ligand density to a ratio of 100:1 on rod shaped particles reduced uptake compared to the intermediate ligand density ratio of 100:20 but not compared to the maximum ligand density of 100:100. Overall, similar total cellular association was observed for spherical and rod shaped particles at each variable IgG density.
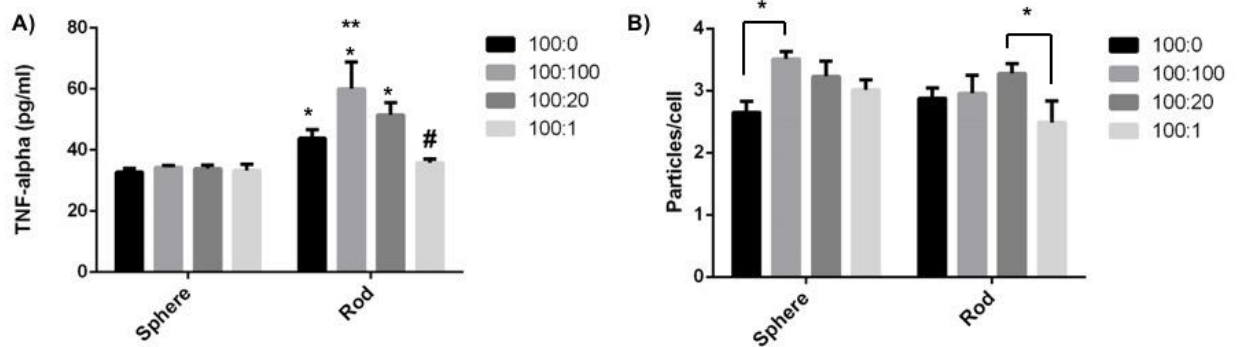
Figure 5.4 Effect of IgG ligand density and its presentation on spherical or rod shaped particles. A) TNF-α production and B) total association in J774 macrophages. A) Quantitative analysis of total particles associated with macrophages, including attached and internalized, at each ligand density when presented on spherical or rod shaped particles. * denotes p< 0.05 between groups as determined by two-way ANOVA with Tukey's multiple comparison test in each condition. B) Concentration of TNF-α produced by macrophages at each ligand density when presented on spherical or rod shaped particles. Error bars indicate averages+/- standard deviation of n=3 and * denotes p< 0.05 between corresponding spherical and rod shaped groups, ** denotes p<0.05 between 100:100 and 100:0 rod shaped groups and # denotes p<0.05 between 100:1 and 100:100 or 100:20 as determined by two-way ANOVA with Tukey's multiple comparison test.

5.2.4 CD200 immobilization and the effect of geometric presentation of CD200 functionalized particles on macrophage response

In contrast to the ligand coated particles in Figure 5.1, which appear foreign to macrophages, CD200, a self-ligand known for its anti-inflammatory nature, was immobilized on particles to further understand the role of geometric ligand presentation[207]. CD200 coated particles were produced by first functionalizing particles with anti-Fc domain, followed by CD200-Fc incubation with particles, as seen in Figure 5.5A. The effect of CD200 immobilization on varying shapes on TNF-α production was assessed in mouse bone-marrow derived macrophages since there is no literature evidence that macrophage cell line J774 responds to CD200. The role of geometric presentation on immune-inhibitory properties of CD200 was evaluated after pre-treating bone marrow derived macrophages with CD200 functionalized particles, followed by incubation with potent stimulators of inflammatory response: lipopolysacharide (LPS) and interferon-gamma (IFN-γ). Despite the anti-inflammatory nature of CD200, immobilization on rods activated greater production of TNF-α in macrophages than spherical particles, as seen in Figure 5.5B. There was no difference in TNF-α production by primary macrophages between non-functionalized spherical and rod shaped PS particles.
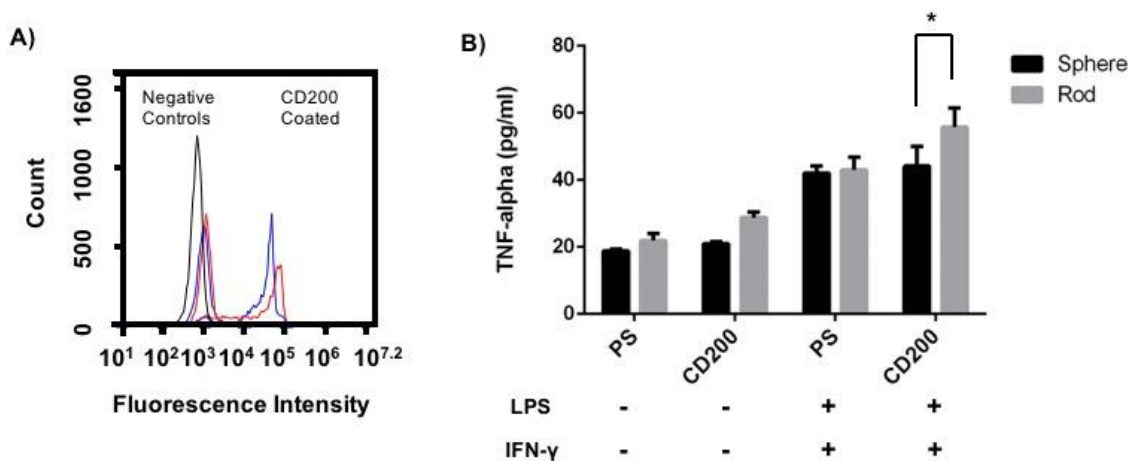
Figure 5.5 Immobilization of anti-inflammatory ligand CD200 on shaped particles and effect of its geometric presentation on TNF-α production in primary mouse macrophages. (A) Spherical (blue) and rod (red) shaped particles were functionalized with CD200-Fc through prior incubation with anti-Fc IgG antibody and probed with secondary anti-mouse CD200 FITC labeled antibody to confirm CD200 presence. The negative control was incubated with anti-Fc and secondary anti-mouse CD200 FITC labeled antibody only. Plain PS particles (black) presented to indicate particle autofluorescence. Traces were consistent across two independent replicates. (B) Concentration of TNF-α produced by primary macrophages when incubated with CD200 coated particles. TNF-α values are averages +/- standard deviation of n=3 and * denotes $p < 0.05$ as determined by two-way ANOVA followed by Tukey's multiple comparison test evaluating differences in TNF-α production due to particle coating on varying shape.

5.2.5   Influence on structure of protein when adsorbed on shaped particles

Enhanced green fluorescent protein (GFP) was used a model protein to evaluate the influence on change in protein structure upon direct adsorption to shaped particles. GFP is known to known to lose fluorescence upon denaturation due to structural changes in its barrel protected chromophore[208,209]. Rods adsorbed with GFP exhibited lower fluorescence than spheres (Figure S1A), Further, this lower fluorescence on rods was similar to fluorescence from GFP coated spheres denatured by heating to 55°C.
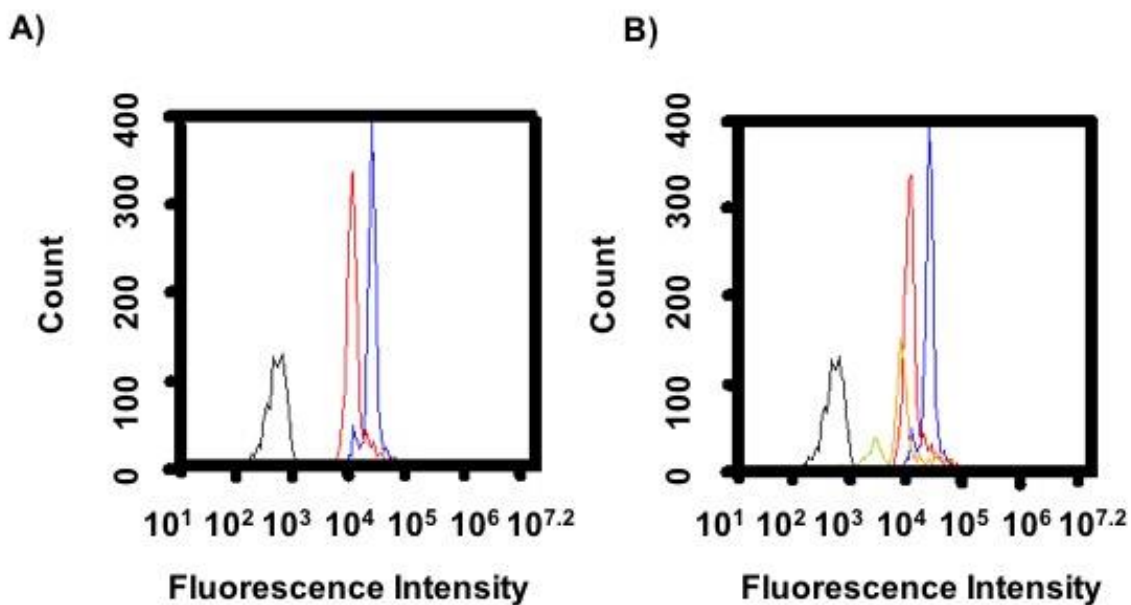
Figure 5.6 GFP undergoes unfolding upon adsorption to rod shaped particles. A) Spherical (blue) or rod shaped (red) particles were incubated with GFP for 15 minutes. B) Spherical or rod shaped GFP coated particles subjected to denaturation by heat. Curves represent GFP coated shaped particles: no denaturation (spherical: blue, rod: red) or denaturation at 55 ° C (spherical, orange) or 65 ° C (spherical, green). Plain particles (black) indicate bare particle autofluorescence. Traces were consistent across three independent replicates.

5.3   Discussion

The tunability of synthetic particles in the field of immune-engineering has led to the development of novel design strategies capable of tailoring an immune response[201]. One such strategy is to replicate native immune interfaces by the functionalization of particle surfaces with ligands to initiate signaling from cognate receptors on immune cells of interest. In addition to functionalization with a ligand of interest, particle shape can be manipulated to augment interactions with immune cells [102]. However, little is known about the effect of presentation of diverse ligands on shaped particles to immune cells like

macrophages. Macrophages bridge the innate and adaptive immune responses by orchestrated secretion of cytokines and chemokines during their interaction with synthetic particles. Thus, our aim in this report was to determine whether geometric presentation of diverse ligands on differing shapes affected macrophage inflammatory response.

We made rod shaped particles from 3 µm spheres by our previously developed technique involving heat liquefaction and stretching [32]. This allowed us to conserve the volume of the particles between the spherical and rod shapes, thereby negligibly affecting the surface area of the altered rod shape in comparison to the corresponding sphere. Therefore, functionalization of the spherical and rod shaped particles through passive adsorption resulted in similar ligand densities on both shapes (Figure 5.1, Figure 5.5A). We presented diverse ligands on these shapes, BSA, IgG, OVA and CD200, that interact with macrophages through varied receptors, scavenger, Fc, mannose and CD200R, respectively[43,150,207,210,211]. We determined the effect of geometric presentation of active ligands on macrophage inflammatory response by monitoring TNF-α production. TNF-α drives inflammatory responses through the activation of the NFκB pathway in cells[212]. We observed a significant enhancement of TNF-α secretion by macrophages when ligands of any type were presented on a rod shape compared to a spherical shape (Figure 5.2, Figure 5.5B). Similar increased TNF-α production was reported for non-functionalized rod shaped PMA$_{SH}$ capsules over spheres and for West Nile virus antigen coated cubic Au nanoparticles over spherical or rod shapes. While comparisons cannot be drawn, due to differing receptor engagement, particle sizes, and uptake processes between these studies and ours, they indicate that shape and ligand influence the magnitude of inflammatory response[120,124].

TNF-α production was increased for rod shapes over spheres irrespective of the nature of the ligand, suggesting the importance of geometric presentation of ligands on varying shapes to immune cells. The functionalization of 3 μm spherical shaped PS particles with inflammatory ligands like IgG or OVA did not enhance TNF-α production by macrophages in comparison to BSA coated spheres (Figure 5.2). In the case of 1 μm PS spheres, IgG coating enhanced TNF-α production by unprimed macrophages compared to BSA coated particles[213]. However, in another study the ability of macrophages to induce differential cytokine response between ligands BSA and IgG was lost with increasing size (0.5 to 1 μm) of spherical particles, suggesting the role of biophysical properties in such signaling[214]. In contrast, the amount of TNF-α produced when these ligands were presented on rods corresponded with the inflammatory nature of the ligand (OVA > IgG > BSA) (Figure 5.2). Further, there was no difference in TNF-α production between non-functionalized spherical or rod shaped particles, despite non-specific adsorption likely from BSA and IgG from serum in the culture media (Figure 5.5B). This suggests that presence of a ligand on the surface is critical for altering inflammatory responses. In addition, with similar ligand immobilization levels between the shapes (Figure 5.2, Figure 5.5A), these results demonstrate that the biophysical attributes of ligand presentation can influence innate immune signaling in macrophages.

Ligand density and particle shape can influence receptor signaling and uptake by cells [52,107]. Especially in the case of macrophages, a high aspect ratio worm-like shape has been shown to inhibit phagocytosis[34], while other shapes, like rods, can only be internalized from particular locations[8]. We therefore investigated the role of geometric presentation on the same ligand density for varying shapes and the influence of ligand density on a

particular shape on TNF-α secretion and total particle association. We chose total particle association with macrophages, which includes both attachment and internalization, as both these processes influence inflammatory responses during phagocytosis [215].

Geometric presentation of all IgG ligand densities, except the lowest (100:1 BSA:IgG), on rod shapes induced greater TNF-α production than the corresponding density on spherical particles (Figure 5.4A). However, there was no difference in cell association between spheres and rods with the same ligand density (Figure 5.4B). This is consistent with our previous study that reported similar total association between IgG coated polyelectrolyte spheres and rods[216]. These results indicate that the upregulation of TNF-α of rods over spheres is not due to an increase in cellular association with particles during phagocytic events.

Inflammatory responses initiated by phagocytosis depend on the type of receptor engagement and subsequent phagosomal processing of the particle[215]. While receptor clustering and subsequent uptake is a hallmark for phagocytosis of particles, it is not known if the clustering of receptors varies when the shape of the particle is altered[210]. It is possible that shaped particles have a different pattern of clustering, which could also depend on the orientation of the particle with respect to the cell, thereby affecting signaling. In addition, the role of biophysical attributes of ligand presentation in signaling during phagosomal processing in macrophages is not known. In a recent study, despite similar acidification of varying sized OVA functionalized protein nanoparticles upon uptake in dendritic cells, medium sized (~ 350 nm) nanoparticles induced larger amounts of TNF-α secretion than small (~ 270 nm) or large nanoparticles (~ 560 nm)[217]. This suggests that particle size has the ability to alter cytokine responses during surface receptor-mediated pathways. Shape

has been shown to influence intracellular trafficking in other cell types. Elongated shaped poly(lactic-co-glycolic acid) microparticles, unlike spheres, were shown to be oriented tangentially when trafficked towards the nucleus of endothelial cells [218]. In another study, disk shaped PS microparticles were shown to reside in pre-lysosomal compartments of endothelial cells longer than spherical particles[219]. Taking these size and shape examples together, it is possible that altered phagosomal processing of ligand coated rods influences inflammatory cytokine production.

In addition to altered processing, the structure of the adsorbed proteins on the particle surface could also influence inflammatory cytokine production[220]. BSA and OVA functionalized rod shaped particles enhanced TNF-α production when compared to spheres (Figure 5.2, Figure 5.4A). This could due to a change in the structure of BSA or OVA upon direct adsorption to a rod shaped particle compared to a sphere. To test this hypothesis, spheres and rods were incubated with enhanced green fluorescent protein (GFP). GFP is known to lose fluorescence upon denaturation due to structural changes in its barrel protected chromophore[208,209]. Rods adsorbed with GFP exhibited lower fluorescence than spheres (Figure 5.6A), even though ligand functionalization levels between shapes were consistent for all ligands (Figure 5.1, Figure 5.5A). Further, this lower fluorescence on rods was similar to fluorescence from GFP coated spheres denatured by heating to $55°C$, suggesting that GFP undergoes denaturation upon adsorption to rods (Figure 5.6B). In addition, it has been shown that albumin adsorption to shaped particles like gold nanorods[221], and cubic[222] or layered silicate nanoparticles[43] leads to denaturation of albumin on the particle surface. In another study, denaturation of BSA upon adsorption to gold nanorods was observed but not for spherical nanoparticles[221]. While the surface

chemistry between these two shapes was different, it is possible that both the shape and the surface chemistry of the particle contribute to this effect. Further, denaturation of protein on a particle surface has been shown to cause alternate receptor engagement and promote inflammatory cytokine production[220,223]. Denaturation of BSA on layered silicate particles has been shown to reveal cryptic epitopes that promote recognition of these particles through a specific macrophage scavenger receptor[43] and could explain the different trends in TNF-α between spherical and rod shaped particles. In the case of IgG and CD200 coated rods, it is possible that their denaturation is prevented as the anchor protein (BSA or anti-Fc IgG) is adsorbed first.

We investigated how ligand density affected TNF-α and total particle association for a particular shape to help understand the differing response in TNF-α due to geometric presentation. Altering the IgG ligand density on spheres did not influence TNF-α production (Figure 5.4A). Similarly, varying the IgG density on 1 μm PS spheres did not affect TNF-α responses in macrophages[214]. The total association of spheres between 100:100 or 100:20 and 100:1 BSA:IgG coating ratios were similar (Figure 5.4B). Again, this is consistent with a previous study that reported that the role of IgG density on macrophage interactions was negligible for PS spheres 3 μm and larger[52]. For the case of rods, a different trend was seen. Reducing the ligand density to a ratio of 100:1 decreased TNF-α production in macrophages (Figure 5.4A) when compared to ratios 100:20 and 100:100. This data correlated to a decrease in total particle association when compared to the ratio 100:20 but not 100:100. While the TNF-α secretion in macrophages is impacted

by altering ligand density on rods, there is no direct correspondence between particle association and TNF-α production (Figure 5.4B).

While BSA, OVA, and IgG ligands appear foreign to macrophages, we also investigated the role of geometric presentation for a self-ligand, CD200. CD200, like CD47, is a membrane protein and serves as a "don't eat me signal" on a broad range of cells[207,224,225]. It ligates to CD200R present exclusively on myeloid cells and is known to deliver a strong inhibitory signal. Disrupting the CD200/CD200R interaction using CD200-knockout mice or blocking antibodies was shown to increase the number of infiltrating macrophages and susceptibility to autoimmune diseases, including collagen-induced arthritis and experimental allergic encephalomyelitis[226,227]. In addition, administration of CD200-Fc fusion protein was shown to suppresses macrophage activation in a number of inflammatory diseases including arthritis [228], multiple sclerosis, [229] influenza infection[230] and organ transplantation[231]. The ability of CD200 to initiate these signals through surface interactions with its corresponding receptor motivated us to investigate if geometric presentation influenced its inhibitory behavior. Similar CD200 functionalization levels were observed between spheres and rods, as seen in Figure 5.5A. The ability of CD200 functionalized particles to attenuate TNF-α secretion was tested in primary macrophages as there is no literature on the function of CD200, in J774 cell line macrophages.

No difference in TNF-α production due to geometric presentation of CD200 was observed in the unstimulated conditions, which is in agreement with studies that indicate CD200 needs an inflammatory environment to exert any inhibitory influence. Similar

results were reported when primary macrophages were seeded on CD200 modified polystyrene surfaces; no influence of CD200 was observed until the cells were stimulated with inflammatory mediators[109]. When the macrophages were stimulated, TNF-α production was enhanced by geometric presentation of CD200 on rods compared to spheres. This suggests that presentation on rods was inhibiting the ability of CD200 to attenuate inflammatory responses. This could be due to overriding of CD200 self-signal when presented on a rigid, rod shaped particle, compared to a softer cell. The ability of physical properties shape and rigidity to override self-ligand signaling in macrophages has been recently established for self-ligand CD47 during erythrocyte phagocytosis [232].

There was no difference in TNF-α produced by primary macrophages when exposed to non-functionalized spherical and rod-shaped PS particles in both the unstimulated and stimulated conditions as depicted in Figure 5.5B. This implies that the particles themselves are not inflammatory, in the absence of ligand functionalization. It is important to note that there was 10% serum present in the media in all experiments, so it is likely there was nonspecific adsorption of serum proteins onto non-functionalized particles, likely including BSA and IgG. However, for non-functionalized particles, the particle material chemistry may play a larger role since rod shaped PMA$_{SH}$ particles were determined to be more inflammatory to unstimulated macrophages than spherical particles[124].

5.4   Conclusion

In this chapter, we have examined the effect of geometric presentation of diverse ligands on macrophage inflammatory TNF-α cytokine production. Our results demonstrate

that presentation of ligands on rod shaped particles is inflammatory to macrophages compared to the same ligands presented on spherical shaped particles. This effect was observed for diverse ligands engaging varied macrophage receptors and for varying ligand densities. The degree of particle association with cells does not correlate with TNF-α cytokine production by macrophages and is not responsible for the shape effects seen. Our results indicate that particle shape can influence macrophage functions, such as cytokine production, when ligands are presented on the particle. The ability to program cell-particle interactions through geometric manipulation can be used as a strategy to influence immunological outcomes. Additionally, these results should inform ligand-targeted drug delivery particle design. A shape should be chosen that balances the goal of the application with any undesired immunological responses caused through the interaction of shaped particles with off-target cells like macrophages.

CHAPTER 6.   CONCLUSIONS AND FUTURE OUTLOOK

The work presented in this thesis focuses on engineering particles for tuning cellular interactions. Methods were developed to produce particles with controlled size, shape, stiffness, and surface chemistry. These particles were then used to probe how macrophage-particle interactions are impacted by these physicochemical properties, either alone or in combination. While the investigation of combinatorial properties is critical for advancing carrier designs, identification of the role of intrinsic particle properties is important to comprehend how the immune system responds to these particles. Particularly, we investigated the intrinsic role of shape on inflammatory responses, when presenting varied chemistries to macrophages. Thus, understanding the role of physicochemical properties through a combination of novel particle fabrication techniques and intrinsic particle property-cell response relationships could help design carriers to alter cellular outcomes based on the type of disease.

The key findings in this work are:

1. Soft templates possess the unique ability to be engineered in a wide variety of sizes and shapes. The development of the modified LbL technique based on hydrogen bonding using an organic solvent enabled the use of soft templates as a core material to create core-shell or hollow capsule particles. This method expanded the wide array of shapes that the versatile LbL process can be applied to and overcame issues such as aggregation that typically plague soft templates during LbL.

2. The combination of modified LbL method on soft templates and thiol chemistry facilitated the development of a particle system whose physical properties size,

shape and stiffness can be tuned independent of one another while retaining the same surface chemistry.

3. Particles with tunable physicochemical properties revealed the complex interplay between size, shape and stiffness in interactions with macrophages. Increase in size but not reduction in stiffness played a critical role in decreasing the internalization of spheres. Internalization of rod shaped particles but not spherical particles was highly dependent on stiffness.

4. The modified LbL technique enabled a simple one step self-assembly process of a zwitterionic polymer that imparted stealth properties to particles and evaded macrophage uptake in vitro.

5. The geometric presentation of active ligands was shown to affect inflammatory responses by macrophages. Particularly, presentation of ligands on rod shaped particles enhanced inflammatory cytokine responses by macrophages compared to spherical particles.

The findings from this work illustrate the feasibility of using hydrogen bonded LbL on soft templates to manipulate multiple physical properties of particles. This system enables experiments to understand how cellular interactions can be altered when multiple properties are combined. This approach is modular, and other polyelectrolytes and biologic drugs could be incorporated to further tune the therapeutic outcome upon interaction with cells. The avenues opened through this modular nature are exciting for exploring the role of fundamental particle properties in biological milieu and extending this knowledge to applications involving biomaterial based tuning of cell responses. While this work helped in understanding the role of particulate stiffness in combination with other properties on

cellular interactions through qualitative measurements of particle stiffness, quantitative stiffness measurements have not been possible due to both experimental and data analysis limitations. Future work involving altered stiffness of anisotropic shapes should seek to obtain quantitative stiffness data on particles. Experimentally, passivation of the AFM probe might be beneficial. Data analysis between stiffness measurements of particles is challenging due to high variability, thereby making statistical interpretations difficult. In addition, establishing correlation of particulate stiffness induced biological changes in actin cup assembly during the phagocytic process can help establish how stiffness regulates this process.

This work provides impetus to further investigate how the physico-chemical approaches to particle design can be manipulated to tune cell interactions based on fundamental properties. In addition, with the emerging applications of LbL in immunotherapy, future work needs to address clinical translatability of these materials. Some potential areas for investigation are as follows:

6.1   Influence of surface topography on cellular interactions

As evident from some studies[77,233] and this work, LbL can be used to alter the surface chemistry of particles and affect the outcome of biological interactions. Another interesting property that can be tuned using this technique is the surface topography. The choice of polyelectrolytes in the LbL assembly process could cause changes in the roughness, thereby altering the surface topography of particles. The influence of surface topography of these multi-layered coated particles on influencing cell interactions has not been explored to the full extent. The interactions between these multi-layers can influence

not only the surface roughness but also the type, amount and conformation of proteins adsorbed[234]. Surface roughness has also been established as a critical parameter in influencing foreign body responses of biomaterials upon implantation[235]. Investigating the influence of this parameter would help in further influencing cellular outcomes from a material's perspective.

Recently, it was shown that the change in surface roughness due to varying polyelectrolyte layers on the surface of AuNP influenced the amount of proteins adsorbed and cellular association[204]. While it isn't clear from this study how roughness was affecting cellular association; it is possible that the change in structure of proteins upon adsorption to surfaces of different roughness influences this phenomenon. It has been established that the secondary structure of proteins adsorbed to particles influences the type of receptors involved in uptake[150]. Thus, investigation of type of proteins adsorbed to LbL particles, their structure and influence of cell association should be considered to understand the role of surface roughness.

6.2   Role of stiffness of anisotropic shapes in tuning phagocytic response

Stiffness of particles has the ability to tune the phagocytic response of macrophages. The role of stiffness of anisotropic shapes in tuning cell interactions is an emerging area. From our data for rods, it is evident that reduction in stiffness of rod shaped particles enhances internalization by macrophages. It is possible that the macrophages are able to change the particle orientation during uptake or experience dynamic mobility of ligands owing to the reduced stiffness. Understanding the role of orientation could be important when multiple ligands are decorated on the surface of particles for targeted drug delivery applications that involve evading macrophage recognition[54]. The dynamic

mobility of ligands imparted due to reduced stiffness could help achieve desired cellular responses at lower ligand densities[236]. The investigation of these aspects would help in designing novel particles capable of replicating natural interfaces between cells in an immunological setting.

6.3   Role of geometric presentation of ligands on phagosomal processing

Our results indicate that geometric presentation of active ligands on varying shapes is inflammatory to macrophages. In another study, ovalbumin conjugated rod shaped but not spherical polystyrene particles were able to induce a Th2 type immune response against ovalbumin in vivo[92]. These studies suggest that there can be crosstalk between innate immune responses and the development of adaptive immunity. It is possible that when antigens are presented on varying shapes, they are processed differently by macrophages due to varying phagosomal activity. The physical property size was shown to affect the cross-presentation efficiency of ovalbumin conjugated spherical polystyrene beads by dendritic cells[202]. While it has been shown that size can influence immunological processing, it is unclear how shape exhibits such influence. In endothelial cells, it has been established that a disk shaped PS particle resided longer in prelysosomal compartment than spherical particles, thereby beneficial for delivering enzymes for antioxidant protection[219]. In addition, elongated shaped particles unlike spheres were shown to be oriented tangentially when trafficked towards the nucleus [218]. The characterization of phagosomes and understanding the process of phagosomal protein degradation when presented on varied shapes can further help comprehend the varying immune responses observed in macrophages. Identifying these mechanisms can lead to the development of altered antigen presentation based either on the shape of the particle or choice of active ligand[237].

6.4 Stability of LbL particles

With the increasing application of LbL in immunological applications, it is crucial to address the stability of particles fabricated with this technique. There is very little evidence on long-term stability and storage of particles that are made with materials of varying properties like pH responsiveness, degradability. Identification of different cryoprotectants might be helpful in determining conditions suitable for lyophilizing these particles.

6.5 Role of stiffness and shape in influencing macrophage function

Stiffness has been identified as an important parameter in influencing the outcome of particle-cell interactions[160]. However, the role of stiffness on cellular functions is an emerging area, both for particulates and bulk materials. Recently, it has been established that stiffness of the substrate presenting antigens influences B cell activation[238]. Presentation from stiffer substrates induced greater B cell activation through enhanced microcluster formation and expression of activation markers. In another study, B cell proliferation was enhanced when antigens were presented on a soft substrate compared to a stiff substrate, highlighting the differences in downstream signaling upon activation based on B cell mechanosensing[239]. This mechanosensing mechanism of B cells depends on differences in microtubule network formation unlike actin cytoskeleton based changes in macrophages. While the mechanisms between these immune cells are different, it is possible that macrophage functions like cytokine production or antigen presentation are influenced during the mechanosensing based phagocytic process. From our data, rod shape particles functionalized with a ligand influences macrophage cytokine production during

the phagocytosis process. When stiffness of this shape is altered, it may not only influence macrophage cytokine production but also antigen presentation, based on the combination of these biophysical properties. Understanding the role of these properties on cellular functions may help design better vaccines and enhance therapeutic efficacy in macrophage induced autoimmune diseases like rheumatoid arthritis[240].

Ultimately, these studies have provided the biomaterials community with a novel technique that enables the fabrication of tunable particles and provides insight on the role of individual or combined particle properties in altering biological outcomes. This platform provides avenues for the design of advanced carriers incorporating varied physical properties and multiple biochemical signals for drug delivery, understanding membrane mechanics, or replicating native immune interfaces. The combination of particle properties and the choice of biochemical signal can enhance the therapeutic outcome based on the type of disease involved. For example, the enhanced internalization of rod capsules upon interaction with macrophages can have applications in rheumatoid arthritis where these cells are the systemic amplifiers of the disease[240]. Functionalization of these capsules with anti-inflammatory self-molecules like CD200 can attenuate inflammation by inducing an anti-inflammatory phenotype in macrophages[241]. Further, signaling ability of functionalized self- molecules on particles has been shown to be dependent on both the particle shape and rigidity[232]. Taking advantage of the rod capsules' ability to deform can enhance the ability of CD200 to signal self and inhibit inflammation. Further, particles can be endowed with new functionalities, such as stimuli- responsiveness, leading to new strategies for immunotherapy. The integration of such tunable particle platforms with the

understanding of intrinsic material properties will lead to exciting applications in the field

of immune engineering.

APPENDIX A. ELASTICITY OF HOLLOW COLLOIDAL

PARTICLES

The elasticity of thin spherical shells like microcapsules has been derived analytically[167] and is known as

$$k_{shell} = \frac{d^2}{R} \frac{2E}{\sqrt{3(1 - \triangle^2)}}$$

where k_{shell} is the shell spring constant, d is the thickness of the shell, R its radius, $\triangle$ the poisson ratio and E the Young's modulus of the material. Thus the stiffness of spherical capsule is inversely proportional to the radius for the same material properties.

APPENDIX B. MPC STRUCTURE
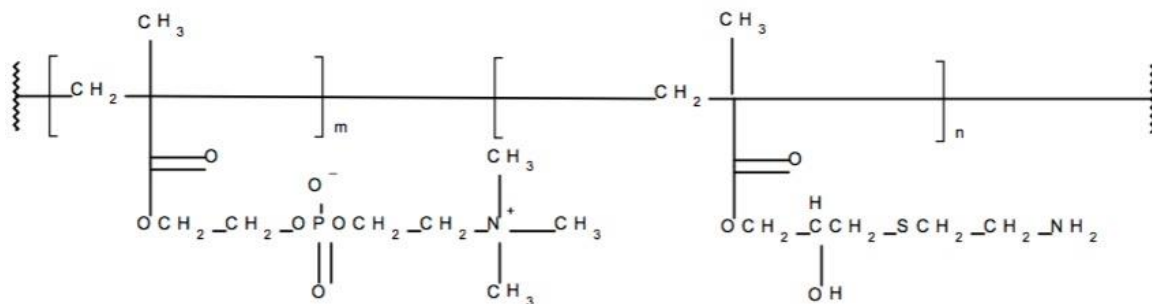
Figure B.1 MPC Structure

REFERENCES

1. Duncan R. Drug-polymer conjugates: potential for improved chemotherapy. *Anticancer Drugs*. 1992;3(3).

2. Mitragotri S, Lahann J. Physical approaches to biomaterial design. *Nat Mater*. 2009;8(1):15-23.

3. Yoo J-W, Irvine DJ, Discher DE, Mitragotri S. Bio-inspired, bioengineered and biomimetic drug delivery carriers. *Nat Rev Drug Discov*. 2011;10(7):521-535.

4. Tiwari G, Tiwari R, Sriwastawa B, et al. Drug delivery systems: An updated review. *Int J Pharm Investig*. 2012;2(1):2.

5. Owens III DE, Peppas NA. Opsonization, biodistribution, and pharmacokinetics of polymeric nanoparticles. *Int J Pharm*. 2006;307(1):93-102.

6. Tabata Y, Ikada Y. Effect of the size and surface charge of polymer microspheres on their phagocytosis by macrophage. *Biomaterials*. 1988;9(4):356-362.

7. Champion JA, Walker A, Mitragotri S. Role of particle size in phagocytosis of polymeric microspheres. *Pharm Res*. 2008;25(8):1815-1821. doi:10.1007/s11095-008-9562-y.

8. Champion JA, Mitragotri S. Role of target geometry in phagocytosis. *Proc Natl Acad Sci U S A*. 2006;103(13):4930-4934.

9. Beningo KA, Wang Y. Fc-receptor-mediated phagocytosis is regulated by

mechanical properties of the target. *J Cell Sci*. 2002;115(Pt 4):849-856.

10. Ahsan F, Rivas IP, Khan MA, Torres Suárez AI. Targeting to macrophages: role of physicochemical properties of particulate carriers—liposomes and microspheres—on the phagocytosis by macrophages. *J Control Release*. 2002;79(1–3):29-40.

11. Young KD. The selective value of bacterial shape. *Microbiol Mol Biol Rev*. 2006;70(3):660-703.

12. Muzykantov VR. Drug delivery by red blood cells: vascular carriers designed by mother nature. *Expert Opin Drug Deliv*. 2010;7(4):403-427.

13. Freiberg S, Zhu XX. Polymer microspheres for controlled drug release. *Int J Pharm*. 2004;282(1):1-18.

14. Berkland C, Kim KK, Pack DW. Fabrication of PLG microspheres with precisely controlled and monodisperse size distributions. *J Control Release*. 2001;73(1):59-74.

15. Moghimi SM, Hunter AC, Murray JC. Long-Circulating and Target-Specific Nanoparticles: Theory to Practice. *Pharmacol Rev*. 2001;53(2):283 LP-318.

16. Tao SL, Desai TA. Microfabricated drug delivery systems: from particles to pores. *Adv Drug Deliv Rev*. 2003;55(3):315-328. doi:http://dx.doi.org/10.1016/S0169-409X(02)00227-2.

17. Zambaux MF, Bonneaux F, Gref R, et al. Influence of experimental parameters on the characteristics of poly (lactic acid) nanoparticles prepared by a double emulsion

method. *J Control Release*. 1998;50(1):31-40.

18.   Kohane DS. Microparticles and nanoparticles for drug delivery. *Biotechnol Bioeng*. 2007;96(2):203-209. doi:10.1002/bit.21301.

19.   Wileman T, Harding C, Stahl P. Receptor-mediated endocytosis. *Biochem J*. 1985;232(1):1.

20.   Champion JA, Katare YK, Mitragotri S. Particle shape: a new design parameter for micro-and nanoscale drug delivery carriers. *J Control Release*. 2007;121(1):3-9.

21.   Stolnik S, Illum L, Davis SS. Long circulating microparticulate drug carriers. *Adv Drug Deliv Rev*. 1995;16(2):195-214.

22.   Acharya S, Sahoo SK. PLGA nanoparticles containing various anticancer agents and tumour delivery by EPR effect. *Adv Drug Deliv Rev*. 2011;63(3):170-183.

23.   Prabhakar U, Maeda H, Jain RK, et al. Challenges and key considerations of the enhanced permeability and retention effect for nanomedicine drug delivery in oncology. *Cancer Res*. 2013;73(8):2412-2417.

24.   Edwards DA, Ben-Jebria A, Langer R. Recent advances in pulmonary drug delivery using large, porous inhaled particles. *J Appl Physiol*. 1998;85(2):379-385.

25.   Castellano F, Chavrier P, Caron E. Actin dynamics during phagocytosis. *Semin Immunol*. 2001;13. doi:10.1006/smim.2001.0331.

26.   Simon SI, Schmid-Schönbein GW. Biophysical aspects of microsphere engulfment by human neutrophils. *Biophys J*. 1988;53(2):163.

27.	Doshi N, Mitragotri S. Macrophages Recognize Size and Shape of Their Targets. *PLoS One*. 2010;5(4):e10051.

28.	Dendukuri D, Pregibon DC, Collins J, Hatton TA, Doyle PS. Continuous-flow lithography for high-throughput microparticle synthesis. *Nat Mater*. 2006;5(5):365-369.

29.	Manoharan VN, Elsesser MT, Pine DJ. Dense packing and symmetry in small clusters of microspheres. *Science (80-)*. 2003;301(5632):483-487.

30.	Mohraz A, Solomon MJ. Direct visualization of colloidal rod assembly by confocal microscopy. *Langmuir*. 2005;21(12):5298-5306.

31.	Ho CC, Keller A, Odell JA, Ottewill RH. Preparation of monodisperse ellipsoidal polystyrene particles. *Colloid Polym Sci*. 1993;271(5):469-479.

32.	Champion JA, Katare YK, Mitragotri S. Making polymeric micro- and nanoparticles of complex shapes. *Proc Natl Acad Sci U S A*. 2007;104(29):11901-11904. doi:10.1073/pnas.0705326104.

33.	Rolland JP, Maynor BW, Euliss LE, Exner AE, Denison GM, DeSimone JM. Direct fabrication and harvesting of monodisperse, shape-specific nanobiomaterials. *J Am Chem Soc*. 2005;127(28):10096-10100.

34.	Champion JA, Mitragotri S. Shape induced inhibition of phagocytosis of polymer particles. *Pharm Res*. 2009;26.

35.	Sharma G, Valenta DT, Altman Y, et al. Polymer particle shape independently

influences binding and internalization by macrophages. *J Control release*. 2010;147(3):408-412.

36.   Barua S, Yoo J-W, Kolhar P, Wakankar A, Gokarn YR, Mitragotri S. Particle shape enhances specificity of antibody-displaying nanoparticles. *Proc Natl Acad Sci*. 2013;110(9):3270-3275. doi:10.1073/pnas.1216893110.

37.   Geng Y, Dalhaimer P, Cai S, et al. Shape effects of filaments versus spherical particles in flow and drug delivery. *Nat Nanotechnol*. 2007;2(4):249-255.

38.   Christian DA, Cai S, Garbuzenko OB, et al. Flexible filaments for in vivo imaging and delivery: persistent circulation of filomicelles opens the dosage window for sustained tumor shrinkage. *Mol Pharm*. 2009;6(5):1343-1352.

39.   Gentile F, Chiappini C, Fine D, et al. The effect of shape on the margination dynamics of non-neutrally buoyant particles in two-dimensional shear flows. *J Biomech*. 2008;41(10):2312-2318.

40.   Tenzer S, Docter D, Kuharev J, et al. Rapid formation of plasma protein corona critically affects nanoparticle pathophysiology. *Nat Nano*. 2013;8(10):772-781.

41.   Tabata Y, Ikada Y. Effect of the size and surface charge of polymer microspheres on their phagocytosis by macrophage. *Biomaterials*. 1988;9(4):356-362.

42.   Kaminskas LM, Boyd BJ. Nanosized Drug Delivery Vectors and the Reticuloendothelial System. In: Prokop A, ed. *Intracellular Delivery: Fundamentals and Applications*. Dordrecht: Springer Netherlands; 2011:155-178.

43. Mortimer GM, Butcher NJ, Musumeci AW, Deng ZJ, Martin DJ, Minchin RF. Cryptic Epitopes of Albumin Determine Mononuclear Phagocyte System Clearance of Nanomaterials. *ACS Nano*. 2014;8(4):3357-3366.

44. Feng W, Zhu S, Ishihara K, Brash JL. Protein resistant surfaces: comparison of acrylate graft polymers bearing oligo-ethylene oxide and phosphorylcholine side chains. *Biointerphases*. 2006;1(1):50.

45. Schellekens H, Hennink W, Brinks V. The Immunogenicity of Polyethylene Glycol: Facts and Fiction. *Pharm Res*. 2013;30(7):1729-1734.

46. Verhoef JJF, Carpenter JF, Anchordoquy TJ, Schellekens H. Potential induction of anti-PEG antibodies and complement activation toward PEGylated therapeutics. *Drug Discov Today*. 2014.

47. Liu S, Jiang S. Zwitterionic polymer-protein conjugates reduce polymer-specific antibody response. *Nano Today*. 2016;11(3):285-291.

48. Hu C-MJ, Zhang L, Aryal S, Cheung C, Fang RH, Zhang L. Erythrocyte membrane-camouflaged polymeric nanoparticles as a biomimetic delivery platform. *Proc Natl Acad Sci*. 2011.

49. Copp JA, Fang RH, Luk BT, et al. Clearance of pathological antibodies using biomimetic nanoparticles. *Proc Natl Acad Sci*. 2014;111(37):13481-13486. doi:10.1073/pnas.1412420111.

50. Toledano Furman NE, Lupu-Haber Y, Bronshtein T, et al. Reconstructed Stem Cell

Nanoghosts: A Natural Tumor Targeting Platform. *Nano Lett*. 2013;13(7):3248-3255. doi:10.1021/nl401376w.

51.   Rodriguez PL, Harada T, Christian DA, Pantano DA, Tsai RK, Discher DE. Minimal" Self" peptides that inhibit phagocytic clearance and enhance delivery of nanoparticles. *Science (80-)*. 2013;339(6122):971-975.

52.   Pacheco P, White D, Sulchek T. Effects of Microparticle Size and Fc Density on Macrophage Phagocytosis. *PLoS One*. 2013;8(4):e60989.

53.   Cui J, De Rose R, Best JP, et al. Mechanically Tunable, Self-Adjuvanting Nanoengineered Polypeptide Particles. *Adv Mater*. 2013;25(25):3468-3472.

54.   Alexander JF, Kozlovskaya V, Chen J, Kuncewicz T, Kharlampieva E, Godin B. Cubical Shape Enhances the Interaction of Layer-by-Layer Polymeric Particles with Breast Cancer Cells. *Adv Healthc Mater*. 2015;4(17):2657-2666.

55.   Anselmo AC, Zhang M, Kumar S, et al. Elasticity of nanoparticles influences their blood circulation, phagocytosis, endocytosis, and targeting. *ACS Nano*. 2015;9(3):3169-3177.

56.   Key J, Palange AL, Gentile F, et al. Soft Discoidal Polymeric Nanoconstructs Resist Macrophage Uptake and Enhance Vascular Targeting in Tumors. *ACS Nano*. 2015;9(12):11628-11641.

57.   Banquy X, Suarez F, Argaw A, et al. Effect of mechanical properties of hydrogel nanoparticles on macrophage cell uptake. *Soft Matter*. 2009;5(20):3984-3991.

58. Sun H, Wong EHH, Yan Y, et al. The role of capsule stiffness on cellular processing. *Chem Sci*. 2015;6(6):3505-3514. doi:10.1039/C5SC00416K.

59. Hartmann R, Weidenbach M, Neubauer M, Fery A, Parak WJ. Stiffness-Dependent In Vitro Uptake and Lysosomal Acidification of Colloidal Particles. *Angew Chemie Int Ed*. 2015;54(4):1365-1368.

60. Johnston APR, Cortez C, Angelatos AS, Caruso F. Layer-by-layer engineered capsules and their applications. *Curr Opin Colloid Interface Sci*. 2006;11(4):203-209.

61. Schuetz P, Caruso F. Copper-Assisted Weak Polyelectrolyte Multilayer Formation on Microspheres and Subsequent Film Crosslinking. *Adv Funct Mater*. 2003;13(12):929-937.

62. Cho J, Caruso F. Polymeric multilayer films comprising deconstructible hydrogen-bonded stacks confined between electrostatically assembled layers. *Macromolecules*. 2003;36(8):2845-2851.

63. Pan HM, Subramanian A, Ochs CJ, Dewavrin J-Y, Beyer S, Trau DW. Edible polyelectrolyte microcapsules with water-soluble cargo assembled in organic phase. *RSC Adv*. 2014;4(66):35163-35166. doi:10.1039/C4RA04750H.

64. Zelikin AN, Quinn JF, Caruso F. Disulfide cross-linked polymer capsules: en route to biodeconstructible systems. *Biomacromolecules*. 2006;7(1):27-30.

65. Correa S, Dreaden EC, Gu L, Hammond PT. Engineering nanolayered particles for

modular drug delivery. *J Control Release*. 2016;240:364-386.

66. Kharlampieva E, Kozlovskaya V, Sukhishvili SA. Layer-by-Layer Hydrogen-Bonded Polymer Films: From Fundamentals to Applications. *Adv Mater*. 2009;21(30):3053-3065.

67. De Temmerman M-L, Demeester J, De Vos F, De Smedt SC. Encapsulation performance of layer-by-layer microcapsules for proteins. *Biomacromolecules*. 2011;12(4):1283-1289.

68. Gittins DI, Caruso F. Multilayered polymer nanocapsules derived from gold nanoparticle templates. *Adv Mater*. 2000;12(24):1947-1949.

69. Neu B, Voigt A, Mitlöhner R, et al. Biological cells as templates for hollow microcapsules. *J Microencapsul*. 2001;18(3):385-395.

70. Balkundi SS, Veerabadran NG, Eby DM, Johnson GR, Lvov YM. Encapsulation of Bacterial Spores in Nanoorganized Polyelectrolyte Shells. *Langmuir*. 2009;25(24):14011-14016. doi:10.1021/la900971h.

71. Sukhishvili SA, Granick S. Layered, Erasable Polymer Multilayers Formed by Hydrogen-Bonded Sequential Self-Assembly. *Macromolecules*. 2002;35(1):301-310. doi:10.1021/ma011346c.

72. Shchepelina O, Lisunova MO, Drachuk I, Tsukruk V V. Morphology and Properties of Microcapsules with Different Core Releases. *Chem Mater*. 2012;24(7):1245-1254. doi:10.1021/cm202820r.

73. Shimoni O, Yan Y, Wang Y, Caruso F. Shape-Dependent Cellular Processing of Polyelectrolyte Capsules. *ACS Nano*. 2013;7(1):522-530.

74. Li H, Zhang W, Tong W, Gao C. Enhanced Cellular Uptake of Bowl-like Microcapsules. *ACS Appl Mater Interfaces*. 2016;8(18):11210-11214. doi:10.1021/acsami.6b02965.

75. Kozlovskaya V, Alexander JF, Wang Y, et al. Internalization of Red Blood Cell-Mimicking Hydrogel Capsules with pH-Triggered Shape Responses. *ACS Nano*. 2014;8(6):5725-5737. doi:10.1021/nn500512x.

76. Sexton A, Whitney PG, Chong S-F, et al. A Protective Vaccine Delivery System for In Vivo T Cell Stimulation Using Nanoengineered Polymer Hydrogel Capsules. *ACS Nano*. 2009;3(11):3391-3400. doi:10.1021/nn900715g.

77. Zhang P, Chiu Y-C, Tostanoski LH, Jewell CM. Polyelectrolyte multilayers assembled entirely from immune signals on gold nanoparticle templates promote antigen-specific T cell response. *ACS Nano*. 2015;9(6):6465-6477.

78. Fooksman DR, Vardhana S, Vasiliver-Shamis G, et al. Functional anatomy of T cell activation and synapse formation. *Annu Rev Immunol*. 2010;28:79.

79. Angus KL, Griffiths GM. Cell polarisation and the immunological synapse. *Curr Opin Cell Biol*. 2013;25(1):85-91.

80. Marcus ME, Leonard JN. FedExosomes: Engineering therapeutic biological nanoparticles that truly deliver. *Pharmaceuticals*. 2013;6(5):659-680.

81. Irvine DJ, Hanson MC, Rakhra K, Tokatlian T. Synthetic Nanoparticles for Vaccines and Immunotherapy. *Chem Rev*. 2015;115(19):11109-11146. doi:10.1021/acs.chemrev.5b00109.

82. Fang RH, Hu C-MJ, Luk BT, et al. Cancer Cell Membrane-Coated Nanoparticles for Anticancer Vaccination and Drug Delivery. *Nano Lett*. 2014;14(4):2181-2188. doi:10.1021/nl500618u.

83. Hu C-MJ, Fang RH, Copp J, Luk BT, Zhang L. A biomimetic nanosponge that absorbs pore-forming toxins. *Nat Nanotechnol*. 2013;8(5):336-340.

84. Mitchell MJ, Wayne E, Rana K, Schaffer CB, King MR. TRAIL-coated leukocytes that kill cancer cells in the circulation. *Proc Natl Acad Sci*. 2014;111(3):930-935.

85. Porotto M, Yi F, Moscona A, LaVan DA. Synthetic protocells interact with viral nanomachinery and inactivate pathogenic human virus. *PLoS One*. 2011;6(3):e16874.

86. Robbins GP, Saunders RL, Haun JB, Rawson J, Therien MJ, Hammer DA. Tunable leuko-polymersomes that adhere specifically to inflammatory markers. *Langmuir*. 2010;26(17):14089-14096.

87. Gao W, Fang R, Thamphiwatana S, et al. Modulating Antibacterial Immunity via Bacterial Membrane-Coated Nanoparticles. *Nano Lett*. 2015.

88. Moon JJ, Suh H, Li A V, Ockenhouse CF, Yadava A, Irvine DJ. Enhancing humoral responses to a malaria antigen with nanoparticle vaccines that expand Tfh cells and

promote germinal center induction. *Proc Natl Acad Sci*. 2012;109(4):1080-1085.

89.   De Geest BG, Willart MA, Lambrecht BN, et al. Surface-Engineered Polyelectrolyte Multilayer Capsules: Synthetic Vaccines Mimicking Microbial Structure and Function. *Angew Chemie*. 2012;124(16):3928-3932.

90.   Powell TJ, Tang J, DeRome ME, et al. < i> Plasmodium falciparum</i> synthetic LbL microparticle vaccine elicits protective neutralizing antibody and parasite-specific cellular immune responses. *Vaccine*. 2013;31(15):1898-1904.

91.   Bershteyn A, Hanson MC, Crespo MP, et al. Robust IgG responses to nanograms of antigen using a biomimetic lipid-coated particle vaccine. *J Control Release*. 2012;157(3):354-365.

92.   Kumar S, Anselmo AC, Banerjee A, Zakrewsky M, Mitragotri S. Shape and size-dependent immune response to antigen-carrying nanoparticles. *J Control Release*. 2015;220:141-148.

93.   Li Z, Sun L, Zhang Y, Dove AP, O'Reilly RK, Chen G. Shape effect of glyco-nanoparticles on macrophage cellular uptake and immune response. *ACS Macro Lett*. 2016;5(9):1059-1064.

94.   Sunshine JC, Green JJ. Nanoengineering approaches to the design of artificial antigen-presenting cells. *Nanomedicine*. 2013;8(7):1173-1189.

95.   Butler MO, Ansén S, Tanaka M, et al. A panel of human cell-based artificial APC enables the expansion of long-lived antigen-specific CD4+ T cells restricted by

prevalent HLA-DR alleles. *Int Immunol*. 2010:dxq440.

96. Steenblock ER, Wrzesinski SH, Flavell RA, Fahmy TM. Antigen presentation on artificial acellular substrates: modular systems for flexible, adaptable immunotherapy. 2009.

97. Ding Q, Chen J, Wei X, et al. RAFTsomes containing epitope-MHC-II complexes mediated CD4+ T cell activation and antigen-specific immune responses. *Pharm Res*. 2013;30(1):60-69.

98. Shen C, Cheng K, Miao S, et al. Latex bead-based artificial antigen-presenting cells induce tumor-specific CTL responses in the native T-cell repertoires and inhibit tumor growth. *Immunol Lett*. 2013;150(1):1-11.

99. Perica K, De León Medero A, Durai M, et al. Nanoscale artificial antigen presenting cells for T cell immunotherapy. *Nanomedicine Nanotechnology, Biol Med*. 2014;10(1):119-129.

100. Perica K, Tu A, Richter A, Bieler JG, Edidin M, Schneck JP. Magnetic field-induced T cell receptor clustering by nanoparticles enhances T cell activation and stimulates antitumor activity. *ACS Nano*. 2014;8(3):2252-2260.

101. Chen B, Jia Y, Gao Y, Sanchez L, Anthony SM, Yu Y. Janus Particles as Artificial Antigen-Presenting Cells for T Cell Activation. *ACS Appl Mater Interfaces*. 2014;6(21):18435-18439.

102. Sunshine JC, Perica K, Schneck JP, Green JJ. Particle shape dependence of CD8+

T cell activation by artificial antigen presenting cells. *Biomaterials*. 2014;35(1):269-277.

103. Steenblock ER, Fadel T, Labowsky M, Pober JS, Fahmy TM. An artificial antigen-presenting cell with paracrine delivery of IL-2 impacts the magnitude and direction of the T cell response. *J Biol Chem*. 2011;286(40):34883-34892.

104. Park JR, DiGiusto DL, Slovak M, et al. Adoptive Transfer of Chimeric Antigen Receptor Re-directed Cytolytic T Lymphocyte Clones in Patients with Neuroblastoma. *Mol Ther*. 2007;15(4):825-833.

105. Rushworth D, Jena B, Olivares S, et al. Universal Artificial Antigen Presenting Cells to Selectively Propagate T Cells Expressing Chimeric Antigen Receptor Independent of Specificity. *J Immunother*. 2014;37(4):204-213.

106. Van Seventer GA, Shimizu Y, Horgan KJ, Shaw S. The LFA-1 ligand ICAM-1 provides an important costimulatory signal for T cell receptor-mediated activation of resting T cells. *J Immunol*. 1990;144(12):4579-4586.

107. Chittasupho C, Shannon L, Siahaan TJ, Vines CM, Berkland C. Nanoparticles targeting dendritic cell surface molecules effectively block T cell conjugation and shift response. *ACS Nano*. 2011;5(3):1693-1702.

108. Lo Y-C, Edidin MA, Powell JD. Selective Activation of Antigen-Experienced T Cells by Anti-CD3 Constrained on Nanoparticles. *J Immunol*. 2013;191(10):5107-5114.

109. Kim YK, Que R, Wang S-W, Liu WF. Modification of Biomaterials with a Self-Protein Inhibits the Macrophage Response. *Adv Healthc Mater*. 2014;3(7):989-994.

110. Gray M, Miles K, Salter D, Gray D, Savill J. Apoptotic cells protect mice from autoimmune inflammation by the induction of regulatory B cells. *Proc Natl Acad Sci*. 2007;104(35):14080-14085. doi:10.1073/pnas.0700326104.

111. Getts DR, Turley DM, Smith CE, et al. Tolerance induced by apoptotic antigen-coupled leukocytes is induced by PD-L1+ and IL-10–producing splenic macrophages and maintained by T regulatory cells. *J Immunol*. 2011;187(5):2405-2417.

112. Lutterotti A, Yousef S, Sputtek A, et al. Antigen-Specific Tolerance by Autologous Myelin Peptide–Coupled Cells: A Phase 1 Trial in Multiple Sclerosis. *Sci Transl Med*. 2013;5(188):188ra75-188ra75.

113. Kontos S, Kourtis IC, Dane KY, Hubbell JA. Engineering antigens for in situ erythrocyte binding induces T-cell deletion. *Proc Natl Acad Sci*. 2013;110(1):E60-E68.

114. Getts DR, Martin AJ, McCarthy DP, et al. Microparticles bearing encephalitogenic peptides induce T-cell tolerance and ameliorate experimental autoimmune encephalomyelitis. *Nat Biotechnol*. 2012;30(12):1217-1224.

115. Tsai S, Shameli A, Yamanouchi J, et al. Reversal of autoimmunity by boosting memory-like autoregulatory T cells. *Immunity*. 2010;32(4):568-580.

116. Maldonado RA, LaMothe RA, Ferrari JD, et al. Polymeric synthetic nanoparticles for the induction of antigen-specific immunological tolerance. *Proc Natl Acad Sci*. 2015;112(2):E156-E165.

117. Hunter Z, McCarthy DP, Yap WT, et al. A Biodegradable Nanoparticle Platform for the Induction of Antigen-Specific Immune Tolerance for Treatment of Autoimmune Disease. *ACS Nano*. 2014;8(3):2148-2160.

118. Thomas SN, Vokali E, Lund AW, Hubbell JA, Swartz MA. Targeting the tumor-draining lymph node with adjuvanted nanoparticles reshapes the anti-tumor immune response. *Biomaterials*. 2014;35(2):814-824.

119. Sharp FA, Ruane D, Claass B, et al. Uptake of particulate vaccine adjuvants by dendritic cells activates the NALP3 inflammasome. *Proc Natl Acad Sci*. 2009;106(3):870-875.

120. Niikura K, Matsunaga T, Suzuki T, et al. Gold Nanoparticles as a Vaccine Platform: Influence of Size and Shape on Immunological Responses in Vitro and in Vivo. *ACS Nano*. 2013;7(5):3926-3938.

121. Sun B, Ji Z, Liao Y-P, et al. Engineering an effective immune adjuvant by designed control of shape and crystallinity of aluminum oxyhydroxide nanoparticles. *ACS Nano*. 2013;7(12):10834-10849.

122. Li WA, Lu BY, Gu L, Choi Y, Kim J, Mooney DJ. The effect of surface modification of mesoporous silica micro-rod scaffold on immune cell activation and infiltration. *Biomaterials*. 2016;83:249-256.

123. Vaine CA, Patel MK, Zhu J, et al. Tuning innate immune activation by surface texturing of polymer microparticles: the role of shape in inflammasome activation. *J Immunol*. 2013;190(7):3525-3532.

124. Chen X, Yan Y, Müllner M, et al. Shape-Dependent Activation of Cytokine Secretion by Polymer Capsules in Human Monocyte-Derived Macrophages. *Biomacromolecules*. 2016;17(3):1205-1212. doi:10.1021/acs.biomac.6b00027.

125. Shima F, Akagi T, Uto T, Akashi M. Manipulating the antigen-specific immune response by the hydrophobicity of amphiphilic poly(γ-glutamic acid) nanoparticles. *Biomaterials*. 2013;34(37):9709-9716.

126. Moyano DF, Goldsmith M, Solfiell DJ, et al. Nanoparticle Hydrophobicity Dictates Immune Response. *J Am Chem Soc*. 2012;134(9):3965-3967.

127. Reddy ST, van der Vlies AJ, Simeoni E, et al. Exploiting lymphatic transport and complement activation in nanoparticle vaccines. *Nat Biotechnol*. 2007;25(10):1159-1164.

128. Thomas SN, van der Vlies AJ, O'Neil CP, et al. Engineering complement activation on polypropylene sulfide vaccine nanoparticles. *Biomaterials*. 2011;32(8):2194-2203.

129. Broaders KE, Cohen JA, Beaudette TT, Bachelder EM, Fréchet JMJ. Acetalated dextran is a chemically and biologically tunable material for particulate immunotherapy. *Proc Natl Acad Sci*. 2009;106(14):5497-5502.

130. Li H, Li Y, Jiao J, Hu H-M. Alpha-alumina nanoparticles induce efficient autophagy-dependent cross-presentation and potent antitumour response. *Nat Nano*. 2011;6(10):645-650.

131. Liu H-L, Zhang Y-L, Yang N, et al. A functionalized single-walled carbon nanotube-induced autophagic cell death in human lung cells through Akt-TSC2-mTOR signaling. *Cell Death Dis*. 2011;2:e159.

132. Getts DR, Terry RL, Getts MT, et al. Therapeutic inflammatory monocyte modulation using immune-modifying microparticles. *Sci Transl Med*. 2014;6(219):219ra7-219ra7.

133. Anselmo AC, Kumar S, Gupta V, et al. Exploiting shape, cellular-hitchhiking and antibodies to target nanoparticles to lung endothelium: Synergy between physical, chemical and biological approaches. *Biomaterials*. 2015;68:1-8.

134. Becker AL, Johnston APR, Caruso F. Layer-By-Layer-Assembled Capsules and Films for Therapeutic Delivery. *Small*. 2010;6(17).

135. Liu Y, Tan J, Thomas A, Ou-Yang D, Muzykantov VR. The shape of things to come: importance of design in nanotechnology for drug delivery. *Ther Deliv*. 2012;3(2):181-194.

136. Fleischer CC, Payne CK. Nanoparticle Surface Charge Mediates the Cellular Receptors Used by Protein–Nanoparticle Complexes. *J Phys Chem B*. 2012;116(30):8901-8907.

137. Kawaguchi H, Koiwai N, Ohtsuka Y, Miyamoto M, Sasakawa S. Phagocytosis of latex particles by leucocytes. I. Dependence of phagocytosis on the size and surface potential of particles. *Biomaterials*. 1986;7(1):61-66.

138. Volodkin D V, Larionova NI, Sukhorukov GB. Protein encapsulation via porous CaCO3 microparticles templating. *Biomacromolecules*. 2004;5(5):1962-1972.

139. Perry JL, Herlihy KP, Napier ME, DeSimone JM. PRINT: a novel platform toward shape and size specific nanoparticle theranostics. *Acc Chem Res*. 2011;44(10):990-998.

140. Fu Y, Bai S, Cui S, Qiu D, Wang Z, Zhang X. Hydrogen-bonding-directed layer-by-layer multilayer assembly: reconformation yielding microporous films. *Macromolecules*. 2002;35(25):9451-9458.

141. Yang S, Zhang Y, Guan Y, et al. Water uptake behavior of hydrogen-bonded PVPON–PAA LBL film. *Soft Matter*. 2006;2(8):699-704.

142. Tian Y, He Q, Cui Y, Tao C, Li J. Assembly of Nanotubes of Poly (4-vinylpyridine) and Poly (acrylic acid) through Hydrogen Bonding. *Chem Eur J*. 2006;12(18):4808-4812.

143. Zhang H, Wang Z, Zhang Y, Zhang X. Hydrogen-bonding-directed layer-by-layer assembly of poly (4-vinylpyridine) and poly (4-vinylphenol): effect of solvent composition on multilayer buildup. *Langmuir*. 2004;20(21):9366-9370.

144. Kim B-S, Lebedeva O V, Koynov K, et al. Effect of organic solvent on the

permeability and stiffness of polyelectrolyte multilayer microcapsules. *Macromolecules*. 2005;38(12):5214-5222.

145. Jang J, Lee K. Facile fabrication of hollow polystyrene nanocapsules by microemulsion polymerization. *Chem Commun*. 2002;(10):1098-1099.

146. Ye S, Wang C, Liu X, Tong Z. Multilayer nanocapsules of polysaccharide chitosan and alginate through layer-by-layer assembly directly on PS nanoparticles for release. *J Biomater Sci Polym Ed*. 2005;16(7):909-923.

147. Rice-Ficht AC, Arenas-Gamboa AM, Kahl-McDonagh MM, Ficht TA. Polymeric particles in vaccine delivery. *Curr Opin Microbiol*. 2010;13(1):106-112.

148. Tang BC, Dawson M, Lai SK, et al. Biodegradable polymer nanoparticles that rapidly penetrate the human mucus barrier. *Proc Natl Acad Sci*. 2009;106(46):19268-19273.

149. Shang L, Nienhaus K, Nienhaus GU. Engineered nanoparticles interacting with cells: size matters. *J Nanobiotechnol*. 2014;12(5):b26.

150. Fleischer CC, Payne CK. Secondary Structure of Corona Proteins Determines the Cell Surface Receptors Used by Nanoparticles. *J Phys Chem B*. 2014;118(49):14017-14026.

151. Gref R, Lu M. " Stealth " corona-core nanoparticles surface modified by polyethylene glycol (PEG): influences of the corona (PEG chain length and surface density) and of the core composition on phagocytic uptake and plasma protein

adsorption. 2000;18:301-313.

152. Ishihara K, Takai M. Bioinspired interface for nanobiodevices based on phospholipid polymer chemistry. *J R Soc Interface*. 2009;6(Suppl 3):S279-S291.

153. Champion JA, Mitragotri S. Shape induced inhibition of phagocytosis of polymer particles. *Pharm Res*. 2009;26(1):244-249.

154. Beningo KA, Wang Y. Fc-receptor-mediated phagocytosis is regulated by mechanical properties of the target. *J Cell Sci*. 2002;115(4):849-856.

155. Zan X, Garapaty A, Champion JA. Engineering Polyelectrolyte Capsules with Independently Controlled Size and Shape. *Langmuir*. 2015;31(27):7601-7608.

156. Kim B-S, Park SW, Hammond PT. Hydrogen-bonding layer-by-layer-assembled biodegradable polymeric micelles as drug delivery vehicles from surfaces. *ACS Nano*. 2008;2(2):386-392.

157. Zelikin AN, Li Q, Caruso F. Disulfide-stabilized poly (methacrylic acid) capsules: formation, cross-linking, and degradation behavior. *Chem Mater*. 2008;20(8):2655-2661.

158. Sangsuwan A, Narupai B, Sae-ung P, Rodtamai S, Rodthongkum N, Hoven VP. Patterned Poly (acrylic acid) Brushes Containing Gold Nanoparticles for Peptide Detection by Surface-Assisted Laser Desorption/Ionization Mass Spectrometry. *Anal Chem*. 2015;87(21):10738-10746.

159. Davis ME, Shin DM. Nanoparticle therapeutics: an emerging treatment modality for

cancer. *Nat Rev Drug Discov*. 2008;7(9):771-782.

160. Anselmo AC, Mitragotri S. Impact of particle elasticity on particle-based drug delivery systems. *Adv Drug Deliv Rev*. 2016.

161. Gilberti RM, Knecht DA. Macrophages phagocytose nonopsonized silica particles using a unique microtubule-dependent pathway. *Mol Biol Cell*. 2015;26(3):518-529.

162. Aderem A, Underhill DM. Mechanisms of phagocytosis in macrophages. *Annu Rev Immunol*. 1999;17:593-623. doi:10.1146/annurev.immunol.17.1.593.

163. Lo S-C, Scearce-Levie K, Sheng M. Characterization of Social Behaviors in caspase-3 deficient mice. *Sci Rep*. 2016;6.

164. Paul D, Achouri S, Yoon Y-Z, Herre J, Bryant CE, Cicuta P. Phagocytosis dynamics depends on target shape. *Biophys J*. 2013;105(5):1143-1150.

165. Tollis S, Dart AE, Tzircotis G, Endres RG. The zipper mechanism in phagocytosis: energetic requirements and variability in phagocytic cup shape. *BMC Syst Biol*. 2010;4(1):1-17. doi:10.1186/1752-0509-4-149.

166. Tang H, Zhang H, Ye H, Zheng Y. Wrapping of a deformable nanoparticle by the cell membrane: Insights into the flexibility-regulated nanoparticle-membrane interaction. *J Appl Phys*. 2016;120(11):114701.

167. Zoldesi CI, Ivanovska IL, Quilliet C, Wuite GJL, Imhof A. Elastic properties of hollow colloidal particles. *Phys Rev E*. 2008;78(5):51401.

168. Gao C, Leporatti S, Moya S, Donath E, Möhwald H. Stability and mechanical

properties of polyelectrolyte capsules obtained by stepwise assembly of poly (styrenesulfonate sodium salt) and poly (diallyldimethyl ammonium) chloride onto melamine resin particles. *Langmuir*. 2001;17(11):3491-3495.

169. Yi X, Gao H. Cell membrane wrapping of a spherical thin elastic shell. *Soft Matter*. 2015;11(6):1107-1115.

170. Mueller R, Daehne L, Fery A. Hollow Polyelectrolyte Multilayer Tubes: Mechanical Properties and Shape Changes. *J Phys Chem B*. 2007;111(29):8547-8553.

171. Mueller R, Daehne L, Fery A. Preparation and mechanical characterization of artificial hollow tubes. *Polymer (Guildf)*. 2007;48(9):2520-2525.

172. Knoche S, Vella D, Aumaitre E, et al. Elastometry of Deflated Capsules: Elastic Moduli from Shape and Wrinkle Analysis. *Langmuir*. 2013;29(40):12463-12471.

173. Li H, Leow WK, Chiu I. Elastic tubes: modeling elastic deformation of hollow tubes. In: *Computer Graphics Forum*. Vol 29. Wiley Online Library; 2010:1770-1782.

174. Shimeta J, Jumars PA. Physical mechanisms and rates of particle capture by suspension-feeders. *Ocean Mar Biol Annu Rev*. 1991;29(19):l-257.

175. Richards DM, Endres RG. Target shape dependence in a simple model of receptor-mediated endocytosis and phagocytosis. *Proc Natl Acad Sci*. 2016;113(22):6113-6118.

176. Bahrami AH, Lipowsky R, Weikl TR. The role of membrane curvature for the

wrapping of nanoparticles. *Soft Matter*. 2016;12(2):581-587.

177. Palankar R, Pinchasik B-E, Schmidt S, et al. Mechanical strength and intracellular uptake of CaCO3-templated LbL capsules composed of biodegradable polyelectrolytes: the influence of the number of layers. *J Mater Chem B*. 2013;1(8):1175-1181.

178. Yi X, Shi X, Gao H. Cellular Uptake of Elastic Nanoparticles. *Phys Rev Lett*. 2011;107(9):98101.

179. Goto Y, Matsuno R, Konno T, Takai M, Ishihara K. Polymer nanoparticles covered with phosphorylcholine groups and immobilized with antibody for high-affinity separation of proteins. *Biomacromolecules*. 2008;9(3):828-833.

180. Ishihara K, Oshida H, Endo Y, Ueda T, Watanabe A, Nakabayashi N. Hemocompatibility of human whole blood on polymers with a phospholipid polar group and its mechanism. *J Biomed Mater Res*. 1992;26(12):1543-1552. doi:10.1002/jbm.820261202.

181. Chen S, Liu L, Jiang S. Strong resistance of oligo(phosphorylcholine) self-assembled monolayers to protein adsorption. *Langmuir*. 2006;22(6):2418-2421.

182. Xu Y, Takai M, Ishihara K. Protein adsorption and cell adhesion on cationic, neutral, and anionic 2-methacryloyloxyethyl phosphorylcholine copolymer surfaces. *Biomaterials*. 2009;30(28):4930-4938.

183. Lewis AL, Cumming ZL, Goreish HH, Kirkwood LC, Tolhurst LA, Stratford PW.

Crosslinkable coatings from phosphorylcholine-based polymers. *Biomaterials*. 2001;22(2):99-111.

184. Lewis AL, Hughes PD, Kirkwood LC, et al. Synthesis and characterisation of phosphorylcholine-based polymers useful for coating blood filtration devices. *Biomaterials*. 2000;21(18):1847-1859.

185. Gref R, Lück M, Quellec P, et al. "Stealth" corona-core nanoparticles surface modified by polyethylene glycol (PEG): influences of the corona (PEG chain length and surface density) and of the core composition on phagocytic uptake and plasma protein adsorption. *Colloids Surfaces B Biointerfaces*. 2000;18(3–4):301-313.

186. Meng F, Engbers GHM, Feijen J. Polyethylene glycol–grafted polystyrene particles. *J Biomed Mater Res Part A*. 2004;70A(1):49-58.

187. Cedervall T, Lynch I, Lindman S, et al. Understanding the nanoparticle–protein corona using methods to quantify exchange rates and affinities of proteins for nanoparticles. *Proc Natl Acad Sci*. 2007;104(7):2050-2055.

188. Moro T, Takatori Y, Kyomoto M, et al. Surface grafting of biocompatible phospholipid polymer MPC provides wear resistance of tibial polyethylene insert in artificial knee joints. *Osteoarthr Cartil*. 2010;18(9):1174-1182.

189. Doorley GW, Payne CK. Cellular binding of nanoparticles in the presence of serum proteins. *Chem Commun*. 2011;47(1):466-468.

190. Deng ZJ, Liang M, Monteiro M, Toth I, Minchin RF. Nanoparticle-induced

unfolding of fibrinogen promotes Mac-1 receptor activation and inflammation. *Nat Nanotechnol*. 2011;6(1):39-44.

191.   Runa S, Hill A, Cochran VL, Payne CK. PEGylated nanoparticles: protein corona and secondary structure. Banerji N, Hayes SC, Silva C, eds. *ProcSPIE*. September 2014:91651F. doi:10.1117/12.2062767.

192.   Wattendorf U, Merkle HP. PEGylation as a tool for the biomedical engineering of surface modified microparticles. *J Pharm Sci*. 2008;97(11):4655-4669.

193.   Fleischer CC, Kumar U, Payne CK. Cellular binding of anionic nanoparticles is inhibited by serum proteins independent of nanoparticle composition. *Biomater Sci*. 2013;1(9):975-982.

194.   Cho EC, Au L, Zhang Q, Xia Y. The effects of size, shape, and surface functional group of gold nanostructures on their adsorption and internalization by cells. *Small*. 2010;6(4):517-522.

195.   Thiele L, Diederichs JE, Reszka R, Merkle HP, Walter E. Competitive adsorption of serum proteins at microparticles affects phagocytosis by dendritic cells. *Biomaterials*. 2003;24(8):1409-1418.

196.   Patil S, Sandberg A, Heckert E, Self W, Seal S. Protein adsorption and cellular uptake of cerium oxide nanoparticles as a function of zeta potential. *Biomaterials*. 2007;28(31):4600-4607.

197.   Chen S, Zheng J, Li L, Jiang S. Strong Resistance of Phosphorylcholine Self-

Assembled Monolayers to Protein Adsorption: Insights into Nonfouling Properties of Zwitterionic Materials. *J Am Chem Soc*. 2005;127(41):14473-14478.

198. Clarke S, Davies MC, Roberts CJ, et al. Surface Mobility of 2-Methacryloyloxyethyl Phosphorylcholine-co-Lauryl Methacrylate Polymers. *Langmuir*. 2000;16(11):5116-5122.

199. Georgiev GS, Kamenska EB, Vassileva ED, et al. Self-Assembly, Antipolyelectrolyte Effect, and Nonbiofouling Properties of Polyzwitterions. *Biomacromolecules*. 2006;7(4):1329-1334. doi:10.1021/bm050938q.

200. Poptoshev E, Schoeler B, Caruso F. Influence of Solvent Quality on the Growth of Polyelectrolyte Multilayers. *Langmuir*. 2004;20(3):829-834. doi:10.1021/la035485u.

201. Garapaty A, Champion JA. Biomimetic and synthetic interfaces to tune immune responses. *Biointerphases*. 2015;10(3):30801.

202. Tran KK, Shen H. The role of phagosomal pH on the size-dependent efficiency of cross-presentation by dendritic cells. *Biomaterials*. 2009;30(7):1356-1362.

203. Qie Y, Yuan H, von Roemeling CA, et al. Surface modification of nanoparticles enables selective evasion of phagocytic clearance by distinct macrophage phenotypes. *Sci Rep*. 2016;6.

204. Wurster E-C, Liebl R, Michaelis S, et al. Oligolayer-Coated Nanoparticles: Impact of Surface Topography at the Nanobio Interface. *ACS Appl Mater Interfaces*.

2015;7(15):7891-7900.

205. Steinkamp JA, Wilson JS, Saunders GC, Stewart CC. Phagocytosis: flow cytometric quantitation with fluorescent microspheres. *Science (80-)*. 1982;215(4528):64-66.

206. Gonçalves R, Mosser DM. The isolation and characterization of murine macrophages. *Curr Protoc Immunol*. 2008:11-14.

207. Holmannová D, Kolackova M, Kondelkova K, Kunes P, Krejsek J, Andrys C. CD200/CD200R paired potent inhibitory molecules regulating immune and inflammatory responses; Part I: CD200/CD200R structure, activation, and function. *acta Medica (hradec Králové)*. 2012;55(1):12-17.

208. Stepanenko O V, Stepanenko O V, Kuznetsova IM, Verkhusha V V, Turoverov KK. Beta-barrel scaffold of fluorescent proteins: folding, stability and role in chromophore formation. *Int Rev Cell Mol Biol*. 2013;302:221.

209. Vessoni Penna TC, Ishii M, Cholewa O, De Souza LC. Thermal characteristics of recombinant green fluorescent protein (GFPuv) extracted from Escherichia coli. *Lett Appl Microbiol*. 2004;38(2):135-139.

210. Sobota A, Strzelecka-Kiliszek A, Gladkowska A, Yoshida K, Mrozinska K, Kwiatkowska K. Binding of IgG-opsonized particles to FcγR is an active stage of phagocytosis that involves receptor clustering and phosphorylation. *J Immunol*. 2005;175.

211. Autenrieth SE, Autenrieth IB. Variable antigen uptake due to different expression

of the macrophage mannose receptor by dendritic cells in various inbred mouse strains. *Immunology*. 2009;127(4):523-529.

212. Vallabhapurapu S, Karin M. Regulation and function of NF-κB transcription factors in the immune system. *Annu Rev Immunol*. 2009;27:693-733.

213. Huang Z, Hoffmann FW, Fay JD, et al. Stimulation of unprimed macrophages with immune complexes triggers a low output of nitric oxide by calcium-dependent neuronal nitric-oxide synthase. *J Biol Chem*. 2012;287(7):4492-4502.

214. Pacheco PM. Fc coated micro/nanoparticles for humoral immune system modulation. 2014.

215. Underhill DM, Goodridge HS. Information processing during phagocytosis. *Nat Rev Immunol*. 2012;12(7):492-502.

216. Garapaty A, Champion JA. Tunable particles alter macrophage uptake based on combinatorial effects of physical properties. *Bioeng Transl Med*. November 2016. doi:10.1002/btm2.10047.

217. Chang TZ, Stadmiller SS, Staskevicius E, Champion JA. Effects of ovalbumin protein nanoparticle vaccine size and coating on dendritic cell processing. *Biomater Sci*. 2017.

218. Yoo J, Doshi N, Mitragotri S. Endocytosis and intracellular distribution of PLGA particles in endothelial cells: effect of particle geometry. *Macromol Rapid Commun*. 2010;31(2):142-148.

219. Muro S, Garnacho C, Champion JA, et al. Control of endothelial targeting and intracellular delivery of therapeutic enzymes by modulating the size and shape of ICAM-1-targeted carriers. *Mol Ther*. 2008;16(8):1450-1458.

220. Deng ZJ, Liang M, Monteiro M, Toth I, Minchin RF. Nanoparticle-induced unfolding of fibrinogen promotes Mac-1 receptor activation and inflammation. *Nat Nanotechnol*. 2011;6(1):39-44.

221. Chakraborty S, Joshi P, Shanker V, Ansari ZA, Singh SP, Chakrabarti P. Contrasting effect of gold nanoparticles and nanorods with different surface modifications on the structure and activity of bovine serum albumin. *Langmuir*. 2011;27(12):7722-7731.

222. Ramezani F, Amanlou M, Rafii-Tabar H. Gold nanoparticle shape effects on human serum albumin corona interface: a molecular dynamic study. *J Nanoparticle Res*. 2014;16(7):2512.

223. Yan Y, Gause KT, Kamphuis MMJ, et al. Differential roles of the protein corona in the cellular uptake of nanoporous polymer particles by monocyte and macrophage cell lines. *ACS Nano*. 2013;7(12):10960-10970.

224. Barclay AN, Wright GJ, Brooke G, Brown MH. CD200 and membrane protein interactions in the control of myeloid cells. *Trends Immunol*. 2002;23(6):285-290.

225. Brown GC, Neher JJ. Eaten alive! Cell death by primary phagocytosis: ‘phagoptosis’ *Trends Biochem Sci*. 2017;37(8):325-332. doi:10.1016/j.tibs.2012.05.002.

226. Hoek RM, Ruuls SR, Murphy CA, et al. Down-regulation of the macrophage lineage through interaction with OX2 (CD200). *Science (80-)*. 2000;290(5497):1768-1771.

227. Wright GJ, Puklavec MJ, Willis AC, et al. Lymphoid/neuronal cell surface OX2 glycoprotein recognizes a novel receptor on macrophages implicated in the control of their function. *Immunity*. 2000;13(2):233-242.

228. Gorczynski RM, Chen Z, Yu K, Hu J. CD200 immunoadhesin suppresses collagen-induced arthritis in mice. *Clin Immunol*. 2001;101(3):328-334.

229. Liu Y, Bando Y, Vargas-Lowy D, et al. CD200R1 agonist attenuates mechanisms of chronic disease in a murine model of multiple sclerosis. *J Neurosci*. 2010;30(6):2025-2038.

230. Snelgrove RJ, Goulding J, Didierlaurent AM, et al. A critical function for CD200 in lung immune homeostasis and the severity of influenza infection. *Nat Immunol*. 2008;9(9):1074-1083.

231. Gorczynski RM, Cattral MS, Chen Z, et al. An immunoadhesin incorporating the molecule OX-2 is a potent immunosuppressant that prolongs allo-and xenograft survival. *J Immunol*. 1999;163(3):1654-1660.

232. Sosale NG, Rouhiparkouhi T, Bradshaw AM, Dimova R, Lipowsky R, Discher DE. Cell rigidity and shape override CD47's "self"-signaling in phagocytosis by hyperactivating myosin-II. *Blood*. 2015;125(3):542 LP-552.

233. Tostanoski LH, Chiu Y-C, Andorko JI, et al. Design of Polyelectrolyte Multilayers

to Promote Immunological Tolerance. *ACS Nano*. 2016;10(10):9334-9345.

234. Wong SY, Han L, Timachova K, et al. Drastically lowered protein adsorption on microbicidal hydrophobic/hydrophilic polyelectrolyte multilayers. *Biomacromolecules*. 2012;13(3):719-726.

235. Vegas AJ, Veiseh O, Doloff JC, et al. Combinatorial hydrogel library enables identification of materials that mitigate the foreign body response in primates. *Nat Biotechnol*. 2016;34(3):345-352.

236. Ben M'Barek K, Molino D, Quignard S, et al. Phagocytosis of immunoglobulin-coated emulsion droplets. *Biomaterials*. 2015;51:270-277.

237. Balce DR, Rybicka JM, Greene CJ, Ewanchuk BW, Yates RM. Ligation of FcγR Alters Phagosomal Processing of Protein via Augmentation of NADPH Oxidase Activity. *Traffic*. 2016.

238. Wan Z, Zhang S, Fan Y, et al. B cell activation is regulated by the stiffness properties of the substrate presenting the antigens. *J Immunol*. 2013;190(9):4661-4675.

239. Zeng Y, Yi J, Wan Z, et al. Substrate stiffness regulates B-cell activation, proliferation, class switch, and T-cell-independent antibody responses in vivo. *Eur J Immunol*. 2015;45(6):1621-1634. doi:10.1002/eji.201444777.

240. Kinne RW, Stuhlmüller B, Burmester G-R. Cells of the synovium in rheumatoid arthritis. Macrophages. *Arthritis Res Ther*. 2007;9(6):1-16.

241. Hayakawa K, Wang X, Lo EH. CD200 increases alternatively activated

macrophages through cAMP-response element binding protein – C/EBP-beta signaling. *J Neurochem*. 2016;136(5):900-906. doi:10.1111/jnc.13492.